Semiconductor Optical Amplifiers to Extend the Reach of Passive Optical Networks

Jenny McGeough

A thesis submitted for the degree of Doctor of Philosophy (Ph.D.)
to the School of Engineering in the College of Science and Engineering,
University of Glasgow

I know quite certainly that I myself have no special talent;
curiosity, obsession and dogged endurance,
combined with self-criticism,
have brought me to my ideas.

-Albert Einstein

Abstract

This thesis reports on Semiconductor Optical Amplifiers (SOAs) and their use in optical communication systems; in particular improving the reach of Passive Optical Networks (PON).

Following a comprehensive overview of the components of optical communication systems a PON is introduced and the standard of Gigabit-PON (GPON) explained. The concept of extending the reach of GPON through the introduction of amplification is presented and the business drivers of the telecommunication operators detailed.

The physics of SOAs are described followed by the parameters used to characterise them. Carrier dynamics of SOAs are explained and the methods of measurement of the carrier dynamics are detailed including the spectrogram technique. This method simultaneously measures the gain and phase recovery which is desirable for applications in long range telecommunications which require unchirped signals with a fast response for both gain and phase.

Parameters of commercially available SOAs are compared with the requirements to extend the reach of PONs. Following this the fabrication tolerances for SOAs insensitive to polarisation dependent gain (PDG) are modelled. Results from SOA modelling showed that the greatest contributing factor to PDG variation was the active region thickness error. In the context of bulk production this requires a realistic tolerance of $\pm$10nm to maintain PDG of $\sim$1dB. A polarisation insensitive high gain SOA is designed and experimentally measured. This SOA is measured in the context of GPON and shown to extend the reach of the current standard by a record margin of 28dB. The limitation of the improvement is attributed to gain modulation sourced intersymbol interference (the patterning effect).

The patterning effect has been reported in literature to be reduced through the introduction of SOAs with an active region made from quantum dot (Qdot) material. A comparative study of the gain and phase recovery time and alpha factor of various dimensional SOAs is presented. Using the spectrogram method it is shown that reducing the power and increasing the bias of the SOA can reduce the carrier recovery time. A Qdot active region SOAs is shown to considerably reduce the gain recovery time compared to a bulk SOA of similar length. The active region of the Qdot SOA alludes to a faster carrier recovery time which could be beneficial to extend the reach of PONs without patterning. However as these are more difficult to fabricate in mass production it is unknown if they are a viable solution on a commercial scale.

In the context of GPON a low α-factor is desired for minimizing chirp and phase nonlinearities during amplification of short pulses. An alpha factor study is presented and the Qdot SOA was measured to have the lowest alpha factor which could be beneficial for reducing chirp in 10G-PON.

Contents

List of Figures

Table of Acronyms and Abbreviations

APD	Avalanche Photodiode
ASE	Amplified Spontaneous Emission
BS	Beamsplitter
CH	Carrier Heating
CO	Central Office
CW	Continuous Wave
BER	Bit Error Rate/Ratio
BERT	Bit Error Rate Testing
BTB	Back to Back
DWDM	Dense Wavelength Division Multiplexing
EAM	Electroabsorption Modulator
EDFA	Erbium Doped Fibre Amplifier
ER GPON	Extended Reach Gigabit-capable Passive Optical Network
ES	Excited State
FCA	Free Carrier Absorption
FFT	Fast Fourier Transform
FOA	Fibre Optical Amplifier
FROG	Frequency Resolved Optical Gating
FTTH	Fibre to the Home
FTTB	Fibre to the Building
FTTK	Fibre to the Kerb
FTTx	Fibre to the x
FWHM	Full Width at Half Maximum
GPON	Gigabit-capable Passive Optical Network
GS	Ground State
IPTV	Internet Protocol Television
ISI	Intersymbol Interference
ITU	International Telecommunication Union
ITU-T	ITU's Telecommunication Standardization Sector

MM	Multimode
MQW	Multiple Quantum Well
NF	Noise Figure
OEO	Optical to Electrical to Optical
OLT	Optical Line Termination
ONU	Optical Network Unit
OPA	Optical Parametric Amplifier
OPO	Optical Parametric Oscillator
OSA	Optical Spectrum Analyser
PB	Petabyte (1024 Terabytes)
PCGPA	Principal Component Generalized Projections Algorithm
PDG	Polarisation Dependant Gain
PEF	Pattern-Effect-Free
PIN	Positive-Intrinsic-Negative
PMD	Polarisation Mode Dispersion
PON	Passive Optical Network
Qdot	Quantum Dot
RHS	Right Hand Side
RMS	Root Mean Square
RZ / NRZ	Return to Zero / Non-Return to Zero
SCH	Separate Confinement Heterostructure
SHB	Spectral Hole Burning
SiO_2	Silicon Dioxide / Silica
SM	Single Mode
SNR	Signal to Noise Ratio
SOA	Semiconductor Optical Amplifier
SONET	Synchronous Optical Network
TDM	Time Division Multiplexing
TDMA	Time Division Multiple Access
TE	Transverse Electric
TM	Transverse Magnetic
TPA/2PA	Two Photon Absorption
VOIP	Voice Over Internet Protocol
WAN	Wide Area Network
WDM	Wavelength Division Multiplexing
WL	Wetting Layer

Chapter 1

Introduction

1.1 Telecommunications Networks

The exchange of information is a integral part of modern life. Whether it is in business or for personal communication, there are continuous developments in the way in which people can interact: telephone, email, mobile device, interactive television, VoIP; the list goes on and the possibilities are endless. The telecommunications network which supports this information interchange of voice, data and video is made up of a series of nodes and links to safely transmit the information to its desired destination.

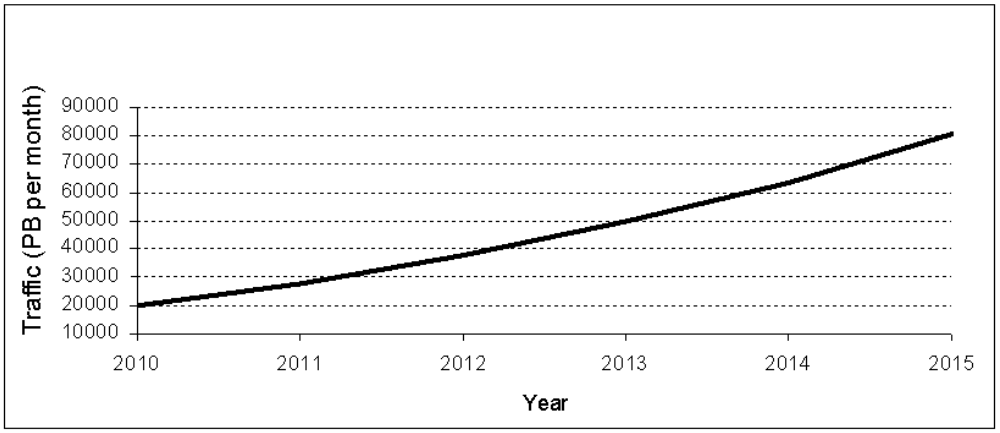

Figure 1.1: Global IP Traffic Forecast from [1].

There has been an increasing rate of traffic growth over the telecoms network in the past twenty-five years and is predicted to increase 32% per year for the next

four years as can be seen in Figure 1.1 and the number of devices connected to IP networks will be twice as high as the global population in 2015 [1]. This is partially due to the continual rise of internet development and users and also following the introduction of new bandwidth consuming applications. As the proportion of broadband connections increase, users tend to spend more time online to utilise bandwidth demanding services such as video-on-demand, IPTV, high speed file sharing, video calling, online gaming etc.

1.1.1 The Last Mile Bottleneck

The telecommunications network is made up of two distinct parts: the backbone (core) network and the access (local) network, as illustrated in Figure 1.2. The backbone is the long distance infrastructure consisting mainly of high capacity links, switches and routers which are responsible for carrying the traffic from one edge of the network to the other. The access network connects the end user to the backbone. The core network has been developed into a high-speed, high-

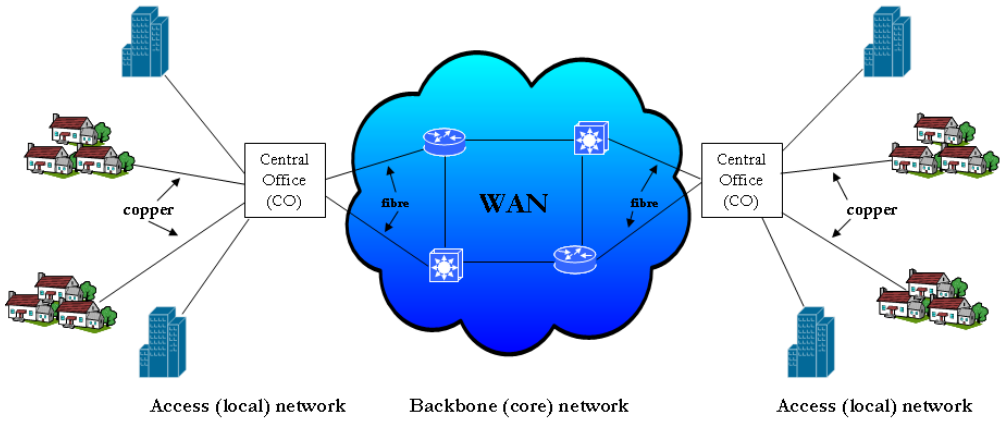

Figure 1.2: Schematic of Telecommunications Network.

throughput service as multiple companies have shared the cost of investment and equipment upgrade such as high speed switches and routers and the adoption of fibre optic cables as the transport links. The access network typically consists of copper telephone wires and in its nature is shared among fewer users. Thus it is a more cost-sensitive project and so there have been fewer outlays to improve the services. In June 2009 the UK Government published its long-awaited Digital Britain report. This made a Universal Service Commitment of 2Mbit/s by

2012 and proposed a 50p levy on phone lines to create a Next Generation Fund which would provide a part subsidy to bring next generation broadband to the 'final third' of homes and small businesses that would otherwise miss out. However following the review of public expenditure, the Government has rescoped the programme but still maintains the target of 90% broadband coverage by 2017. As public pressure increases and the requirement for speed and for greater throughput increases, the network providers are under pressure to find a cost-effective solution to provide broadband access all the way to the end user.

1.1.2 The Last Mile Solution

One of the most promising solutions to the access network bottleneck situation are Passive Optical Networks (PONs). PONs are a point-to-multipoint network architecture which utilise the huge bandwidth potential of optical fibres to bring data at high speed and high bit rates all the way to the end user while minimising the amount of equipment within the network [7]. This technology introduces splitters into the network to replace the more expensive traditional active optoelectronic devices. The splitters are passive; they transmit and split the optical signal without optoelectronic conversions therefore require no power supply and have very low maintenance costs. This allows many users to share one fibre, increasing their individual available link capacity while reducing their overall cost.

This thesis models and develops a high gain, low polarisation sensitive semiconductor optical amplifier (SOA) as a solution to extending the reach of Passive Optical Networks. It then looks at quantum confined SOAs as a way to improve the reach further.

1.2 Thesis Overview

Chapter 2 provides an introduction to optical communications. The major components of a communications system are described including optical transmitters, fibre, amplifiers and receivers; and the methods of optical processing and testing are explained. Following this, the concept of a Passive Optical Network is presented and the current standard for Gigabit-capable Passive Optical Networks (GPON) is outlined. Finally the need for amplification to improve the reach of this standard is discussed.

Chapter 3 analyses the basic principles of optical amplification and the relationship to semiconductor devices. SOA structures and the types of active regions to be explored in this thesis (bulk, multiple quantum well and quantum dot) are introduced. The SOA characterisation parameters are outlined, including gain, gain bandwidth, saturation output power, polarisation dependence and noise. The gain and phase dynamics of the carriers in an SOA are presented and a literature review details the carrier dynamics characterisations reported to date. Following this the techniques implemented to measure the carriers are given including an introduction to the pump-probe and spectrogram techniques.

Chapter 4 reviews the opportunities for SOAs to extend the reach of GPON. The requirements for an SOA specification in this context are reviewed. Modelling is presented to identify the parameters affecting the mass fabrication of high gain SOAs suitable for serving GPON. A high gain SOA with low polarisation dependence is designed, fabricated and experimentally measured to show a record margin improvement in a Passive Optical Network with the inclusion of an SOA. The SOA is shown to have gain modulation sourced ISI (patterning) effects at high power which limits the performance in the PON scenario.

Chapter 5 investigates quantum confined SOAs and their reduced patterning effect. An introduction to the gain saturation effect which leads to the patterning effect is given and a literature review of 'Pattern-effect-free' quantum dot SOAs is presented. The structures and emission properties of the bulk, multiple quantum well and quantum dot SOAs studied in this chapter are described. This chapter then identifies the range of ideal launch conditions for an amplifier in a Passive Optical Network. Following this the spectrogram characterisation facility used for the measurements are described and the experimental measurements are presented of the gain and phase recovery dynamics. An alpha factor study is presented. It is commented how introducing quantum dot active region SOAs could improve the reach of PONs further.

Chapter 6 summarises the thesis and draws conclusions from the work contained herein.

1.3 Summary of Contribution

Table 1.1 shows the activities undertaken in the research of this thesis and highlights the specific involvement of the author.

Activity	Author's Involvement
SOA Modelling	Complete
High Gain SOA Design	Significant
High Gain SOA Fabrication	Nil
High Gain SOA Measurements	Complete
High Gain SOA Analysis	Complete
GPON Launch Conditions Measurements	Complete
GPON Launch Conditions Analysis	Complete
MQW / Qdot SOA Design / Fabrication	Nil
Gain and Phase Measurements	Complete
Gain and Phase Analysis	Complete
Alpha Factor Measurements	Complete
Alpha Factor Analysis	Complete

Table 1.1: Summary of Contribution

1.4 Publications

Journal Papers

A. E. Kelly, C. Michie, I. Armstrong, I. Andonovic, C. Tombling, *J.McGeough*, and B. C. Thomsen, 'High-Performance Semiconductor Optical Amplifier Modules at 1300nm', IEEE Photon. Technol. Lett, vol. 18, no. 24, pp. 2674–2676, 2006.

C. Michie, A. E, Kelly, *J.McGeough*, I. Armstrong, I. Andonovic and C. Tombling, 'Polarization-Insensitive SOAs Using Strained Bulk Active Region', J. Lightw. Technol., vol. 24, no. 11, pp. 3920–3927, 2006.

C. Michie, A. E. Kelly, *J.McGeough*, S. Karagiannopoulos and I. Andonovic, 'Optically Amplified Passive Optical Networks: A Power Budget Analysis', Journal of Optical Networking, vol. 8, no. 4, pp. 370–382, 2009.

Conferences

C. Michie, A. E. Kelly, I. Andonovic and *J.McGeough*, 'Reach Extension of Passive Optical Networks using Semiconductor Optical Amplifiers', In Proceedings

International Conference on Transparent Optical Networks, ICTON, June 2008, pp. 194–197.

J.McGeough, A. E. Kelly and C. Michie, '1300nm Semiconductor Optical Amplifiers for Passive Optical Networks', Semiconductor and Integrated Optoelectronics Conference, SIOE, Cardiff, April 2008.

Chapter 2

Optical Communications

2.1 Introduction

Any communications system can be thought to consist of three main parts: the transmitter which sends the data, the transmission line which carries the data to its destination and the receiver which picks up the data at the destination as can be seen in Figure 2.1(a).

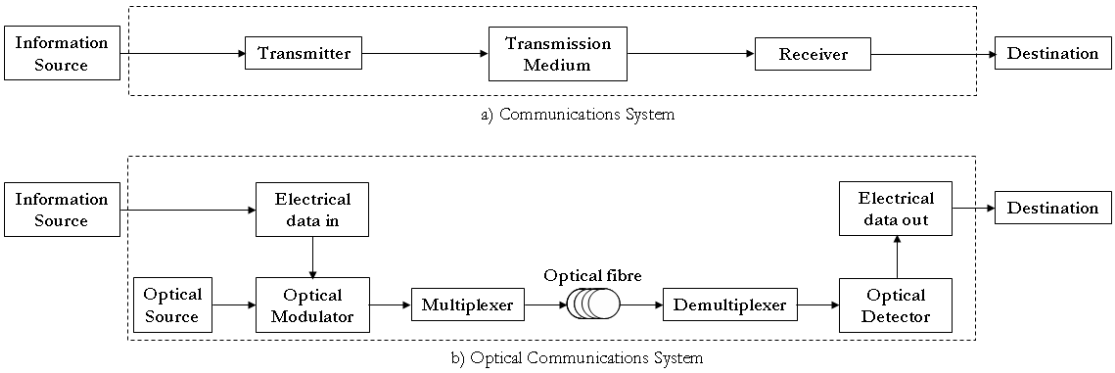

Figure 2.1: Basic block diagram of (a) generic communications system (b) optical communications system.

An optical communications system is no different. As can be seen in Figure 2.1 (b), the carrier signal is transmitted from an optical source such as a semiconductor laser. The electrical information to be conveyed is imprinted upon the carrier signal via an optical modulator. The signal then undergoes multiplexing to improve the data rate throughput before it is sent down the optical fibre transmission line. At the receiving end a demultiplexer is used to separate the

signals before a photodetector receives the signal and converts it back into an electrical signal allowing the information to be extracted for use in audio, video or data handling.

Other actions common during the transmission process are amplification to maintain signal strength, switching to send the signal to its destination and testing to ensure the signal received is correct.

This chapter will introduce the key components of an optical communications system, the processes that are employed during transmission, a method of testing the data and an overview of optical networks.

2.2 Components

This section will look at the key components of an optical communication system: optical transmitters, optical fibre, optical receivers and optical amplifiers.

2.2.1 Optical Transmitters

An optical transmitter converts an electrical signal into an optical signal and launches the optical signal into an optical waveguide or fibre. In optical communications networks the ideal optical transmitter is one which outputs a high quality of light. This can be defined by having a narrow spectral width, high stability, low power consumption and a tuneable central wavelength. The most common light sources found in fibre optic communication systems are light-emitting diodes (LEDs) and laser diodes (LDs). Both are small semiconductor devices that convert electrical signals into light.

Light Emitting Diodes

Light Emitting Diodes (LEDs) emit light through spontaneous emission and are used extensively in fibre optic communication systems due to their small size, long lifetime and low cost. They are mostly found in short distance, low bandwidth networks such as local area networks as they are limited in their transmission capabilities by their low output intensity, poor beam focus and incoherent radiation.

Laser Diodes

In comparison to LEDs, lasers emit light through amplification of radiation by stimulated emission. Lasers have a higher output power than LEDs and so they are capable of transmitting information over longer distances. Also lasers have a much narrower spectral width and can provide high bandwidth communication over long distances, thus are an excellent light source for long haul fibre optics links.

2.2.2 Fibre

An optical fibre used for communication links is a cylindrical dielectric waveguide made of low-loss materials as shown in Figure 2.2. It has a high refractive index inner glass core in which the light is guided, surrounded by a lower refractive index outer cladding. This is covered with a protective buffer and outer jacket. This design of fibre is lightweight and has very low loss (maximum attenuation for CAT 5e cable over 100 metres at 100MHz is 22dB whilst multimode fibre over the same distance is 0.1dB) making it ideal for transmission of information over long distances. The light is maintained within the glass core and cladding by careful design of the relative refractive indices leading to total internal reflection. The normalised frequency, V (or V number) defines the number of modes that are able to propagate within the fibre:

$$V = \frac{\pi d}{\lambda}\sqrt{{n_1}^2 - {n_2}^2} \tag{2.1}$$

where d is the core diameter, λ is the wavelength in vacuum, n_1 is the refractive index of the core and n_2 the refractive index of the cladding.

Every telecommunications fibre falls into one of two categories: single-mode or multimode. It is virtually impossible to distinguish between single-mode and multimode fibre with the naked eye. There is no difference in outward appearance, only in core size. Both fibre types act as a transmission medium for light, but they operate in different ways, have different characteristics and serve different applications.

Single-mode fibre (SM) allows for only one pathway, or mode, of light to travel within the fibre. For this to be the case, $V < 2.405$, where the core size is

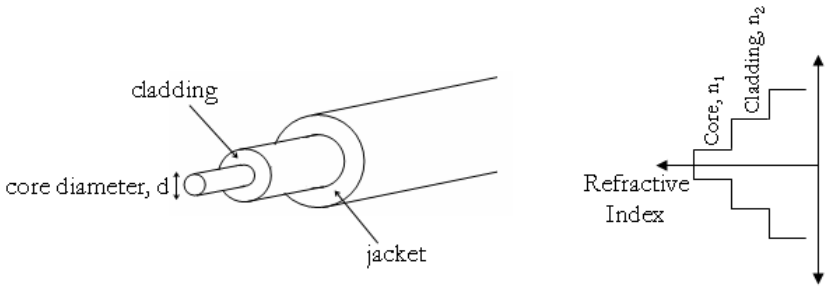

Figure 2.2: Optical fibre core with surrounding cladding and protective jacket where the core has the highest refractive index.

typically 8-10μm. Single-mode fibres are used in applications where low signal loss and high data rates are required, such as in long distance communications where repeater/amplifier spacing needs to be maximized.

Multimode fibre (MM) allows more than one mode of light to travel concurrently within the fibre. Common multimode core sizes are 50μm and 62.5μm. Multimode fibre is better suited for shorter distance, lower bandwidth applications and is more economical because it can be used with inexpensive connectors and LED transmitters, making the total system cost lower.

The loss along fibre is low (maximum attenuation of 1dB/km for multimode fibre at 1300nm [8] and 0.5dB/km for single mode fibre at 1310nm and 0.4dB/km at 1550nm [9]) and the signal is not subject to electromagnetic interference which plagues other methods of signal transmission such as radio or copper wire links. The signal is however, degraded by other means particular to the fibre such as dispersion and non linear effects (caused by a high power density in the fibre core).

There are three main bandwidth 'windows' of interest in the spectrum of fibre as can be seen in Figure 2.3. These three windows exist where the weakest effects of attenuation and dispersion are found, making them the most favourable for transmission. The first window is at 800-900nm, where there is a good source of cheap silicon based detectors. Fibre losses are relatively high in this region and so it is only suitable for short distance transmission. The second window, the original band or O band, is at 1260-1360nm, where there is low fibre attenuation coupled with zero material dispersion. The third window of interest is at 1430-1580nm where fibre has its attenuation minimum. The most popular transmission range in this window is 1530-1565nm where erbium amplifiers operate and is known as

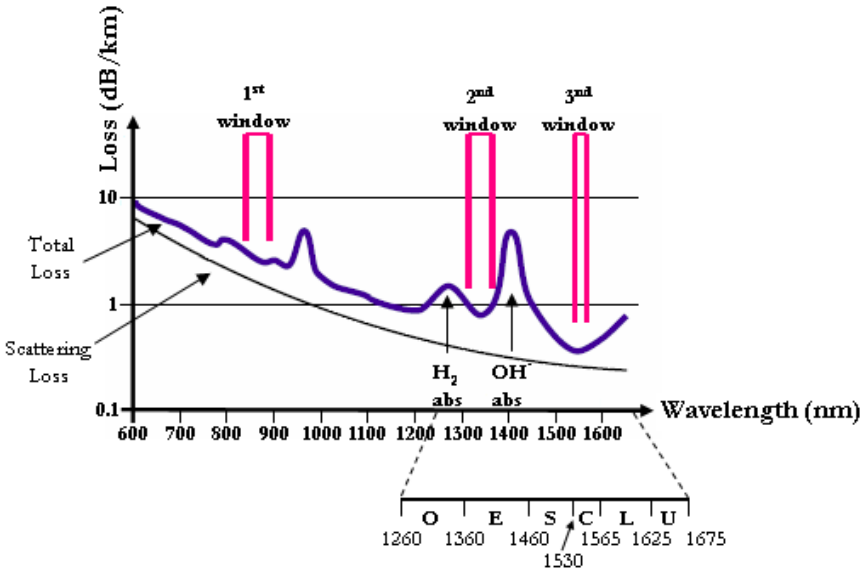

Figure 2.3: Optical fibre attenuation spectra for low loss single-mode silica fibre and the three telecommunications operating windows.

the conventional band or C band.

Fibre Attenuation

Attenuation is the loss of optical power of a signal as it travels down a fibre. Attenuation depends on the wavelength of the light propagating within it and is measured in decibels per length (dB/m, dB/km). Attenuation characteristics can be classified as intrinsic or extrinsic. Intrinsic attenuation occurs due to substances inherently present in the fibre, whereas extrinsic attenuation occurs due to external influences such as bending or connection loss.

Dispersion

The output from a optical communications source (LED or LASER) is not a single wavelength but in fact a distribution of wavelengths. These various wavelength components propagate along the fibre at different speeds and arrive at the receiver at different times thus causing the pulse to spread i.e. disperse. This is characterised by the dispersion parameter, D, which is given by [10]:

$$D = \frac{d}{d\lambda}\left(\frac{d\beta}{d\omega}\right) \tag{2.2}$$

where λ is the operating wavelength, β is the propagation constant and ω is the optical frequency.

Dispersion is measured in picoseconds of pulse widening per nanometre of the signal spectral width per kilometre of the path length i.e. ps/nm.km. When a pulse spreads to the degree where it overlaps with an adjacent pulse it causes detection problems at the receiver resulting in errors in transmission. This is called intersymbol interference (ISI) or patterning. Dispersion is a limiting factor in fibre bandwidth, as the shorter the pulses, the shorter the possible time between the pulses, the more susceptible they are to patterning. There are three types of dispersion found in fibre optical communications: chromatic, intermodal and polarisation mode dispersion. Chromatic dispersion occurs in all types of fibres; intermodal dispersion only occurs in multimode fibres and polarisation mode dispersion is only significant in single mode fibres.

1. Chromatic (Intramodal) Dispersion

   Chromatic dispersion occurs in all types of fibres and occurs due to the individual wavelength components of the signal traveling through a material at different speeds. Chromatic dispersion is composed of two mechanisms, material dispersion and waveguide dispersion.

   Material dispersion occurs because the spreading of a light pulse is dependent on the wavelengths' interaction with the refractive index of the fibre core. Different wavelengths travel at different speeds in the fibre material. Different wavelengths of a light pulse that enter a fibre at one time exit the fibre at different times. Material dispersion is a function of the source spectral width. The spectral width specifies the range of wavelengths that can propagate in the fibre. Material dispersion is lower at longer wavelengths. Waveguide dispersion is relatively small compared to material dispersion in multimode fibres and is more significant in single mode fibres. In single mode fibre, waveguide dispersion occurs because the mode propagation constant, β, is a function of the size of the fibre's core relative to the wavelength of operation. Waveguide dispersion also occurs because light propagates differently in the core than in the cladding.

2. Intermodal Dispersion

Intermodal dispersion only occurs in multimode fibre and is the major limiting factor in multimode fibre bandwidth. In multimode fibre there is more than one mode and intermodal dispersion occurs because each mode travels a different distance over the same time span. This condition causes the light pulse to spread in time as light is coupled, by scattering events, between differently propagating modes. As the length of the fibre increases, intermodal dispersion increases.

3. Polarisation Mode Dispersion

   A third type of dispersion found in fibres is called polarisation mode dispersion (PMD). The fundamental mode which travels in a single mode fibre has two polarisation components. Ideally these two states carry half of the total power each and when the fibre is symmetric PMD is not an issue in the signal transmission. PMD is caused when the fibre's cross section is not symmetric i.e. the refractive indices along the fibre's x and y axes are not equal, which leads to the broadening of the optical signal. This generally occurs during fibre-cabling and fibre-spicing processes. In early installed fibres PMD was found to severely limit the propagation distance at high bit rates [11]. Research into PMD continues as there exists a great deal of installed standard fibre which has a comparatively large PMD value which is a potential problem at high bit rates.

Intermodal dispersion does not exist in single mode fibres as only the fundamental mode propagates thus single mode fibres exhibit the lowest amount of total dispersion. Single mode fibres also exhibit the highest possible bandwidth therefore are used for long distance transmission.

2.2.3 Optical Amplifiers

As has been established in the previous section, attenuation reduces the optical signal as it travels down a fibre. Thus optical amplifiers are greatly beneficial in lengthening the transmission distance capability of a communication system while still enabling the signal to meet the sensitivity requirements of the optical receiver.

Optical amplifiers are categorized in terms of the function which they perform. There are three basic types: boosters, in-line amplifiers and preamplifiers as

can be seen in Figure 2.4. A booster, also called a post-amplifier, is a power amplifier that magnifies a transmitter signal before sending it down a fibre. A booster raises the power of an optical signal to its maximum power, which maximises the transmission distance. An in-line amplifier or mid-span amplifier operates with a signal in the middle of a fibre-optic link and is used to compensate for power losses caused by fibre attenuation. A preamplifier magnifies a signal immediately before it reaches the receiver, thus generally operates with a weak input signal as it is located at the end of the transmission line. Good sensitivity, high gain and low noise are key requirements for a good preamplifier.

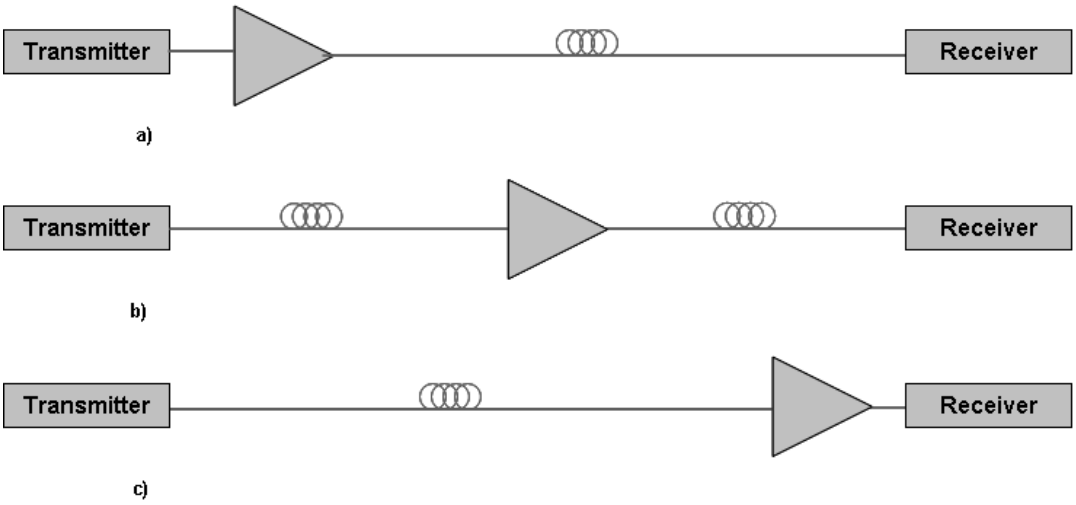

Figure 2.4: Functional types of optical amplifiers (a) booster (b) mid-span (in-line) amplifier (c) preamplifier.

There are three main classes of optical amplifiers in use today: semiconductor optical amplifiers (SOA), fibre optical amplifiers (FOA) and fibre Raman amplifiers. This section will detail SOAs and FOAs.

A semiconductor optical amplifier (SOA) can be thought of as laser diode without, or with very low, optical feedback. A fibre optical amplifier is a piece of speciality fibre spliced with a transmission fibre and connected to a pump laser. Both these amplifier types work on the principle of stimulated emission, (see section 3.1). Fibre amplifiers, specifically erbium-doped fibre amplifiers (EDFAs), are widely used in telecommunication networks. EDFAs operate only in the 1550nm window while SOAs can function in either 1300nm or 1550nm communications windows.

Erbium Doped Fibre Amplifiers (EDFA)

An erbium doped fibre amplifier is one of the most widely used optical amplifiers at 1550nm [12]. EDFAs contain a length of fibre working as an active region that is heavily doped with erbium ions and is pumped optically at 980nm, 1480nm or both using a semiconductor laser in the 10 to 100 milliwatt output range. The optical information and the optical pumping beams are combined onto the same fibre by a coupler; they propagate together along the doped section of the fibre where the information signal is amplified at the expense of the pumping wavelength. A second coupler removes residual pumping light from the fibre. An isolator is incorporated to prevent backwards travelling amplified spontaneous emission (ASE) from penetrating the amplifier. The gain saturation and gain recovery have a time characteristically in the millisecond range. The data which is being amplified does not have any frequency components in this range and therefore the signal is not distorted by amplification. Very high gains (54dB) with low noise figures (3.1dB) have been achieved [13].

The greatest drawback of the EDFA is its wavelength restriction. It is possible to tailor the fibre length to achieve good performance in the L-band (1565-1625nm) [14] but satisfactory performance has not been achieved in the O-band despite a great deal of research [15].

Semiconductor Optical Amplifiers (SOA)

A semiconductor optical amplifier is essentially a semiconductor active region with very low optical feedback. SOAs are pumped electrically and can have their gain peak designed to operate over a large range of wavelengths including 1300nm, 1490nm and 1550nm. They have a bandwidth up to 100nm and are small, thus can be easily integrated into optoelectronic integrated circuits. In addition to linear amplification, an SOA can be used as a high-speed, high-extinction-ratio gate and a nonlinear waveguide for all-optical switching. This allows a variety of functions to be realized with this technology such as wavelength selectors [16, 17], broadcast-and-select space switches [18], and all-optical gates such as wavelength converters and regenerators [19]. The ultrafast dynamics in an SOA give an almost instantaneous nonlinear response that is large enough to allow all-optical switching in a very short device. The large gain and large differential gain of SOAs allow switching with power levels in the range of milliwatts, and various functionalities

have been demonstrated in a number of different schemes at speeds in excess of 100Gb/s, e.g. wavelength conversion at 168Gb/s [20].

The SOA structure and carrier dynamics will be explained in greater detail in sections 3.2 and 3.3.

2.2.4 Optical Receivers

An optical receiver or detector is an electro-optical device that accepts optical signals and converts them into electrical signals. An ideal optical receiver in an optical communications system will have high sensitivity, large bandwidth, low temperature sensitivity, low power consumption and polarisation independence. The most common optical receivers found in fibre optic communication systems are PIN photodiodes and avalanche photodiode (APD) receivers. Both are highly sensitive semiconductor devices that convert light pulses into electrical signals.

PIN Receivers

A PIN photodiode consists of a thick intrinsic (undoped) depletion region sandwiched between thin positive and negative doped regions i.e. positive-intrinsic-negative. The material of the p and n layers is chosen so that there is no absorption of the incident photons in these layers. It is generally operated by applying a reverse-bias voltage, typically less than a few volts. Most of the incident photons will enter the thick intrinsic layer and produce electron-hole pairs which will generate a photocurrent. This photocurrent is in direct proportion to the absorbed optical power:

$$I_p = RP_{in} \tag{2.3}$$

where I_p is the photocurrent, R is the constant of proportionality called the responsivity of the photodetector and P_{in} is the incident optical power.

A current known as dark current is still produced by the leakage current that flows when the reverse bias is applied without any incident light on the photodiode. Dark current is temperature dependent and will increase as the device temperature increases. The PIN photodiode allows high bandwidths and responsivity to be achieved simultaneously [21]. The speed of the PIN photodiode is limited by the carrier drift time across the depletion region. PIN photodiodes are

the most commonly employed receivers in fibre optic communication systems due to their ease in fabrication, high reliability, low noise, low voltage and relatively high bandwidth.

Avalanche Photodiode Receivers

An avalanche photodiode (APD) is a photodiode that internally amplifies the photocurrent by an avalanche process thus making it a more sensitive receiver than a PIN photodiode. The more sensitive the receiver is, the longer the communications link can be with the given losses. The APD has a greater sensitivity by internally amplifying the photocurrent without introducing the noise associated with external electronic circuitry. A reverse bias is applied to the active region which causes the electrons generated by the incident photons to accelerate. These electrons strike neutral atoms in the structure which gain enough energy to ionize other carriers thus increasing the photocurrent.

The gain increases as the reverse bias voltage increases to approach the breakdown voltage. However in the vicinity of the breakdown voltage, a large current flows through the APD which can easily cause it permanent damage. The high bias also increases the noise levels and limits the useful gain of the APD.

An APD has higher gain and bandwidth than a PIN but it requires a much greater voltage to be applied across the active region. This requirement for higher power reduces the capability of miniturization of a receiver unit and limits the possibilities of integration in communication systems.

2.3 Optical Processes

This section will look at the key processes of an optical communication system. First a few terms used in optical communications shall be defined.

2.3.1 Bandwidth and Bit Rate

Bandwidth is the frequency range within which a signal can be transmitted without significant deterioration and is measured in Hertz, Hz. It is the information carrying capacity characteristic of a communications channel used for analogue transmission.

Bit rate is the number of bits that can be transmitted per second and is measured in bits per second, bit/s. It is the direct measure of information carrying capacity of a digital communications link. The bit rate of a system is limited by $BR < 1/(4\Delta t)$ where Δt is pulse spreading which is caused by dispersion in the transmission fibre.

2.3.2 Optical Multiplexing

An optical fibre has a theoretical bandwidth of 50Tbit/s while electronic transmitters and receivers are limited to around 100Gbit/s [22] thus a point-to-point transmission system utilises only 1/500 portion of the available bandwidth. In order to take advantage of the huge bandwidth of the fibre, optical multiplexing techniques are used. These can either be in time (optical time division multiplexing, (O)TDM) or in wavelength (wavelength division multiplexing, WDM) where many channels are transmitted over the same fibre to increase the overall capacity.

A common analogy exists between methods of optical multiplexing and road networks. TDM is analogous to increasing the speed of the cars moving down a motorway and WDM is analogous to adding more lanes on the same road.

Wavelength Division Multiplexing (WDM)

Wavelength division multiplexing is shown schematically in Figure 2.5. It is based on the principle that several light beams at different wavelengths can simultaneously travel over the same optical path without interference except through non-linear effects such as four wave mixing and self and cross phase modulation [23].

A passive wavelength multiplexer is used to combine N signals at N wavelengths and transmit them simultaneously over the same optical fibre. The signal is demultiplexed at the receiver end to output the N signals. This system increases the fibre throughput by a factor of N. WDM systems have the advantage that the aggregate bit rate is increased while the tolerance to factors such as dispersion are exactly the same as a single channel system. Furthermore, the multiplexing and demultiplexing is passive and asynchronous and therefore simple and potentially cheap.

The capacity of a WDM system is related to the transmission wavelength window of the fibre. Due to limitations in demultiplexers, wavelength stability of

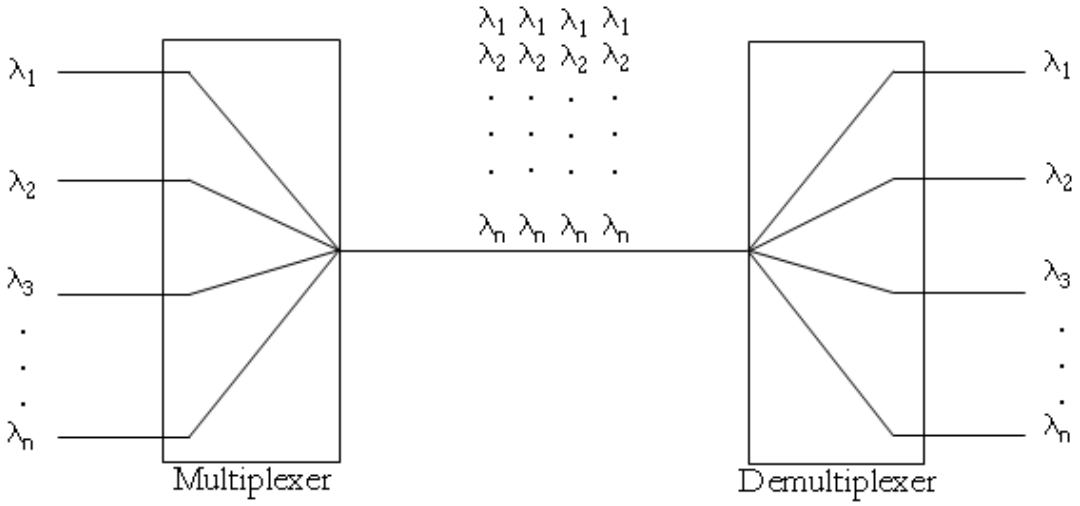

Figure 2.5: Illustration of Wavelength Division Multiplexing.

the optical sources and nonlinear transmission effects, WDM channels have to be separated by more than the data bandwidth of each individual channel (usually around four times the bit rate is required). Recently it was shown that a WDM network with 140 channels of 111Gbit/s is capable of transmitting 14Tbit/s over a single 160km long optical fibre [24].

Optical Time Division Multiplexing (TDM or OTDM)

Optical time division multiplexing is shown schematically in Figure 2.6. In TDM a multiplexer takes a sample of each signal, assigns a specific time slot to this sample, combines the samples and transmits them over the same line.

The relative delay between channels is determined by the number of channels to be multiplexed i.e. if there are N channels the delays generally are $\frac{1}{N}$, $\frac{2}{N}$, ... $\frac{N-1}{N}$ of the bit period. The demultiplexing process is more complicated than that of WDM as active, rather than passive, demultiplexing is required and there is a requirement for high speed clock recovery and a risk of losing the clock pulses. Despite these limitations very high bit rate systems have been achieved using TDM [25, 26].

Combining WDM and TDM techniques is a simple method for realizing high bit rates exceeding 1Tb/s, as has been shown to 3Tb/s over 40km with 19 WDM carriers and 16 TDM channels at a bit rate of 10Gb/s [27].

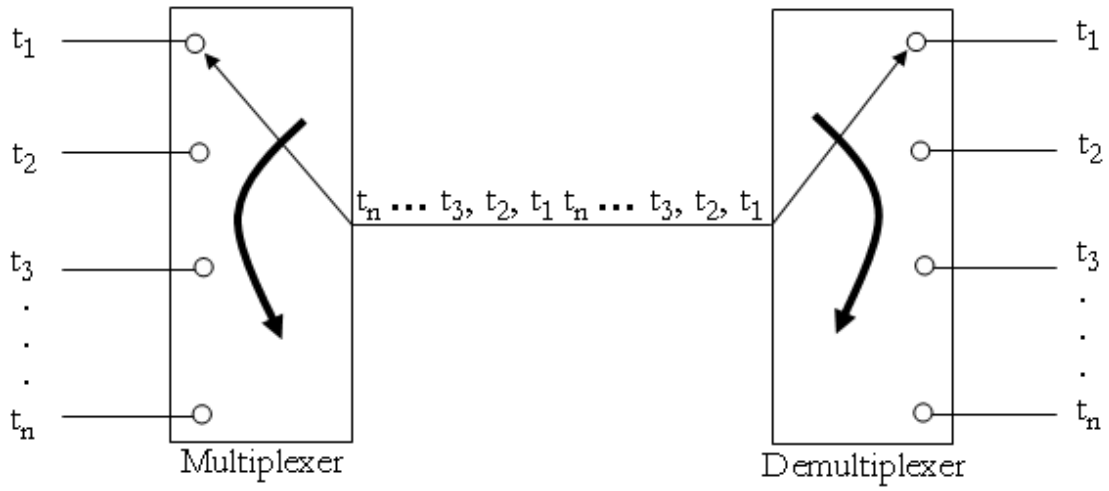

Figure 2.6: Illustration of Time Division Multiplexing.

Time Division Multiple Access (TDMA)

Time Division Multiple Access is a type of time division multiplexing. TDMA works in a similar manner as TDM except instead of the signal being multiplexed from the same node, as in Figure 2.6, there are many transmitters. Each transmitter is given a dedicated time slot in which it can transmit data, in effect a point-to-point scheme. The transmitters only send a signal in their allocated slot when they have something to transmit and so burst mode receivers are required. Every time a burst of data arrives from a transmitter, the burst-mode receiver must synchronize with the clock in the burst before it can decode the data within it.

2.4 Optical Testing

For a communications system to be of any value, the data arriving at the destination must accurately reflect that which was transmitted. In optical transmission systems one method of testing the received data is bit error rate testing (BERT). This is a measure of the bit error rate (BER) (also known as bit error ratio) which is defined as the ratio of the number of erroneous bits received to the total number of bits transmitted in a given time period.

2.4.1 Bit Error Rate Testing

There are many noise processes and distortion mechanisms in the optical path such as dispersion and patterning which can reduce the signal power. The total effect of all the deleterious mechanisms can be characterised by the receiver sensitivity. This is defined as the maximum signal power which is required to fall on the receiver in order to achieve a particular BER (Bit Error Rate/Ratio). The receiver sensitivity is usually defined at a BER of $1x10^{-9}$.

2.4.2 Transmitter Mask or Eye-Diagram

A transmitter mask, or eye-diagram, is commonly used to evaluate optical data transmission. The word eye is used because of the pattern's similarity to the open human eye. An example pattern is formed by superimposing 010 and 101 signals as shown in Figure 2.7. The extinction is the ratio of the power in a binary '1' to that of a binary '0' of a data signal.

An ideal eye, shown in Figure 2.7, can degrade due to common transmitter problems as shown in Figure 2.8. Jitter is a slight variation in the digital signal with respect to reference time which makes the signal diffuse. An increased rise or fall time closes the eye and pulses that overshoot or undershoot also close the eye and distort its shape.

In optical communications it is desirable to have a system which has fast switching between the zero and one states and when measured outputs a high extinction ratio. When measuring eye diagrams it should be noted that increasing input ASE raises the zero line away from the electrical ground line.

2.4.3 Intersymbol Interference (ISI) (Patterning Effects)

Intersymbol interference (ISI), also known as patterning, limits the error free distance in a transmission line. This occurs when a pulse spreads to the degree where it overlaps with an adjacent pulse, which causes detection problems at the receiver resulting in errors in transmission. Patterning is dependent on the 'prehistory' of the pulse and can be avoided by ensuring the repetition rate is higher than the gain recovery time so the gain can fully recover before the next pulse arrives at the receiver.

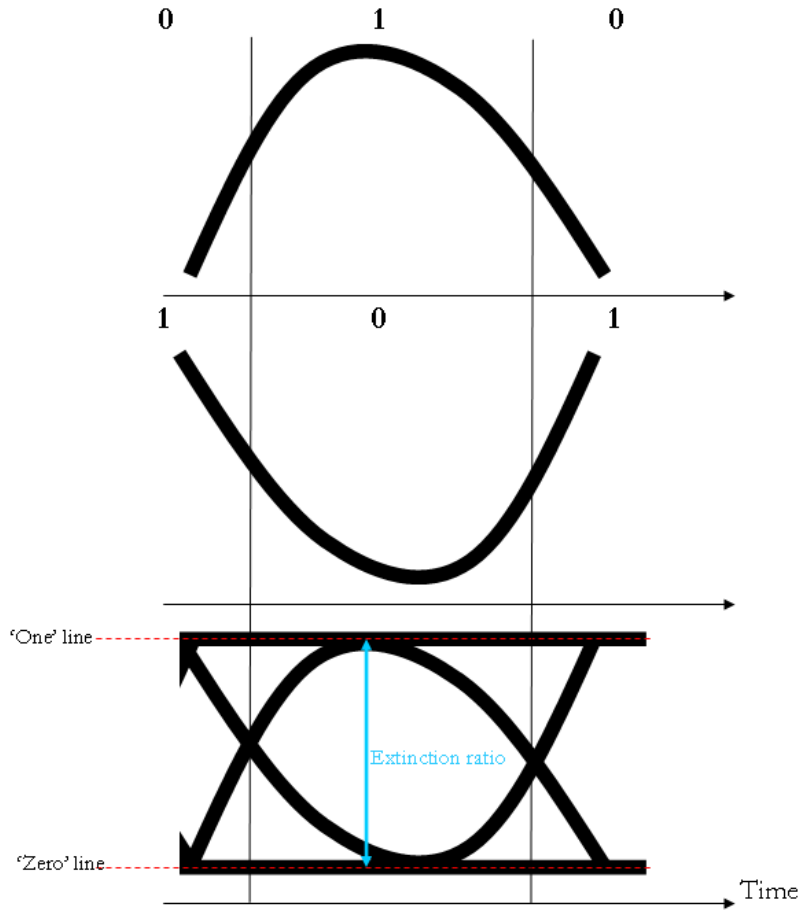

Figure 2.7: Eye diagram showing zero and one lines and the maximum extinction ratio.

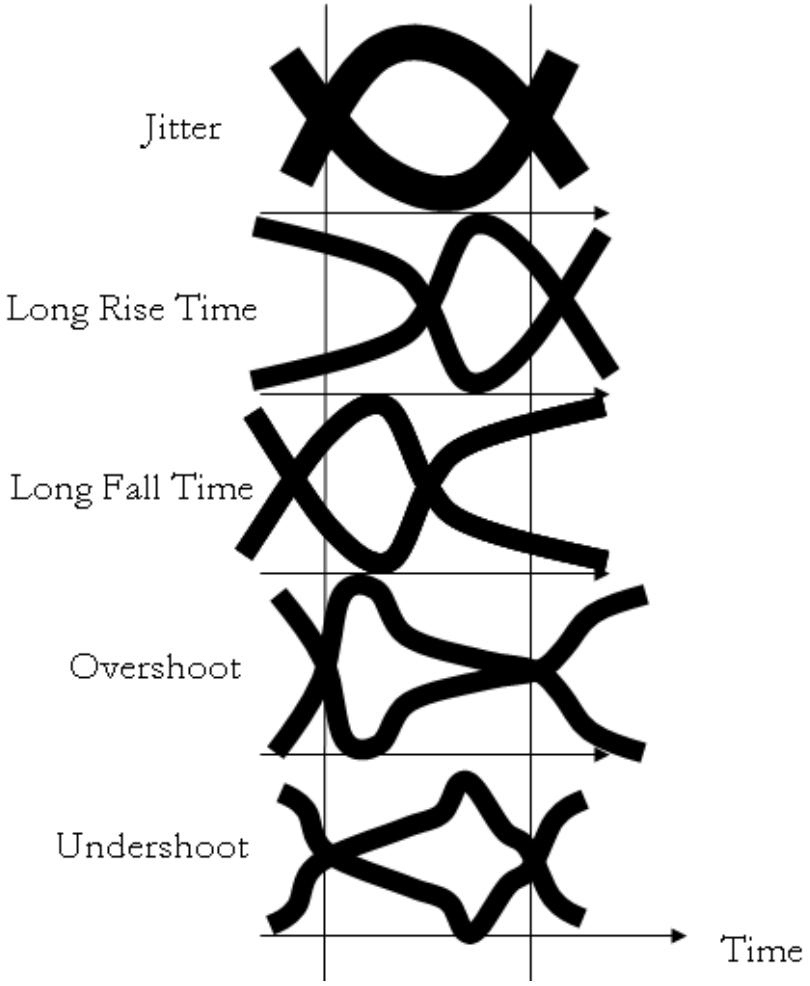

Figure 2.8: Eye Diagram Degradations.

2.5 Passive Optical Networks (PONs)

Passive Optical Networking is a point-to-multipoint optical network architecture. As can be seen in Figure 2.9, a PON consists of an Optical Line Terminal (OLT) at the telecommunications providers' Central Office (CO) which represents the physical interface between the core and access networks. An optical fibre is installed between the OLT and an optical splitter, which divides the signal into several signals without optoelectronic conversion, and distributes it to the Optical Network Units (ONUs) near the end user through a multiplexing technique. The signal is then transformed into electrical form and transmitted to the user's equipment.

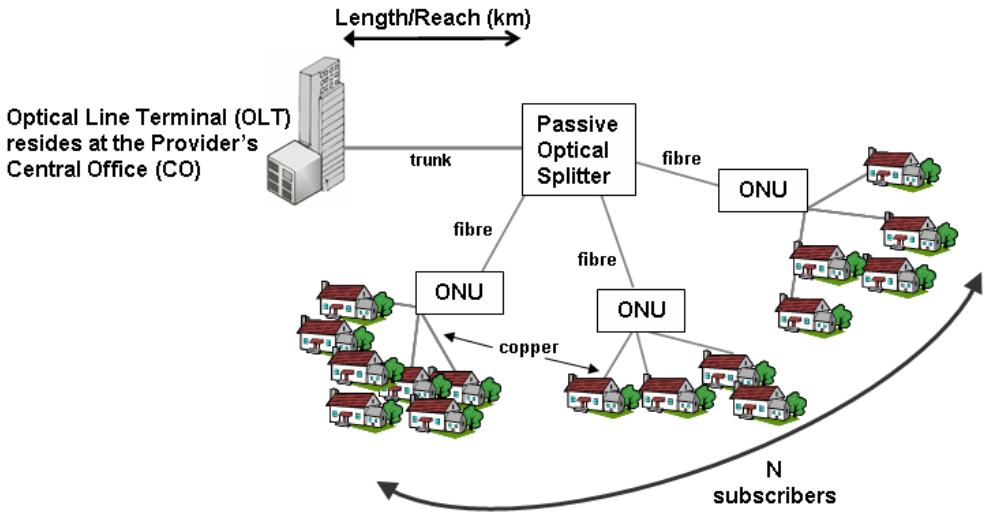

Figure 2.9: Passive Optical Networking Diagram.

Various PON topologies exist and the schematic representation of the most common: tree, bus and ring architectures can be seen in Figure 2.10. Depending on the relevant proximity between the ONU and the user's premises, the architecture is called Fibre To The Home (FTTH), Fibre To The Kerb (FTTK), Fibre To The Building (FTTB) or collectively Fibre to the x (FTTx). Downstream transmission is data traveling from the OLT to the ONU. The traffic first reaches the passive splitter which forwards the data to the ONUs. Then each ONU has to identify which packets are intended for it and discard the rest. This can be achieved through WDM or TDM (see section 2.3.2).

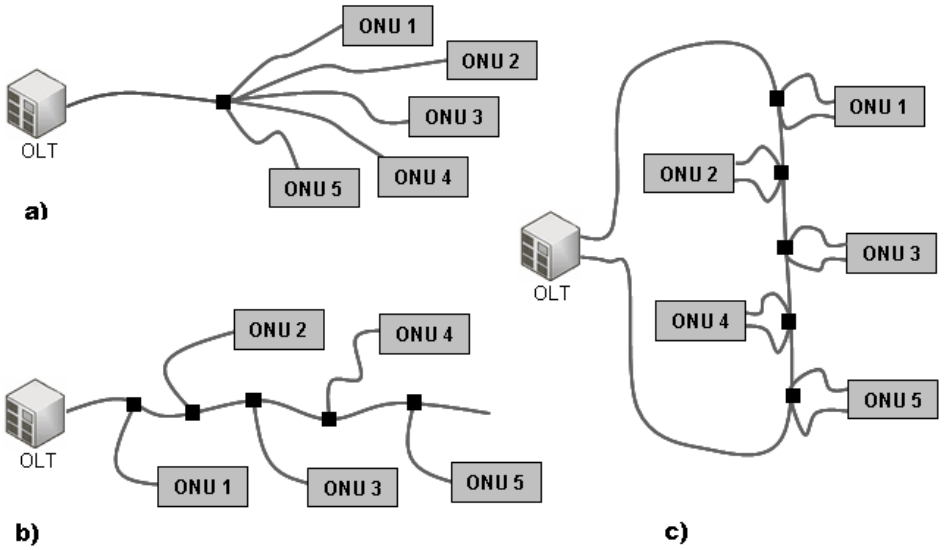

Figure 2.10: PON Topologies: (a) Tree topology, (b) Bus topology, (c) Ring topology.

2.5.1 Gigabit-capable Passive Optical Networks (GPON)

The International Telecommunication Union's Telecommunication Standardization Sector (ITU-T) standardized G.984 or Gigabit-capable PON (GPON) in 2003 with revisions in 2008. Through WDM for data separation, GPON supports asymmetrical streams in a single fibre of 2.5Gb/s downstream at 1490nm and 1.25Gb/s in the upstream direction at 1310nm, avoiding broadcast video in the C-band. TDM is used downstream and TDMA is implemented upstream as can be seen in Figure 2.11. Its maximum physical coverage is up to 20km and its logical reach can be up to 60km. There is a trade off between the PON length and its splitting capability, with a maximum of 128 ONUs per OLT, however a split ratio of 32 is common today.

Operators in Asia have largely settled on Ethernet-PON, whereas North American and European operators have tended to advocate GPON. US operator Verizon started GPON deployments with its fibre-based service FiOS in 2008, and is now servicing more than 9 million homes, half the FiOS rollout target. Europes five main operators BT, Deutsche Telekom, France Telecom, Telefonica (Spain) and Telecom Italia have all backed GPON [28, 29].

Further to this 10G-PON has been standardised: 10 Gbit/s at 1577nm downstream and 2.5 Gbit/s at 1270nm upstream allowing simultaneous use of the GPON

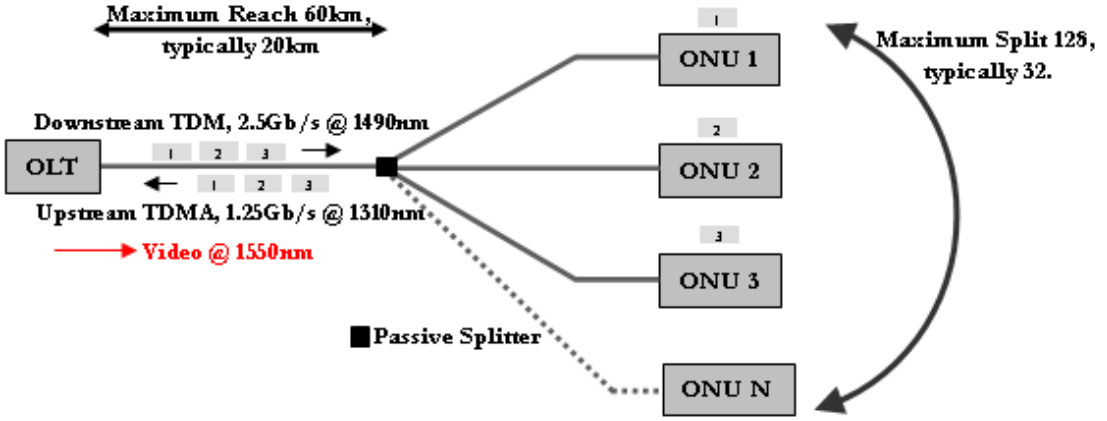

Figure 2.11: ITU-T GPON Standard G.984: Single Fibre.

fibre. This discussion in this thesis primarily refers to GPON however the analysis will be applicable to 10G-PON also.

2.5.2 Extended Reach GPON

A further progression in the pursuit for a cost effective access network is long reach or extended reach GPON (ER GPON) as outlined in G.984.6 and illustrated in Figure 2.12. Ideally there are no active components between the CO and the end user, however if an 'extender box' is included in the system it may be possible to increase the reach of the OLT from 20km up to 100km thus enabling more subscribers to be served from a single OLT.

ER GPON enables an increase in the optical splitting capability allowing it to serve a larger number of users; the minimum splitting ratio is defined as 64 ONUs per OLT. ER GPON can improve the customer experience by allowing rural customers the opportunity to access broadband networks at a lower cost. This is also attractive to the operators as it allows an increase in the geographical range of the network without the requirement for additional central office premises thus a reduction in the unit bandwidth cost. The capital expenditure of the operators will be reduced as the backbone network equipment is replaced with a power splitters and optical amplifiers. The operational expenditure will be reduced also as the majority of the central office premises can be eliminated as the optical amplifying nodes rather than electronic equipment could be placed in street cabinets thus a considerable reduction in real estate costs. The optical solution requires a much

reduced power consumption making it an energy efficient and environmentally friendly solution. A quantitative economic study is presented in detail in [30].

The extension will require an OEO or optical amplifier based reach extender as the wavelengths of interest are outside the erbium window.

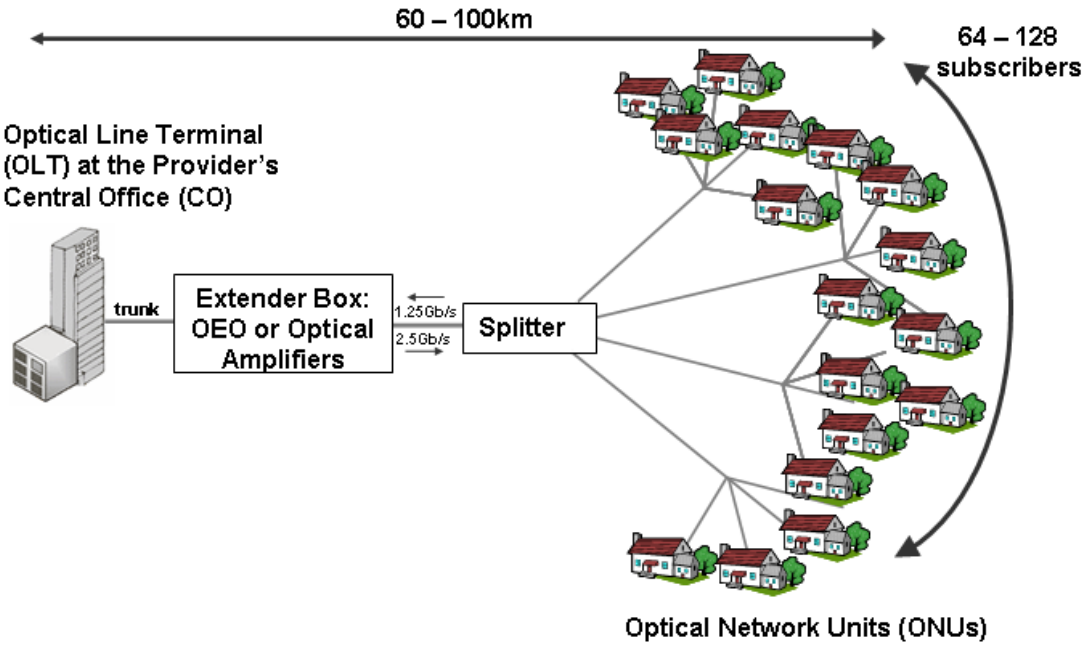

Figure 2.12: Extended Reach GPON.

2.5.3 Amplifiers in Passive Optical Networks

Due to the burst mode nature of TDMA (section 2.3.2) in the upstream the OEO repeater implementation can lead to erosion of the burst mode preamble, meaning that optical amplification may be desirable. In addition the amplifier will need to adjust its gain fast enough when packets with different DC levels pass through it in order to output packets with uniform signal amplitude.

The choice of wavelengths in the GPON standard clearly precludes erbium based fibre amplification leaving SOAs and Raman based amplification as solutions [31]. InGaAsP SOAs are a less expensive option than Raman amplifiers and these devices can be designed for use across the bands required by the standard through varying their composition. There has been much recent interest in increasing the loss budget of GPON [32, 33]. These optical link budgets are determined by the

vendor's active components within the system. Class B+ GPON systems offer a maximum loss budget of 28dB allowing a 32 way split and a 20km trunk loss. This thesis shows the improved loss budget of GPON through the introduction of an SOA.

2.6 Conclusions

This chapter has introduced the key components of an optical communications system and Passive Optical Networks as an architecture for providing last mile connectivity. An amplifier can be inserted into the PON in a bid to extend the reach of the network to enable more users provision from a single OLT and to provide broadband access to more rural locations. Semiconductor amplifiers can be designed to operate at either wavelength of this standard and so can be considered a viable solution for PON reach extension.

Chapter 3

Background Theory

3.1 Light Material Interactions

The dynamics of a semiconductor amplifier (as well as lasers and detectors) are dictated by the distribution of electron-hole pairs, 'carriers', within the conduction-band, the valence-band and their interaction with the incident light upon them. Three general mechanisms are used to explain the interaction between the carrier distributions of the optical semiconductor device and the light incident upon it: absorption, spontaneous emission and stimulated emission.

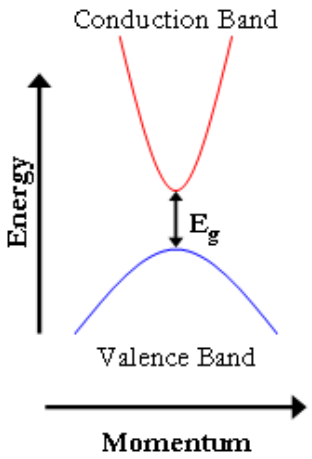

Figure 3.1: Diagram of local energy levels around (direct) material band gap (E_g).

A photon, with energy greater than the bandgap (E_g), incident upon a material may cause excitation of a carrier to a higher energy state across the bandgap

(Figure 3.1), whose energy is given by:

$$E_g = E_c - E_v = h\upsilon = \frac{hc}{\lambda} \tag{3.1}$$

where E_c and E_v are the energies in the conduction band and valence bands respectively, h is Planck's constant, υ and λ are the frequency and wavelength of the incident photon and c is the speed of light in a vacuum.

The absorption process (Figure 3.2(a)) results in an carrier being elevated to a higher (excited) state by the photon energy, annihilating the photon in the process. This carrier can relax to its unexcited state and emit light through one of two decay processes.

The first relaxation process, whereby the carrier may decay of its own accord if left unperturbed in its excited state, is known as spontaneous emission (Figure 3.2(b)). This carrier will stay in the higher state for a period of time known as the (average) carrier lifetime of the excited states (τ) and is dependent on the material of the device. When this carrier returns to the lower level, the energy difference is emitted in the form of a photon with random phase, direction and polarisation. Its wavelength is determined by the energy difference of the two states involved in the carrier's transition (Equation 3.1).

Secondly, a carrier may be induced to make a transition to a lower energy level. Here the presence of a photon which has the correct wavelength, i.e. energy close to that of the electronic transition in the atom, causes the excited carrier to decay to a lower energy state emitting the energy as a photon (Figure 3.2(c)). This is known as stimulated emission. This second photon has the same phase, polarisation, direction and energy as the incident photon; which is the mechanism that allows for the amplification of light signals.

In order to produce optical amplification, stimulated emission must be the dominant process between the incident photons and the carriers in the material. To sustain this process, a surplus of carriers are required in the conduction band which are capable of dropping back across the bandgap and releasing their energy in the form of light. This situation is called a 'population inversion' as normally the valence band is much more heavily populated than the conduction band. To create this population inversion, external energy is applied to the active region through optically or electrically pumping the material to its transparency point or threshold point at the wavelength of interaction. When at transparency (where

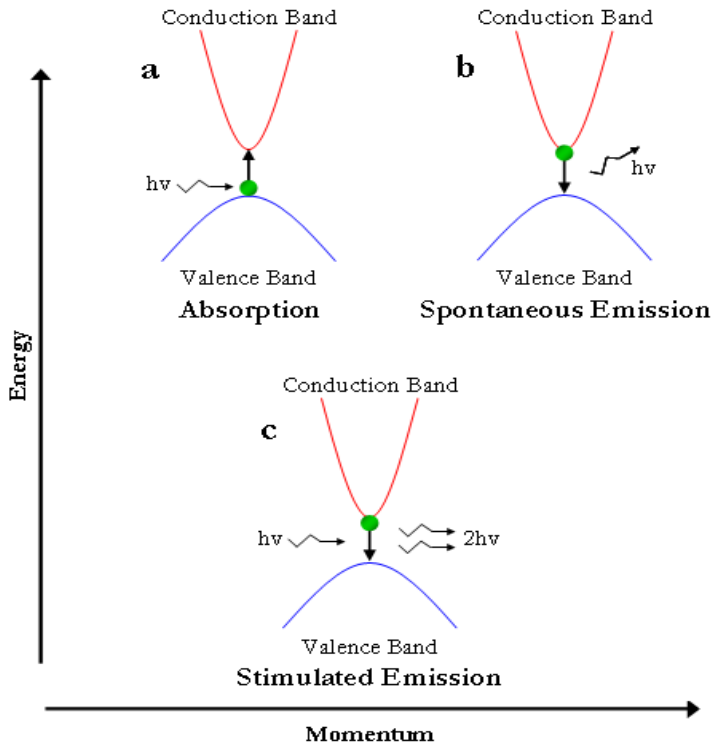

Figure 3.2: Light-Material Interaction Concepts (a) Photon Absorption, (b) Spontaneous Emission and (c) Stimulated Emission.

gain is equal to loss) the carriers are equally likely to be excited to the conduction band by absorption as they are to be returned to the valence band by stimulated emission, regardless of the input signal powers involved.

In early lasers, optical pumping was achieved by external light sources and other laser systems. A more practical method of achieving the desired population inversion in semiconductor laser and optical amplifier devices is to 'pump' with an electric current. Through this method, the current is converted directly into energetic electrons and holes as it passes through the body of the component. Successful creation of a population inversion requires knowledge of how the carriers flow through the device structure.

3.2 Basic SOA structure

This section illustrates certain structural constraints which must be considered in the design of SOAs in order to maximize their efficiency. The confinement

of the carriers and the optical signal through the device depend considerably on the physical dimensions and material compositions of the structure.

3.2.1 Energy Confinement of Carriers

In order to create a useful population inversion, the excited carriers must be confined in energy and in space to allow optical signals to be amplified efficiently. It is not enough to simply sweep carriers through a device as they will have little chance to recombine across the band gap to produce light. In reality this is achieved through the creation of an electrical barrier which restricts the carrier movement in the material; the carriers build up, spend longer in proximity, thus increasing probability of recombination [34]. A pn-junction is a convenient system for creating this energy barrier to establish a population inversion of the energy levels (Figure 3.3).

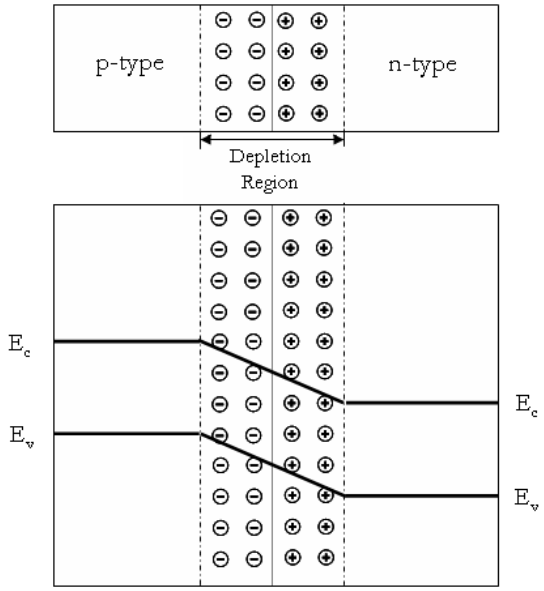

Figure 3.3: pn-junction carrier migration and energy diagram of the resulting depletion region.

P-type (positive) and n-type (negative) semiconductors are created by introducing a dopant species with the correct choice of impurity. When utilizing a dopant material with fewer valence band electrons than the host material, a p-type semiconductor is created as the lack of electron is considered to be a positive 'hole' carrier. Choosing a material with an extra valence band electron will result in a n-

type semiconductor due to the additional negative charge from the extra electron. At the junction interface, carriers from the two materials diffuse a short distance into the other; holes from the p-type migrate into the n-type and electrons from the n-type into the p-type material. The donor species are left behind when the carriers diffuse, thus there is a net charge in the lattice generating a field opposing the carrier migration. This diffusion of electrons and holes produce a 'depletion' region which is devoid of free carriers due to their recombination. In optical devices the depletion region is more commonly known as the 'active region' because it is in this section of the pn-junction that light-material interactions are most likely, as both carrier types are present under forward bias conditions. Applying a forward bias reduces the built-in field resulting in a diffusion of carriers into the depletion region, the positive and negative carriers recombine generating photons by spontaneous or stimulated emission. Figure 3.4 shows the basic SOA structure.

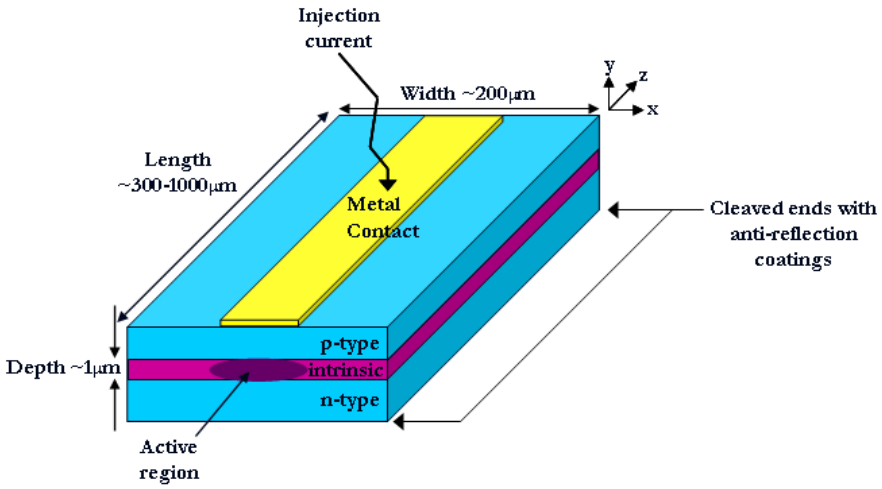

Figure 3.4: Basic SOA Structure.

3.2.2 Spatial Confinement of Carriers and Optical Signals

In designing an efficient semiconductor laser or amplifier the spatial confinement of the material being used is as important a consideration as the energy confinement. The injected electrons and holes require to be constrained in such a way to efficiently pass through the energy band structure. A method to improve the efficiency of the recombination process is to use materials of different band gap energies; i.e. a heterojunction [35]. In this case the active region is a thin layer

of material between two layers of a higher band gap material of the same lattice constant. If the active region is designed with a smaller band gap than the p-type and n-type sections then the carriers will tend to collect in the active region further confining their movement and aiding the recombination process [10].

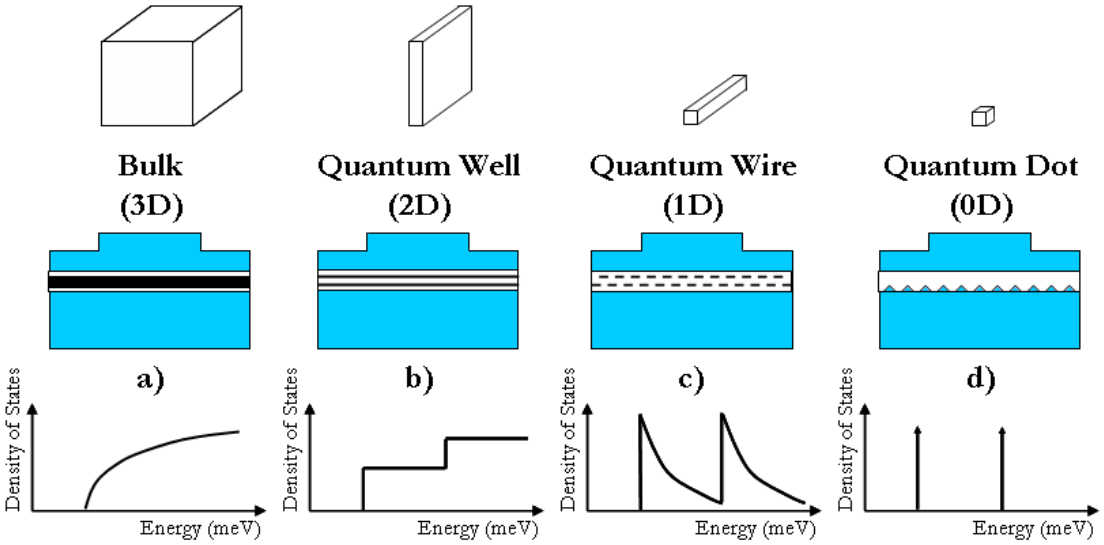

Figure 3.5: Density of states for (a) bulk (3D) (b) quantum well (2D) (c) quantum wire (1D) (d) quantum dot (0D).

Figure 3.5 shows the schematic structures for bulk (three dimensional i.e. the electrons are free to move in all directions), quantum well (two dimensional), quantum wire (one dimensional) and quantum dot (zero dimensional) and their corresponding carrier density of states (DOS). The active region can be quantum confined in 0, 1 or 2 dimensions where they are scaled to near the de Broglie wavelength (material dependent, ∼20nm). The electrons and holes try to occupy the lowest possible energy positions in the conduction and valence bands of the material and are limited by quantum mechanics in the maximum amount of carriers allowed for any given energy. This is called the density of states and is defined as the available number of states N per energy per unit volume. The electronic and optical properties of a semiconductor structure are strongly dependent on its density of states for the carriers. The use of these different structures as active regions in semiconductor amplifiers results in different performance characteristics because of the differences in their density of states as shown in Figure 3.5. For 0-dimensional quantum dot it can been seen that the density of states, and the resulting spectrum of optical transitions, is a series of discrete energy levels in

contrast to the continuum of states obtained for a bulk (3-dimensional), quantum well (2-dimensional), or a quantum wire (1-dimensional).

The discrete energy levels illustrated for the quantum dots assumes that all dots are identical and that there are no interactions among them. In reality the spectrum for the quantum dot does not appear as a delta function due to homogeneous broadening due to the finite lifetime of the excitation and inhomogeneous broadening in which there is broadening of the emission spectrum due to size variations of the dots [36].

Bulk SOAs

Various structures of bulk SOAs are shown in Figure 3.6. The first (Figure 3.6(a)) is the oxide stripe structure, an example of a structure which has poor lateral confinement of the carriers, thus an uneven population inversion throughout the active region. This is known as a 'gain guided' approach. The carriers are injected through the gap in the dielectric layer and are free to diffuse as they travel towards the active region leading to a spatial variance in the carrier distribution in the active region. Outwith this region the light is absorbed quickly by the regions failing to achieve population inversion causing low efficiency. A buried ridge structure (Figure 3.6(b)) attempts to force the injected carriers through the mesa ridge in an effort to spatially confine them until they reach the active region.

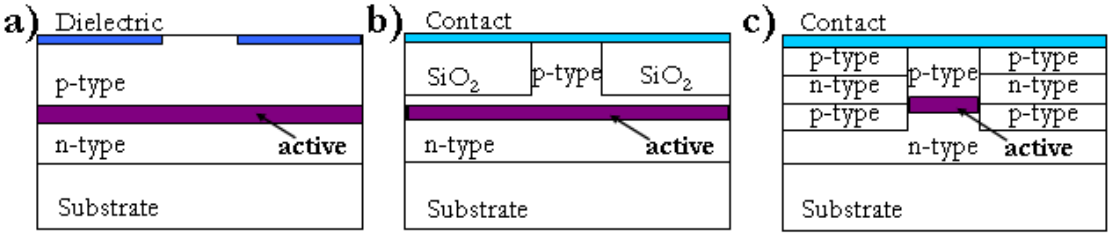

Figure 3.6: Semiconductor Amplifier Structure Evolution (a) oxide stripe structure, (b) buried ridge structure (c) buried heterostructure design.

The SiO_2 has a lower refractive index to aid the optical guidance of the device and assists to confine the light to the mesa by blocking the carriers. However a thin layer of material remains above the active region following the etching process along which some of the current is able to diffuse away from the optical mode reducing the efficiency of the structure. The third structure (Figure 3.6(c)) is the buried

heterostructure design. This is an improvement on the buried ridge structure as the mesa is etched all the way through the active region to the n-type material below. A thin pn-junction is grown either side of the active region so that when the mesa is forward biased these two pn-junctions are reversed biased thus forcing the carriers into the active region. If the active region has a higher refractive index than the material surrounding it, then the buried heterostructure will optimally confine the optical mode and the injected current. The bulk SOAs modelled and tested in this thesis are based on the buried heterostructure design.

Multiple Quantum Well SOAs

The active region of SOAs can be grown in layers a few nanometers thick which allow electrons and holes to be confined to two dimensions i.e. a quantum well is formed. This quantisation of energy levels results in sub-bands within the semiconductor bands, the density of states become step like (Figure 3.5(b)) which can lead to improvements in the active layer performance. Multiple Quantum Well (MQW) active regions are created by growing many layers separated by higher bandgap material and have been shown to improve the performance of SOA characteristics [21]. This modified density of states results in several improvements in characteristics such high saturation power which arises in part due to the lower confinement factor and high gain at low currents compared to bulk [36].

Quantum Dot SOAs

Self-assembled quantum dots are manufactured by growing a semiconductor on a substrate to which it is strongly lattice mismatched. When the material is deposited slowly, one or two monolayers (the so-called wetting layer) are formed. As the number of deposited layers increases, the strain increases and the atoms form islands to relax the lattice strain. The sample is capped with barrier material transforming the islands into quantum dots that can confine the carriers in all three spatial dimensions.

As shown in Figure 3.5 the theoretical width of the electron energy distribution of quantum dots is zero, implying that the electrons in those structures are distributed in certain discrete energy levels and the energy distribution width is fundamentally independent of temperature. In reality a certain width in the electron energy distribution exists; however the temperature dependence is expected

to be much smaller compared to bulk or MQW [37].

Reducing the density of states increases the maximum material gain and differential gain, the quantum dot is at least 2-3 orders higher than MQW SOAs [36]. Qdot SOAs have been shown to have ultrafast response (up to 7 times faster gain recovery than bulk or MQW SOAs [4]), feature larger saturated gain at the same current density [38] and have a broader gain bandwidth [39].

3.2.3 Separate Confinement Heterostructures

Separate Confinement Heterostructure (SCH) layers are used in bulk and MQW devices to increase the amount of high index material and hence adjust the confinement factor. SCH are illustrated in Figure 3.7 and consist of a thin layer of passive material which has a refractive index (n_2) between that of the active material (n_1) and the surrounding blocking layers (n_{p-type}, n_{n-type}). The confinement factors can be modified by varying the thickness and composition of the SCH thus polarisation insensitivity can be achieved. More detail can be found in section 4.2.4.

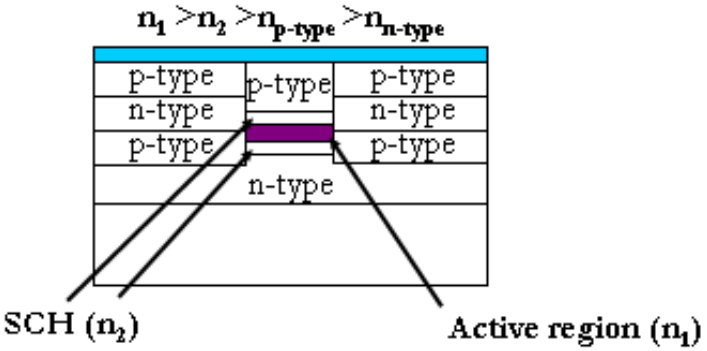

Figure 3.7: Schematic of SOA with an SCH region.

3.2.4 Modal Confinement

Figure 3.8 illustrates the optical modal confinement in a buried heterostructure SOA with SCH layers, similar to that of Figure 3.7. The mode can be seen to be centered in the high refractive index active region.

The modal confinement factor (Γ) can be defined as the fraction of the optical power which travels in the waveguide core:

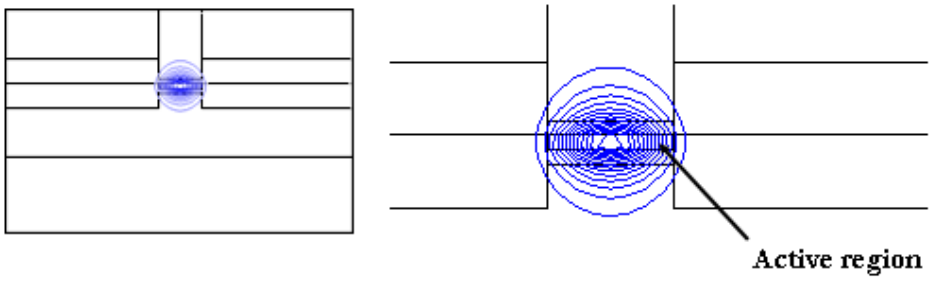

Figure 3.8: Modelling of SOA mode

$$\Gamma = \frac{\int\limits_{active\ region} |E|^2 dA}{\int\limits_{all\ space} |E|^2 dA} \tag{3.2}$$

If the waveguide is sufficiently narrow it will only support a single transverse mode, transverse electric (TE) where the electric field is polarised along the active region plane or transverse magnetic (TM) where the magnetic field is polarised along the active region plane.

3.2.5 Angled Facets

Reflections along the transmission path which are coupled back into the active cavity of an SOA cause spectral distortion [40] as they are captured by the guiding structure and amplified during multiple passes within the gain medium. In order to provide a smooth gain spectrum, it is necessary to reduce the effective reflectivity of the amplifier facets [41].

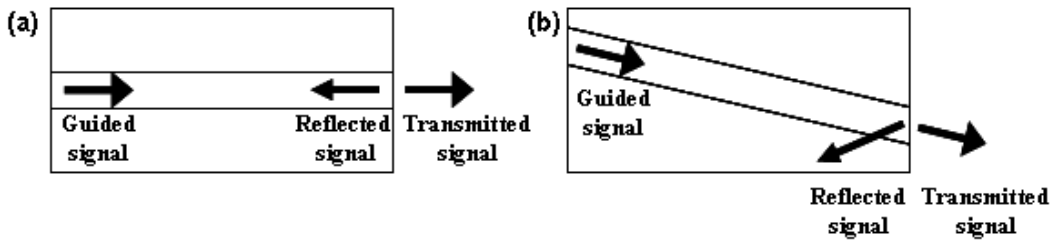

Figure 3.9: Direction of reflected signal at (a) normal cleaved facet and (b) angled facet

If the facet is perpendicular to the direction of propagation (Figure 3.9(a)) reflections will be produced which are directed straight back into the active medium

of the amplifier. Figure 3.9 (b) illustrates tilting the facet of the amplifier from the normal to the propagation direction reflects light away at a greater angle than the waveguide structure can accept and thus prevents it re-entering the active region of the SOA. Angled facets are achieved during fabrication by orienting the waveguide structures at an angle to the cleavage plane of the device during lithography.

3.2.6 Lateral Guide Tapers

The active region of an SOA has a small cross section thus the optical mode is tightly confined. Introducing tapered sections to the gain region alters the mode spot size as it propagates [42] in order to maximise coupling between the active region and the input and output optics. Through the introduction of tapers as illustrated in Figure 3.10 the amplifier can accept a larger diameter mode. The device is cleaved perpendicular the the straight taper extensions to ensure no impact to the adiabatic taper through cleaving. Lateral tapers combined with angled facets leads to a reduction in the effective facet reflectivity.

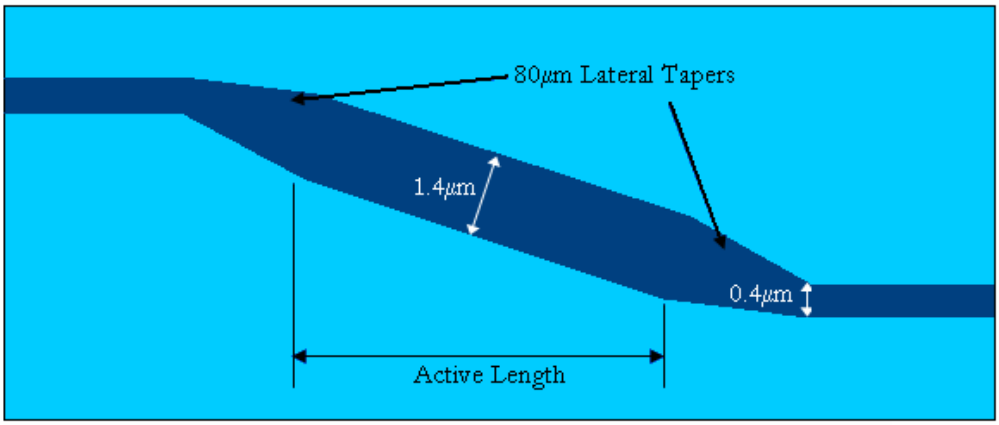

Figure 3.10: Top-down view of angled facet SOA with lateral tapers to provide mode-size control

3.3 SOA Characterisation Parameters

Once the SOA has been designed and fabricated as outlined in the previous section it is essential to be able to measure the performance of the device against other SOAs. This section covers the major parameters used to characterise the

efficiency and overall performance of the SOA; gain (G), saturation output power (P_{sat}), optical bandwidth, noise figure (NF) and polarisation dependence. The carrier dynamics are detailed in section 3.4.

3.3.1 Gain

In a semiconductor medium the time taken for the carriers to reach equilibrium after a perturbation, the intraband relaxation time, is in the order of femtoseconds thus it is reasonable to consider that there is only one mode in the output i.e. it is homogeneously broadened. The carrier and photon densities can be modelled using rate equations [43]. The rate of change of the carriers within the conduction band is given by:

$$\frac{dn}{dt} = -\frac{n}{\tau_c} - \Gamma A_g(n - n_0)\frac{I}{h\upsilon} + \frac{J}{ed} \tag{3.3}$$

where n is the conduction band carrier (electron) population, n_0 is the carrier density at transparency, τ_c is the (average) carrier lifetime of the excited states, Γ is the modal confinement factor (the proportion of the optical mode in the active region), A_g is the differential gain cross-section, I is the optical beam intensity, h is Planck's constant, υ is the frequency of light, J is the injected current density, e is the electronic charge and d is the depth of the active region. The first term on the right represents the recombination due to spontaneous emission with a lifetime of τ_c, the second term is recombination due to stimulated emission and the third term is the *addition* of carriers in the conduction band due to the applied bias current.

Equation 3.3 does not define optical gain, merely the carrier movements within the conduction band. To define gain, first the rate equation for the photon density within the SOA active region should be considered:

$$\frac{dI}{dz} = \Gamma A_g(n - n_0)I - \alpha I \tag{3.4}$$

where Γ is the modal confinement factor of the active region, A_g is the differential gain, n is the conduction band carrier (electron) population, n_0 is the carrier density at transparency, I is the optical beam intensity and α is the waveguide loss coefficient.

The steady state solution of Equation 3.3 can be found and substituted into

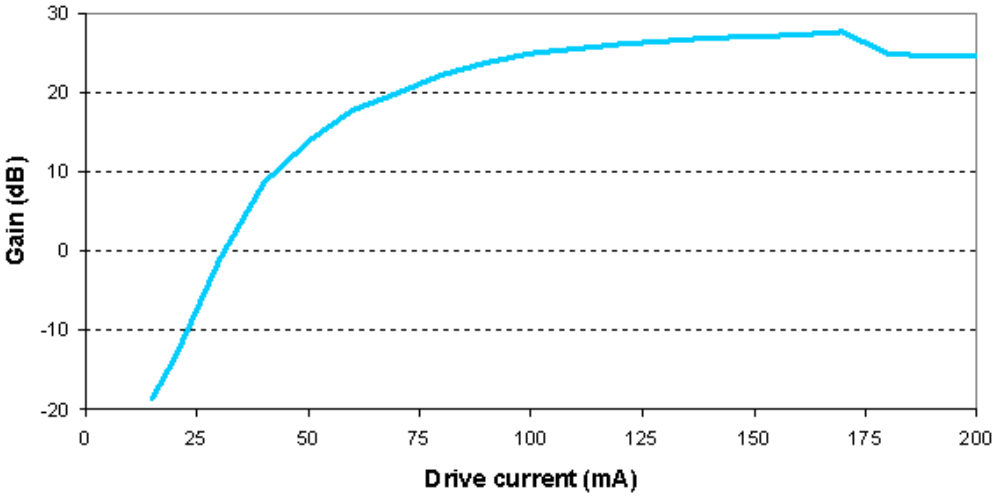

Figure 3.11: Measured gain versus drive current for a bulk InGaAsP active region SOA at 1530nm.

Equation 3.4 to give:

$$\frac{dI}{dz} = I(\frac{\Gamma(A_g(\frac{\tau_c J}{ed} - n_0))}{1 + \frac{I}{I_s}} - \alpha) = I(\frac{\Gamma g_0}{1 + \frac{I}{I_s}} - \alpha) \tag{3.5}$$

where g_0 is the gain coefficient, and I_s is the light saturation intensity (see section 3.3.3).

Assuming I $< I_s$, the emitted power can be found by integrating Equation 3.5 over the length (L) of the amplifier to give:

$$P_{out} = P_{in} exp((\Gamma g_0 - \alpha)L) \tag{3.6}$$

The SOA optical gain can be obtained by rearranging Equation 3.6:

$$G = \frac{P_{out}}{P_{in}} = exp((\Gamma g_0 - \alpha)L) \tag{3.7}$$

It can be seen from Equation 3.7 that the gain in an SOA can be increased ($\uparrow$ G) by increasing the material gain ($\uparrow$ g_0), increasing the device length ($\uparrow$ L), increasing the confinement factor ($\uparrow$ Γ) or decreasing the internal loss ($\downarrow$ α). Figure 3.11 shows the typical gain characteristic of an SOA as the drive current is increased.

3.3.2 Optical Bandwidth

The gain of an SOA is not the same for all frequencies of an input signal. This is more commonly known as the amplified spontaneous emission (ASE) spectrum of the amplifier and a typical bulk SOA characteristic is shown in Figure 3.12. It can be seen that the gain peak wavelength shifts towards the shorter wavelength as the injection current, and therefore the carrier density, increases. This is due to band filling. Figure 3.12 also shows the gain increases with bias up to 150mA after which point the gain cannot be increased by further increasing the bias. When the drive current is increased to 200mA the SOA blocking structure begins leaking current and the electrical confinement begins to break down thus reducing efficiency.

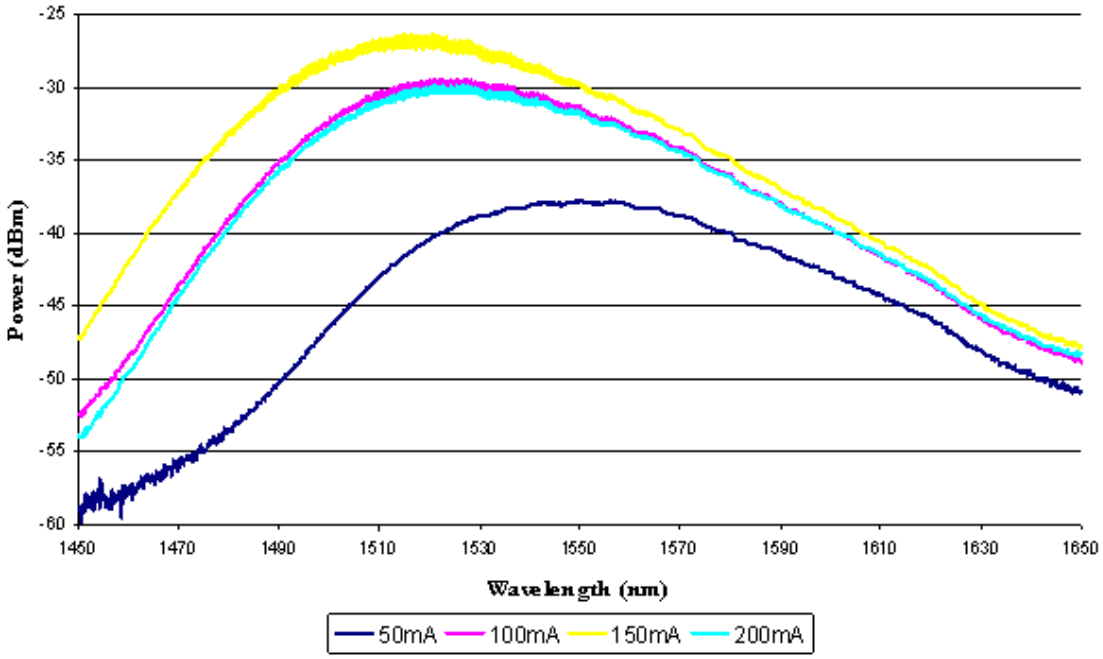

Figure 3.12: Measured ASE spectra at different bias currents for a bulk InGaAsP active region SOA

3.3.3 Saturation Output Power

The gain of an SOA is not only a function of applied bias current but is also modulated by the optical signal passing through the active region of the SOA.

I_s, the optical saturation intensity introduced in (Equation 3.5), is defined as the optical intensity required to halve the gain coefficient and is expressed as:

$$I_s = \frac{h\upsilon}{\tau_c A_g} \tag{3.8}$$

In practice this saturation is the limitation of the achievable gain in the SOA [44]. It is caused by the stimulated emission process removing the carriers from high energy states faster than they can be replenished by the injected current, depleting the population inversion thus curtailing the gain.

This saturation intensity is related to the cross sectional area of the device thus it is not ideal for device characterisation comparisons. A more useful and comparable parameter is known as the saturation output power (P_{sat}) which is the point where the device gain is reduced by 3dB (Figure 3.13) [45]:

$$I_s = \frac{G_0 - 2}{G_0 In(2)} P_{sat} \tag{3.9}$$

where G_0 is the small signal gain value.

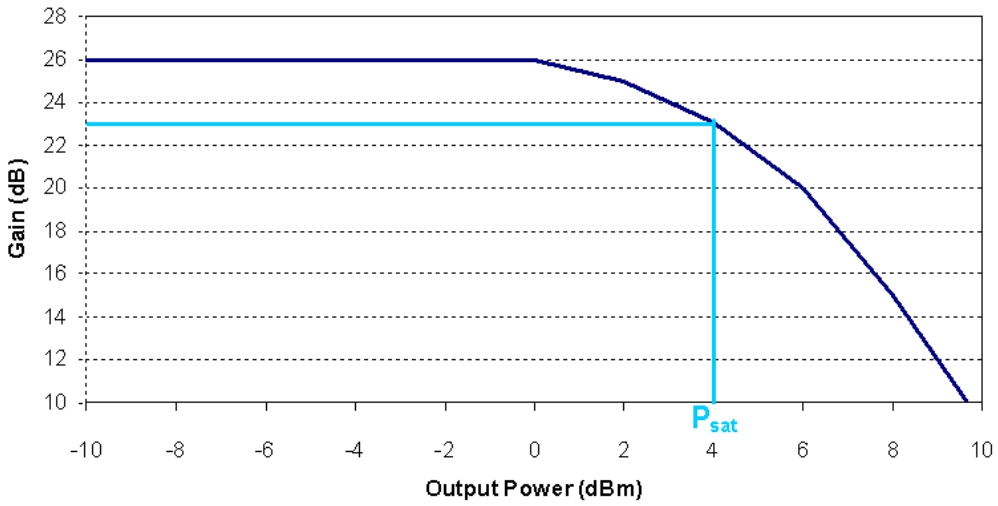

Figure 3.13: Typical SOA saturation characteristics measured on a bulk InGaAsP active region SOA at 100mA.

Saturation of the gain will occur when the total spontaneous emission power approaches P_{sat}. The gain of an SOA is limited to around 40dB for realistic values of P_{sat}. In general, the maximum gain will increase with increasing output power and can be increased through decreasing the gain bandwidth. Gain saturation

causes a shift of the gain maximum towards longer wavelengths as gain saturation means reduction of the carrier density at a given injection current.

3.3.4 Noise

The noise generated by the active medium of an SOA is caused primarily by amplified spontaneous emission (ASE). As outlined in section 3.1 the spontaneously emitted photons in a semiconductor are in the same frequency range as the input signal but they are random in phase and direction. In an SOA the spontaneously emitted photons that follow in the direction of the information signal are amplified by the active medium. As they are randomly generated, they do not contribute to the information signal but generate noise within the signal's bandwidth. The signal wavelength beats with the ASE components and the ASE beats with itself to produce signal-spontaneous and spontaneous-spontaneous beat noise components at the receiver.

The noise performance of an optical amplifier can be characterised by the noise figure (NF). The noise figure of a device is defined as the reduction of signal to noise ratio (SNR) caused by the presence of the device in the system:

$$NF = \frac{SNR_{in}}{SNR_{out}} \tag{3.10}$$

Assuming that the input signal is shot noise limited and $G >> 1$, then the noise figure of the device can be expressed as [43]:

$$NF = 2n_{sp}\chi + \frac{n_{sp}m_t\Delta f}{< n_{in} >} \tag{3.11}$$

where the first term on the RHS is due to signal-spontaneous beat noise and the second term is due to spontaneous-spontaneous beat noise. n_{sp} is the population inversion parameter, χ is the increase in ASE caused by non zero facet reflectivity, m_t is the number of optical modes in the amplifier guide (there are two modes, TM and TE, for a single mode waveguide), Δf is the ASE noise bandwidth and $< n_{in} >$ is the average number of photons injected into the amplifier per second.

The parameters defining the noise figure in Equation 3.11 are difficult to measure and therefore of little practical use. Equation 3.11 is rearranged [43] to give the noise figure for one polarisation state which allows the noise performance of an SOA to be determined experimentally by measuring the gain and the ASE

spectral density at the wavelength of the signal:

$$NF = \frac{2P_{sp}}{h\upsilon(G-1)\delta\upsilon} \tag{3.12}$$

where P_{sp} is the ASE power in a single polarisation state, h is Plank's constant, υ is the optical frequency, G is the signal gain and $\delta\upsilon$ is the optical noise bandwidth.

3.3.5 Polarisation Dependent Gain (PDG)

In general the optical fibre installed in an optical communications system is not polarisation maintaining. Therefore it should be assumed that the polarisation state in a device is not known, thus many applications require SOAs to be polarisation insensitive over their designed wavelength range. Polarisation dependence of an SOA's gain profile is dependent on its manufacture and is demonstrated in the differing modal confinements and energy band structures of the TE and TM modes of the waveguide. Section 3.3.1 introduced the confinement factor (Γ) and the gain coefficient (g_0), these are related to definable physical parameters within the device. In general when a device is designed and fabricated the confinement factor of the TE and TM polarisation states are not equal with the TE usually being more tightly confined in the active region.

PDG in Bulk SOAs

Figure 3.14 shows two schemes for achieving polarisation insensitivity in bulk material. In Figure 3.14 (a) the confinement factors and the material gains for both polaristion states are equal through the square cross sectional unstrained symmetric core. The limitation of this symmetric approach is in mass scale production as the fabrication tolerances are very fine. The mesa has to be etched to a width of around 500nm to match the layer thickness to achieve polarisation insensitivity. This is difficult to achieve reliably across a wafer but is feasible in the fabrication of a small number of devices. The second approach for achieving polarisation insensitivity is using a strained, asymmetric core to balance the effects of mode confinement and material gain as shown in Figure 3.14 (b). The rectangular core causes the TE polarisation confinement coefficient to be greater than that of the TM mode. Tensile strain is placed upon the crystal lattice by choosing the mate-

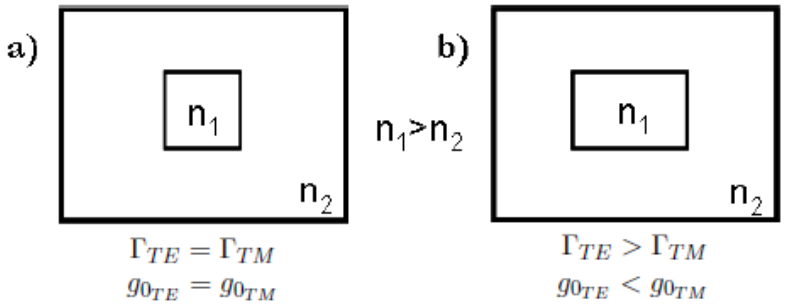

Figure 3.14: Polarisation insensitive SOAs (a) symmetric unstrained core (b) asymmetric strained core designs.

rial composition so that there will be a mismatch in the lattice constant relative to the substrate material. If the appropriate amount of strain is applied then the gain difference will be balanced resulting in polarisation insensitive operation.

PDG in Quantum Confined SOAs

Polarisation independence in quantum well and quantum dot SOAs is not as straightforward as that in bulk SOAs as the gain provided by the quantum structures is primarily polarisation sensitive, requiring strain to be applied in order to achieve polarisation insensitive material gain [46].

Different optimisation processes have been used to increase the polarisation independence in MQW devices. One method [47] assumes the gain for TE and TM radiation occur in the same part of the active region, and the MQW material as a whole is designed to give polarisation independent gain. This is achieved by the use of barriers and wells of different strain directions. Another approach employs tensile and compressively strained quantum wells grown alternatively providing gain separately for the two polarisation states [48]. Qdot SOAs have been designed to output polarisation independent gain through the introduction of tensile-strained side-barriers surrounding high aspect ratio columnar quantum dots [49].

3.4 Physics of Carrier Dynamics

The terms defined in section 3.3 are all measurable parameters using CW signals and measurement techniques. This section investigates the carrier dynamics in semiconductor devices. It has been shown in section 3.3.1 that the gain of an

SOA is supplied by optical transitions between valence and conduction bands. In order to distinguish the different physical processes affecting the free carriers in the SOA it is necessary to upset the population inversion in order for there to be a recovery. This can be achieved by considering the effects of an optical pulse input signal to the carrier distribution.

There are two important regimes in the response, the long-lived carrier density change that results from stimulated emission/absorption, ($\tau \sim 100$ps), as well as various short-lived subpicosecond dynamics. The long lived responses are due to interband relations and involve the exchange of carriers between the conduction band and the valence band which affects the carrier density. The subpicosecond dynamics are intraband relations which do not change the carrier density but change the energy distribution of the carriers in the conduction and valence bands.

The long-lived response can be observed experimentally using pump-probe measurements with pulses 10 to 25ps in duration [3, 50]. However when the pulse duration is reduced, the resolution of the measurement is increased resulting in responses with life times on the order of a few picoseconds being observed around zero time delay [2,3,51]. These responses have been explained phenomenologically, and have been attributed to two-photon absorption, carrier heating, spatial and spectral hole burning, gain dispersion (spectral artifacts), and the optical Stark effect. These additional amplitude and index dynamics perturb the desired ideal instantaneous step response for switching and wavelength conversion on short time scales, and are the focus of modern pump-probe studies.

3.4.1 Intraband Effects

Two Photon Absorption

Two-photon absorption (TPA/2PA) is a non-linear absorption where two photons cooperate in exciting an electron to an energy level equal to the sum of the energies of the two photons [52]. The basic theory for this process was formulated by Maria Goeppert-Mayer in 1931 [53], and its first experimental observation was reported by Kaiser and Garrett in 1961 [54] after the development of the laser. Bechtel and Smith [55] initiated further theory and experimental characterization of some common semiconductor materials.

In semiconductors it is possible to have TPA from a single light pulse with angular frequency ω if twice the photon energy, $2\hbar\omega$, exceeds the semiconductor

energy gap E_g. As two-photon absorption is a nonlinear optical phenomenon, the TPA coefficient can be expressed in terms of nonlinear optical susceptibilities [55].

This process occurs with significant rates only at high optical intensities. The TPA coefficient α_2 is proportional to the optical intensity squared:

$$\frac{dI}{dz} = \alpha_1 I + \alpha_2 I^2 \tag{3.13}$$

where I is the intensity of the electric field and α_1 is the linear absorption coefficient. Thus, it is detrimental to the performance of devices that involve the use of short pulses and large optical intensities.

Spectral Hole Burning

Spectral hole burning (SHB) is a contributor to nonlinear gain (and absorption) of semiconductor materials that is fundamental to the material itself and is less dependent on device structure. This occurs when stimulated transitions preferentially deplete or create carriers between specific energy levels, not across the entire gain or absorption spectrum. In a semiconductor material, this implies that stimulated transitions tend to distort i.e. burn a hole in the Fermi distribution.

In the gain region, an optical beam with centre wavelength, λ_1, will stimulate emission, but will tend to deplete the carrier density over a limited range. In the absorption regime, an optical beam generates carriers over only a limited energy range, bleaching a hole in the absorption. At the transparency point, where there are no net stimulated transitions, there is no spectral hole burning. The nonlinear change in gain due to spectral hole burning should recover quickly, on a sub-ps timescale, as a new thermalised distribution is achieved via carrier-carrier scattering. At high carrier densities, the carrier-carrier scattering time constant has been measured to be 100fs or less [56].

Carrier Heating

Carrier heating is another nonlinearity that is fundamental to the semiconductor gain medium illustrating that carrier temperatures may be different from the lattice temperature. Heating the carrier distribution reduces the gain of the active region. The two predominant physical processes that contribute to carrier heating are stimulated transitions and free carrier absorption (FCA) induced by

the pump signal heating the carrier distributions.

In the process of stimulated transitions, stimulated emission will remove 'cold' carriers (carriers below the average energy) from near the bottom of the band and will increase the temperature of the remaining carrier distribution. Stimulated absorption, however, can either raise or lower the temperature depending on the energy of the excited carrier. Any temperature decrease in this case would be minimal as the difference between the energy of the excited carrier and the average distribution is small.

FCA will serve to heat up the distribution in both the conduction and the valence bands. Through carrier-carrier scattering, these 'hot' carriers share their energy with the rest of the distribution thus the carrier distribution heats up.

Both of these heating processes will cause unequal changes in the electron and hole temperatures, with the electrons being heated more in each case. The heated electron and hole distributions cool to the lattice temperature on a picosecond timescale through the emission of longitudinal optical phonons [57].

The carrier distribution may also be heated by higher-order effects, such as two-photon absorption (TPA) [58], but this effect is much smaller than other heating effects in active semiconductor materials biased in the gain regime. Typically the stimulated transmission probability is orders of magnitude higher than the FCA probability. However, each FCA event changes the total energy of the distribution by almost 1eV, the single photon energy. Each stimulated transition changes the total energy by only a few meV.

3.4.2 Interband Effects

The long-lived carrier density changes of active semiconductor waveguides result from stimulated emission/absorption. These are interband effects known as the free-carrier recovery time or the interband recombination time that have a lifetime in the order of 0.1-1ns. Switching speeds in some SOAs are fundamentally limited by this free-carrier recovery time.

There are various recombination mechanisms in direct-band-gap semiconductors that contribute to carrier lifetime. Three main contributors are:

1. Non-radiative recombination in which an electron in the conduction band recombines with a hole in the valence band and the excess energy is emitted in the form of heat in the semiconductor crystal lattice.

2. Spontaneous emission in which an electron in the conduction band recombines with a hole in the valence band and a photon is spontaneously emitted.

3. Auger recombination involves the interaction of three electrons or holes. In this process, the energy released by recombination of an electron-hole pair is transferred to another electron or hole that decays through the emission of phonons.

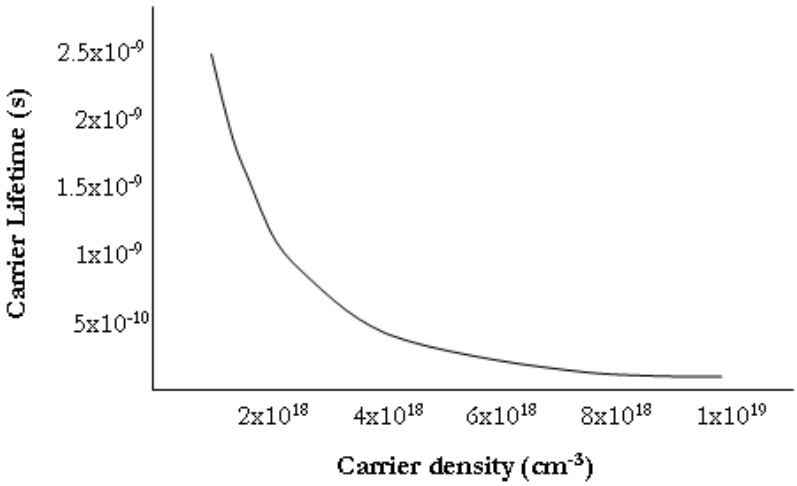

Figure 3.15: Carrier lifetime versus carrier density.

The recombination rate in absence of stimulated processes can be approximated:

$$R = A_{nr}n + B(n)n^2 + Cn^3 \tag{3.14}$$

where A_{nr} is the non-radiative recombination, B is the radiative recombination and C is the Auger recombination mechanism. Figure 3.15 illustrates the relation of these terms to carrier lifetime given the typical values [59]: $A_{nr} = 2\text{x}10^8 s^{-1}$, $B(n) = 1\text{x}10^{10} cm^3 s^{-1}$, $C = 1\text{x}10^{-28} cm^6 s^{-1}$. The carrier lifetime, τ, may be approximated by:

$$\tau = (\frac{dR}{dn})^{-1} = \frac{1}{A_{nr} + 2B(n)n + 3Cn^2} \tag{3.15}$$

Carrier densities in the range $5\text{x}10^{18}$are achievable at high bias currents.

3.4.3 Amplitude Dynamics

The ultrafast response of active semiconductor waveguides gives information that is important for the basic understanding of semiconductor material dynamics as well as for the assessment of the high-speed potential of photonic devices.

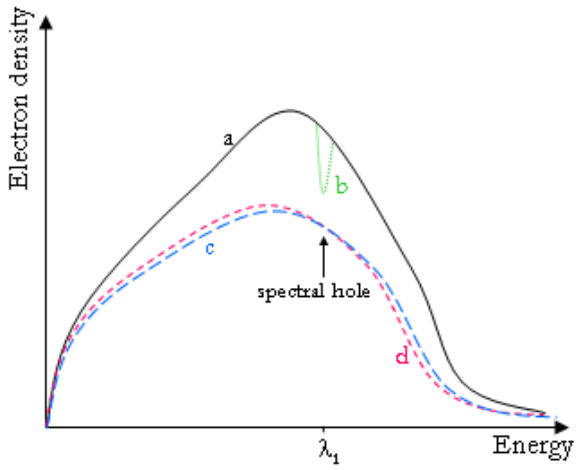

Figure 3.16: Schematic of carrier distribution (a) before and (b-d) after optical pulse injection.

Figure 3.16 gives a schematic of the carrier density changes during interaction with an optical pulse. Curve (a) depicts the unperturbed steady state distribution. When the input pulse (wavelength λ_1) interacts with the SOA at t=0 the carriers are depleted by stimulated emission in a narrow spectral range. A spectral hole is formed instantaneously reducing gain at the corresponding wavelength (λ_1) as shown in curve (b). Curve (c) portrays carrier-carrier scattering processes which washes out the spectral hole and creates a distribution with temperature higher than the steady state situation resulting in a reduced electron density curve. The electron temperature cools down to lattice temperature as shown in curve (d). When the carriers are resupplied to the SOA by the external circuitry the steady state density of curve (a) is reachieved.

The graph on the left in Figure 3.17 depicts a typical pump probe amplitude response of an SOA in the gain regime and illustrates the relative timescales of interband and intraband carrier dynamics. Section 3.4.5 explains the response of the pump probe measurements of an SOA operating in each of the absorption, transparency and gain regimes.

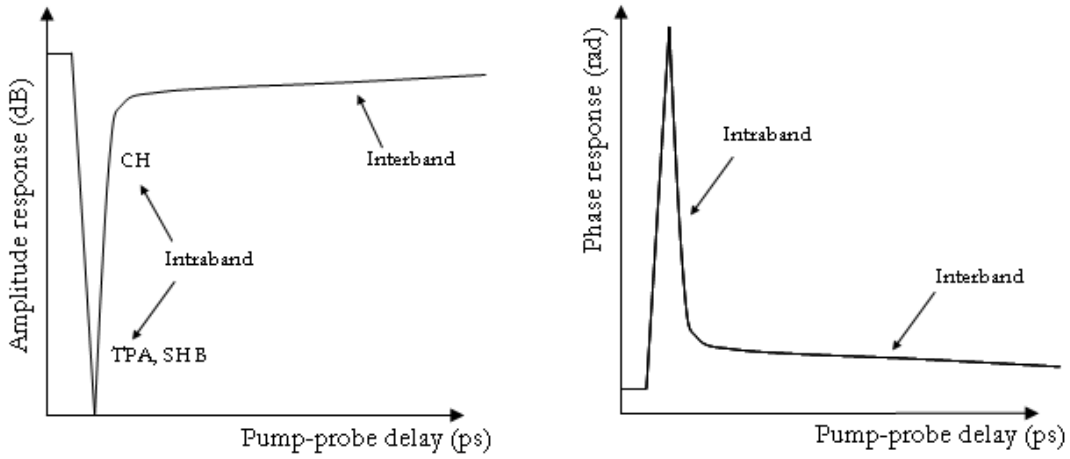

Figure 3.17: LHS depicts typical pump probe response in the gain regime revealing both intraband and interband carrier dynamics. RHS depicts corresponding phase response.

3.4.4 Refractive Index Dynamics

In semiconductor materials, gain changes have associated refractive index changes (phase changes) which influence the phase of the signal. The phase changes cause frequency chirp in lasers as well as in amplifiers amplifying short pulses, and phase effects are used to perform switching in phase-based optical signal processing schemes. While SOAs in amplification systems are generally used as a gain medium, the information on the phase of the pulses is required for predicting and mitigating the degradation due to chromatic dispersion. The integration of SOAs in interferometric all-optical switches is based on utilisation of the corresponding refractive index changes, therefore it is necessary to investigate both the gain and refractive index nonlinearities. The graph on the right in Figure 3.17 depicts a typical pump probe phase response of an SOA in the gain regime. Section 3.4.5 explains the phase response of the pump probe measurements of an SOA operating in each of the absorption, transparency and gain regimes.

The phase shift ($\Delta\phi$) of a medium is caused by changes in the refractive index (Δn) given by:

$$\Delta\phi = \frac{2\pi L}{\lambda}\Delta n \tag{3.16}$$

where L is the length of the active waveguide region. The index changes are further related to the gain changes through the linewidth enhancement factor or

α-factor [35]:

$$\alpha = -\frac{4\pi}{\lambda}\frac{\Delta n}{\Delta g} \tag{3.17}$$

where n is the refractive index and g is the gain. Rearranging Equation 3.16 for Δn and substituting into Equation 3.17 gives:

$$\alpha = -\frac{2}{L}\frac{\Delta \phi}{\Delta g} \tag{3.18}$$

The changes in refractive index and gain are opposite in sign giving a positive value of α. It is useful to define the effective linewidth enhancement factor (α_{eff} factor) [60] as it can be used to compare the qualitative behaviour of nonlinear phenomena in SOAs:

$$\alpha_{eff} = -2\frac{\Delta \phi}{\Delta ln(g)} \tag{3.19}$$

α-factor values have been reported to range from zero to 20 and above [59,61]. The variations in the reported values are largely due to the differences in the device structures and materials, the different bias current and wavelength ranges over which the measurements are made and from differences in the measurement techniques. However the reports have consistently found that the α-factor increases with bias current.

3.4.5 Review of SOA Carrier Dynamics

Numerous characterisations of SOAs have been reported in the last 20 years providing a thorough insight and understanding of the expected carrier dynamics in SOAs. The carrier dynamics in bulk, quantum well and quantum dot SOAs are of interest to determine the effect of the different degrees quantum confinement has on the carrier recovery times [62]. Section 3.2.2 outlined the consequence of the differing levels of quantum confinement in the density of states which can significantly modify the carrier dynamics from that of bulk material. This section details the pertinent results for bulk, quantum well and quantum dot devices.

Figure 3.18 shows experimentally obtained probe amplitude transmission responses from [2] for AlGaAs devices using 440fs pulses These were obtained using the pump-probe technique, explained in section 3.6.1. Similar results were

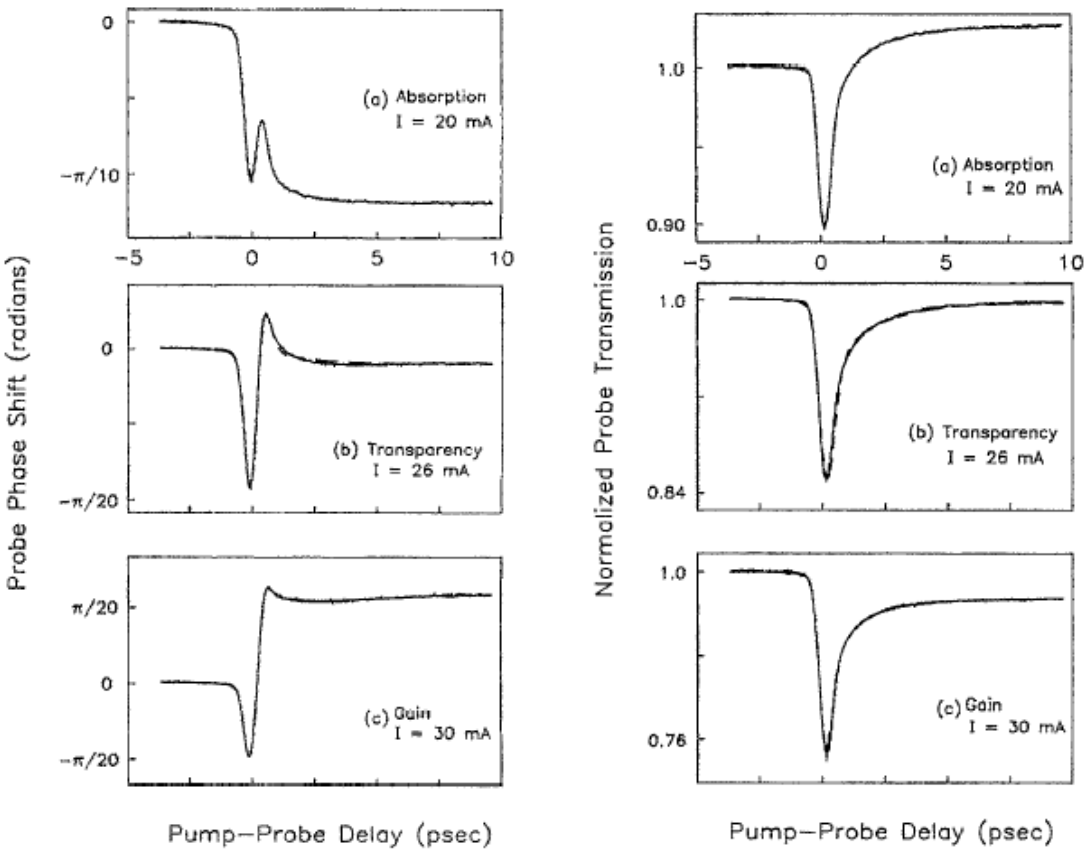

Figure 3.18: Measurements from [2] on AlGaAs devices using 440fs pulses. Change in probe phase (LHS) and amplitude transmission (RHS) versus pump-probe delay with the SOA biased (a) in the absorption regime, (b) at the transparency point, and (c) in the gain regime.

obtained on AlGaAs laser diodes in [63]. The responses fall into three regimes: absorption, transparency and gain.

When the pump energy is greater than the bandgap energy, absorption dominates over stimulated emission and so the carrier density increases due to the presence of the pump. This results in a step increase in amplitude transmission as can be seen in Figure 3.18 (a). This step increase in amplitude leads to a step decrease in phase (α is negative (Equation 3.18)).

Figure 3.18 (b) shows the transparency regime, which occurs at the precise point when gain exactly matches absorption. Here there are no carrier density changes and there is no step response.

When the pump energy is near the band-gap within the gain spectral region, stimulated emission dominates, which is known as the gain regime and is shown in Figure 3.18 (c). In this case the pump-induced stimulated emission reduces the carrier density and so the probe pulse experiences a reduction in gain. This results in an initial step reduction in amplitude transmission (step increase in the phase) which recovers (decays) as the carrier density returns to its unperturbed equilibrium state exponentially with the carrier recovery time.

The different regimes are achieved experimentally by changing the bias voltage of the device if the pump and probe photon energies lie within the gain spectrum of the SOA. For low bias the SOA is absorbing and as the bias is increased the SOA moves through transparency and into the gain regime. The three regimes are clearly seen in the plots for different injected currents.

Figure 3.19 shows measurements on bulk InGaAsP SOAs from [3] with greater resolution than Figure 3.18 thus the intraband effects can be better identified. The instantaneous decrease in phase at zero time delay (i.e. when the pump and probe overlap) is attributed to the electronic Kerr effect, the optical Stark effect and electronic Raman effects [64]. This is equivalent to TPA (section 3.4.1) in the amplitude trace as it has no measurable time constant and is only weakly dependent on carrier density and pump-probe wavelength. The ultrafast component in the amplitude measurements is attributed to spectral hole burning despite its unexpected presence at transparency. The SHB component is not expected in the phase results as the SHB is symmetric about the centre frequency so gives zero index change [4, 51].

The presence of carrier heating can be observed in all three regimes for both amplitude and phase dynamics. This can be measured with an exponential recov-

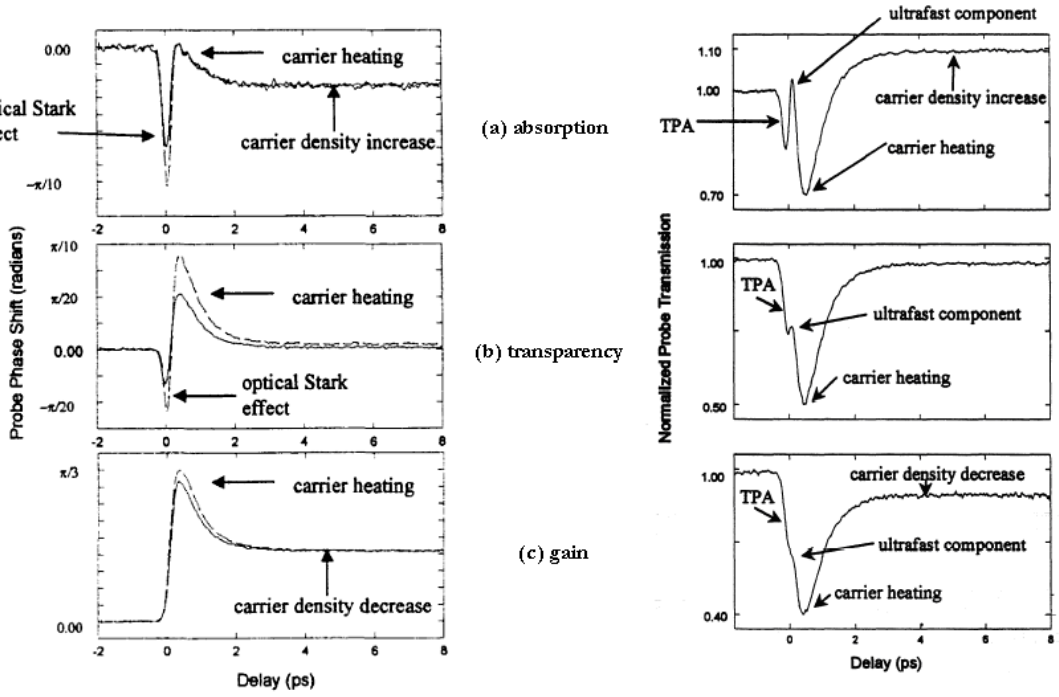

Figure 3.19: Measurements of bulk InGaAsP SOAs from [3] showing different processes attributed to the features observed for cross polarised pump-probe measurements. Co-polarised measurements are shown in the dashed line for the phase change measurements.

ery ($\tau_1 \approx$1ps) which is the most significant contributor to the intraband dynamics. As mentioned previously the negative change in amplitude in both the gain and absorption regimes leads to a positive phase change as α is negative.

Typical carrier recovery lifetimes in MQW or bulk SOAs are a few hundred picoseconds [3, 51, 65, 66] although lifetimes as short as 25ps have been measured in small active area buried waveguide SOAs [67].

Devices with Qdot active region have shown reduced carrier heating for both gain and refractive index dynamics and so it is of interest to explore the potential of Qdot SOAs for ultrafast processing [68]. Modelling results indicate the possibility of operating Qdot SOAs in a new dynamical regime, where spectral hole burning effects are used to increase the speed [69]. Experimental results presented in [70] indicate the possibility of achieving very fast relaxation times.

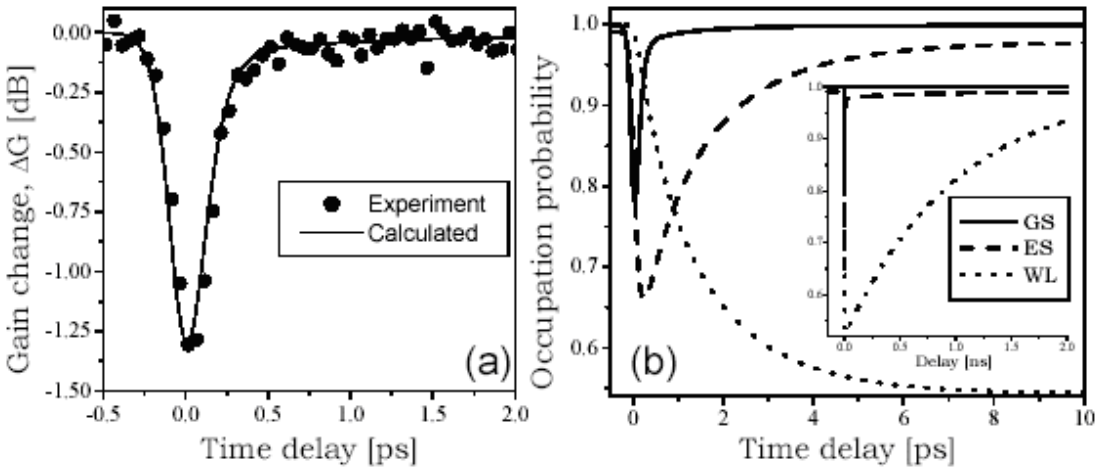

Figure 3.20: From [4] (a) Measured and calculated gain change in an InAs Qdot amplifier following short pulse excitation and (b) the corresponding calculated carrier dynamics in the dot ground state (GS), excited state (ES) and wetting layer (WL). The insert in (b) shows the recovery process on a longer timescale.

Figure 3.20(a) shows the measured (dots) and calculated (solid line) gain recovery of a Qdot amplifier. The modelling of the corresponding carrier dynamics (Figure 3.20 (b)) shows the ground state (GS) of the dot recovers on a short timescale (150fs). The carriers refilling the GS are transferred from the excited states (ES), which recover on a picosecond timescale by capture from the wetting layer (WL). The wetting layer recovers by current injection on a timescale determined by the spontaneous lifetime of the WL, in this case nanoseconds (see insert

of Figure 3.20(b)). It is thus important to realize that the dynamics of the upper energy levels of the system become important when the long timescale dynamics are considered; e.g. in the case where the amplifier is excited by a pulse train rather than a single pulse [71].

3.5 Rate Equation for the Carrier Dynamics

Having reviewed the physics of the different relaxation processes in the previous section, a set of rate equations and impulse response models can now be developed to model optical amplifier dynamics. The gain dynamics *g(t)* and the phase dynamics $\phi(t)$ can be fitted to a phenomenological model of an impulse response for the gain, Equation 3.20, and the phase, Equation 3.21 [72]:

$$g(t) = [a_0 e^{-t/\tau_0} + a_1 e^{-t/\tau_1} + a_2 e^{-t/\tau_2} + a_3\delta(t)] \otimes I_p(t) \tag{3.20}$$

$$\phi(t) = [\frac{\alpha_0 a_0}{2} e^{-t/\tau_0} + \frac{\alpha_1 a_1}{2} e^{-t/\tau_1} + \frac{\alpha_2 a_2}{2} e^{-t/\tau_2} + \frac{\alpha_3 a_3}{2}\delta(t)] \otimes I_p(t) \tag{3.21}$$

The first term on the RHS in these equations represents the interband effects (i.e. carrier depletion, $\tau_0 \approx 0.1-1$ns), the second term is associated with carrier heating (CH) ($\tau_1 \approx 1$ps) and the third term arises from intraband carrier relaxation (i.e. spectral hole burning (SHB) $\tau_2 \approx 0.1$fs). The last term is responsible for instantaneous electronic processes such as two-photon absorption (TPA) that result in gain compression and the Kerr effect for the phase response. It should be noted that the Kerr effect induces a negative phase change in contrast to all other effects that result in gain compression and hence induce a positive phase shift. The individual amplitude coefficients (a_n) and linewidth enhancement factors (α_n) depend on both the physical device parameters and the experimental conditions.

3.6 Ultrashort Pulse Measurement Techniques

The pulses used for optical communications become shorter as the bit rates get higher, thus the limitations of conventional opto-electronic detection are becoming more apparent. An alternate pulse measurement tool with a better time resolution and phase sensitivity is desperately needed. In optical communications, the need for temporal and phase characterisation is due to the impact of processes

such as chromatic dispersion in optical fibres, nonlinear effects and amplification on the electric field of a data-encoded source. The characterisation of these impairments is valuable for system design and operation. Short pulse time-domain measurements can provide the basis for a comprehensive diagnostic technology to characterise both linear and nonlinear optical properties in waveguides. Time-domain measurements have a number of potential advantages for waveguide characterisation. Femtosecond optical pulses can be viewed as delta functions in the time domain (in relation to the timescale of the measurement); time resolved measurements thus provide information about the impulse response of the waveguide. The inherent bandwidths of these techniques are extremely high. Short pulses can provide high peak intensities necessary for the characterisation of nonlinear optical properties. Two experimental methods for time domain measurements are explored: the pump-probe technique which outputs amplitude measurements and spectrography which measures amplitude and phase.

3.6.1 Pump Probe

The common experimental method for characterising the temporal optical response on a very short time scale is the pump-probe technique [73]. Pump-probe experiments are valuable because they provide direct, time-domain measurements of ultra-fast nonlinearities in bulk materials and waveguides [51]. These experiments have a wide range of applications because the technique is relatively straightforward and requires no high-speed detectors with the temporal resolution being limited by the pulse duration.

The fundamental concept is to use two synchronized optical beams of short-duration pulses, one as a pump to induce a response in the medium being measured, and one as a probe whose change in transmission due to the presence of the pump is measured as a function of time delay. The pulses are typically derived from the same source, an ultrafast-pulse mode-locked laser that produces a beam of pulses of picosecond, or subpicosecond duration and a certain repetition rate. The resolution of the pump-probe measurement is dictated by the duration of the pulses, and the repetition rate (i.e. the time between pulses) must be longer than the time needed for the dynamics induced by the previous pulse to be completely recovered. The pump and probe beams are derived from the same source so that they are synchronized, and one beam is sent through a delay stage that can regulate

the delay between the pump and probe pulses. The change in transmission of the probe pulses is then measured as their delay from the pump pulses is changed. The remaining criteria is for the pump and probe pulses to be filtered by wavelength or polarisation. The probe pulses must only respond to the change in the medium due the presence of the pump pulse, and not directly to the presence of the pump pulse itself (i.e. via interference with the pump), even for time delays less than the duration of the pulse when they overlap temporarily.

There are many different systems which realise the pump-probe functionality, with the most popular utilising pulses generated with crossed polarisation states [51, 74–77] or differing wavelengths [50, 78, 79] to allow easy selection of the probe signal. Over the years these measurement systems have been used to investigate different semiconductor material systems [63, 78] and device structures including bulk [74], Multiple Quantum Well [75,76,78–80], Quantum Dash [81] and Quantum Dot [4, 70] amplifiers.

Whilst being a straightforward technique to implement, the limitation of pump-probe measurements is that no phase information is retrieved during the experiment.

3.6.2 Spectrography

Spectrography is an extension of the pump probe technique which measures both phase and amplitude. For optical communications the information on the phase and the amplitude of the pulses is required for predicting and mitigating the degradation from the chromatic dispersion and various optical nonlinearities. An ideal characterisation scheme should permit a waveform characterisation with a time resolution of ∼1ps. Section 3.7 outlines different spectrographic techniques and section 3.8 gives detail about linear spectrograms.

3.7 Spectrographic Techniques

Spectrographic techniques aim at measuring a time-frequency representation of a pulse, from which the analytical signal of the pulse is reconstructed. From a practical point of view, first the experimental trace is measured and then a set of mathematical operations are applied to the measured data in order to reconstruct the electric field. Spectrographic techniques make use of two sequential filters, one

time-stationary (spectral filter) and one time-nonstationary (time gate) followed by a square-law detector. The recorded signal is either a measure of the spectrum of a series of time intervals (spectrogram) or a measure of the time of arrival of a series of spectral intervals (sonogram) depending upon the ordering of the filters. Although the shape of this experimental trace can in some cases be interpreted to give an overview of the shape of the pulse, complete reconstruction of the analytic signal can only be obtained with an iterative algorithm. The sonogram and FROG (Frequency Resolved Optical Gating) spectrogram belong to this class and are popular tools for ultrashort pulse characterisation.

3.7.1 Sonogram

A sonogram of the electric field of the test pulse is obtained by measuring the temporal spectrum of the pulse after spectral gating (Figure 3.21) for various delays between the pulse and the gate [82] [83].

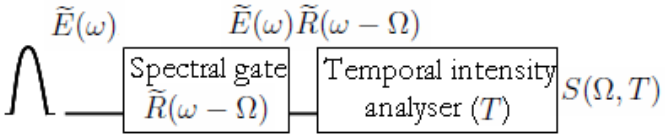

Figure 3.21: Conceptual Implementation of a Sonogram.

Typically, the pulse is first spectrally filtered using a spectrometer with a variable centre frequency Ω. The temporal intensity of the filtered pulse is then measured, and the sonogram is constructed from the set of the measured temporal intensities for various central frequencies Ω:

$$S(\Omega,T)=\left|\int \widetilde{E}(\omega)\widetilde{R}(\omega-\Omega)exp(-i\omega T)d\omega\right|^2 \tag{3.22}$$

In this case the temporal resolution should be very high to ensure the measured trace is a true sonogram. In practice, the sonogram is usually implemented by means of a nonlinear cross-correlation of the spectrally gated signal with the test pulse, which has a shorter duration than the filtered pulse. Therefore, the experimental trace is given by a convolution of the sonogram of Equation 3.22 with the unknown temporal intensity of the pulse under test, a fact that can be included in the inversion algorithm [83].

Time Resolved Optical Gating (TROG) is a well known example of a sonogram, being capable of determining the complex amplitude profile of an ultrashort pulse without any fundamental ambiguities.

3.7.2 Spectrogram

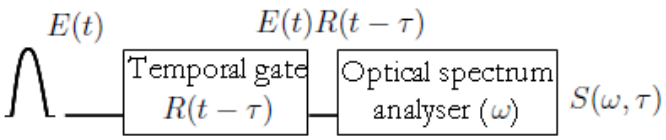

Figure 3.22: Conceptual Implementation of a Spectrogram.

The spectrogram can be measured by reversing the order of the temporal and spectral gate from a sonogram thus gating in time instead of frequency (Figure 3.22). The experimental trace is therefore

$$S(\omega,\tau) = \left| \int E(t)R(t-\tau)exp(-i\omega t)dt \right|^2 \tag{3.23}$$

where ω is the optical frequency and τ the relative delay between the gate and the test pulse. It is important that the resolution of the spectral filter is very high in order to ensure that the measured trace is effectively the spectrogram of the test pulse.

Nonlinear Spectrogram

Frequency resolved optical gating (FROG) is a well known spectrography technique that generates a nonlinear spectrogram of an input pulse by interacting one or more pulses in an nonlinear medium to form a gate that interacts with the input pulse. The interaction forms a signal pulse which is spectrally resolved and recorded as a function of delay between the input pulse and the gate. The spectrogram is a plot of signal intensity versus frequency and time [84]. The FROG technique has been used for ultrashort pulse characterisation in a range of applications [84, 85]. Its versatility lies in the fact that the pulse itself acts as its own gate, thus, the gate duration is optimally tailored to the pulse duration, with a measurement bandwidth only limited by the phase matching bandwidth of the

nonlinear process. However the use of a nonlinear optical process results in low sensitivity and high polarisation sensitivity [86].

Linear Spectrogram

Dorrer and Kang demonstrated a variation on this pulse characterisation technique that employs linear optical gating using an electroabsorption modulator (EAM) [87]. This linear-spectrographic technique has much greater sensitivity, is much less polarisation sensitive and it does not suffer from the temporal ambiguity in the measured fields that is associated with FROG [86].

3.8 Linear Spectrograms for the Characterisation of Short Optical Pulses

Linear characterisation of optical pulses using a temporal modulator as a gate rather than nonlinear optical interaction has been demonstrated [87]. The spectrogram of the pulse is constructed by means of measuring the spectrum of the gated pulse as a function of the delay between the pulse and gate [88]. The complete information of the pulse and gate can be extracted from this time-frequency representation without any assumptions. Assume that there is an optical pulse E(t) and a temporal gate with response R(t), both quantities being complex. A programmable delay τ between the output pulse is related to the input pulse by $E'(t,\tau) = E(t)R(t-\tau)$ as modelled in Figure 3.23. A single time interval of the spectrogram trace is the intensity spectrum of the product of these two functions where the gate is delayed relative to the pulse by τ. The complete spectrogram S(ω,t) is obtained when the gate is scanned in time across the pulse E(t).

The spectrogram S(ω,τ) is then built by measuring the spectrum of the gated pulse as a function of the optical frequency ω and the relative delay τ:

$$S(\omega,\tau) = \left| \int E'(t,\tau) exp(-i\omega t) dt \right|^2 \tag{3.24}$$

$$= \left| \int E(t)R(t-\tau) exp(-i\omega t) dt \right|^2 \tag{3.23}$$

From this experimental trace, both the pulse E(t) and the gate R(t) can be

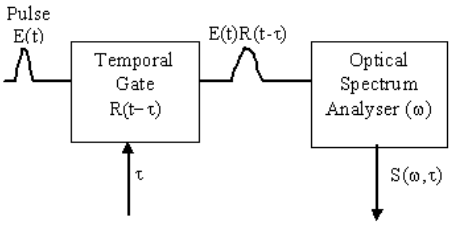

Figure 3.23: Schematic of the measurement of a spectrogram for simultaneous retrieval of the electric field of an optical pulse E and the response of the temporal gate R.

extracted using a phase retrieval algorithm without any assumptions [87] using the principal component generalised projection algorithm [89, 90]. This approach provides accurate and sensitive measurements of optical pulses without bandwidth limitations.

3.8.1 Principal Component Generalized Projections Algorithm

Principal Component Generalized Projections Algorithm (PCGPA) is a very robust inversion algorithm which uses projections derived from the experimentally measured spectrogram and from the functional form of the spectrogram (Equation 3.23).

An input pulse can be represented by Equation 3.25

$$E(t) = Re\left|\sqrt{I(t)}exp(i\omega_o t - i\phi(t))\right| \tag{3.25}$$

where $I(t)$is the time-dependent intensity, ϕ(t) is the time-dependent phase, and ω_o is the carrier frequency.

Equation 3.25 is the magnitude squared of the Fourier transform of the product E(t)R(t-τ) with respect to t. Virtually all practical data collection methods rely on discretizing τ and t. Suppose E(t) and R(t) are sampled at given values of t with a constant spacing of Δt. Then E(t) and R(t) can be thought of as vectors of length N whose elements sample E and R at discrete times, the electric fields become:

$$E_{pulse} = \left[E\left(-\frac{N}{2}\Delta t\right), E\left(-\left(\frac{N}{2}-1\right)\Delta t\right), E\left(-\left(\frac{N}{2}-2\right)\Delta t\right), \cdots, E\left(\left(\frac{N}{2}-1\right)\Delta t\right)\right] \tag{3.26}$$

$$E_{response} = \left[R\left(-\frac{N}{2}\Delta t\right), R\left(-\left(\frac{N}{2}-1\right)\Delta t\right), R\left(-\left(\frac{N}{2}-2\right)\Delta t\right), \cdots, R\left(\left(\frac{N}{2}-1\right)\Delta t\right)\right] \tag{3.27}$$

For simplicity, the vectors are written as

$$E_{pulse} = [E_1, E_2, E_3, \ldots, E_N] \tag{3.28}$$

$$E_{response} = [R_1, R_2, R_3, \ldots, R_N] \tag{3.29}$$

The outer product of E_{pulse} and $E_{response}$ is then expressed by:

$$\begin{array}{cccccc}
E_1R_1 & E_1R_2 & E_1R_3 & E_1R_4 & \cdots & E_1R_N \\
E_2R_1 & E_2R_2 & E_2R_3 & E_2R_4 & \cdots & E_2R_N \\
E_3R_1 & E_3R_2 & E_3R_3 & E_3R_4 & \cdots & E_3R_N \\
E_4R_1 & E_4R_2 & E_4R_3 & E_4R_4 & \cdots & E_4R_N \\
\vdots & \vdots & \vdots & \vdots & & \vdots \\
\vdots & \vdots & \vdots & \vdots & \ddots & \vdots \\
\vdots & \vdots & \vdots & \vdots & & \vdots \\
E_NR_1 & E_NR_2 & E_NR_3 & E_NR_4 & \cdots & E_NR_N
\end{array}$$

The outer product (or outer product form) matrix contains all the points required to construct the time domain spectrogram because it contains all of the interactions between the pulse and the gate for all the discrete delay times. Consequently, a one-to-one mapping of the elements of the outer product can transform the outer product into the time domain of the spectrogram. This is the key to PCGPA. Because the mapping is one-to-one it is invertible; transitions can be made from the outer product form to the time domain spectrogram and vice versa. This transformation can be accomplished by rotating the elements of the rows in the outer product matrix to the left by the row number minus one.

This is the time domain transform of the outer product matrix. The τ=0 column is the first column, where τ is the time delay in increments of Δt, a point-

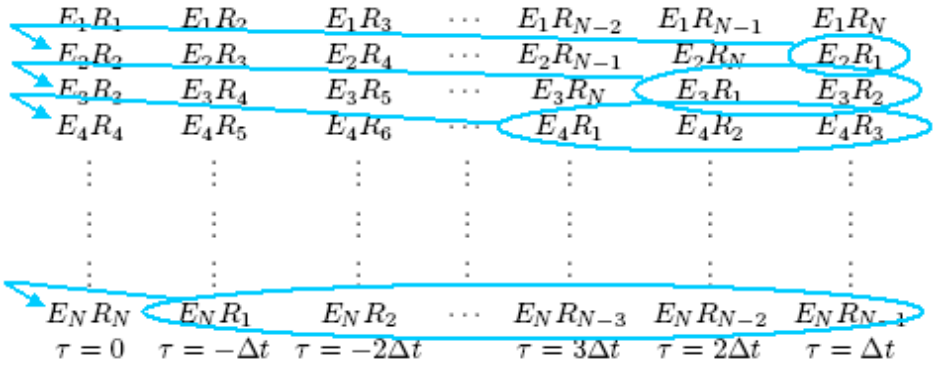

by-point multiplication of the pulse by the gate with no time shift between them. The next column is the τ=-1 column where the gate is delayed relative to the pulse by one resolution element, Δt. The gate appears to be shifted 'up' by one resolution element with the first element wrapped around to the other end of the vector. Column manipulation places the most negative τ on the left and the most positive on the right. The columns are constant in τ(delay) while the rows are constant in t (time).

There is only one image that can be formed by the outer product of a single pair of nontrivial vectors that has the same magnitude as the spectrogram to be inverted. In order to find the proper (principal) vector pair, the phase of the spectrogram must be determined using a 2-D phase retrieval algorithm.

The Power Method

The principal vector pair may be found through the power method [91]. If the intensity and phase of the outer product form matrix are correct then it is a true outer product and has a rank of one. That is, it would have only one nonzero eigenvalue and one right eigenvector and one left eigenvector. The right eigenvector, the pulse, spans the range of the outer product matrix. The complex conjugate of the left eigenvector of the transpose of the outer product matrix (left eigenvector) is the gate. The outer product form matrix produced by the initial estimation however, is not rank one and has several eigenvectors. It will probably have (for an NxN trace) N right eigenvectors and N left eigenvectors (eigenvectors of the transpose): instead of describing a single line in N-space, the matrix represents an ellipsoid in N space. The best next estimation may actually be a superposition of two or more different but linearly independent eigenvectors,

requiring an optimisation such as minimisation of the spectrogram trace error to find the correct superposition.

Suppose the outer product form matrix is an NxN matrix, A. There are two sets of N orthonormal eigenvectors B_i and C_i such that

$$\begin{aligned} AA^T B_i &= \lambda_i B_i \\ A^T A C_i &= \lambda_i C_i \end{aligned} \tag{3.30}$$

where λ_i are the eigenvalues and the superscript T is the transpose operator. A may be constructed by

$$A = \sum_{i=1}^{N} \sqrt{\lambda_i} B_i {C_i}^T \tag{3.31}$$

where B_i and C_i require to correspond to the largest $|\lambda_i|$, or the principal eigenvectors. Suppose an arbitrary nonzero vector x_0 is multiplyed by AA^T. Then

$$AA^T x_0 = \sum_{i=1}^{N} \kappa_i \lambda_i B_i \tag{3.32}$$

where B_i are the eigenvectors of AA^T, λ_i the eigenvalues, and κ_i a set of constants. AA^T can be thought of as an operator that maps onto a superposition of eigenvectors. The process can be repeated resulting in $\mathrm{AA}^T \kappa_i \lambda_i B_i = \kappa_i {\lambda_i}^2 B_i$.

Multiplying by $\left(AA^T\right)^{b-1}$ gives

$$\left(AA^T\right)^b x_0 = \sum_{i=1}^{N} \kappa_i {\lambda^b}_i B_i \tag{3.33}$$

As b becomes large, the largest eigenvalue,λ_i, dominates the sum so that

$$\left(AA^T\right)^b x_0 \approx \kappa_i {\lambda_i}^b B_i \tag{3.34}$$

After a few iterations, a very close approximation to the principal eigenvector (the eigenvector with the greatest eigenvalue) is obtained. Consequently the next estimate for the pulse can be obtained by multiplying the previous estimate for the pulse by AA^T and the next estimate for the gate can be obtained by multiplying

the previous estimate for the gate by $A^T A$. While better approximations for the eigenvectors may be obtained by using these operators several times per iteration, once per iteration is adequate in practice [89]. The power method depends on the outer product form matrix having only one dominant eigenvalue. In practice, this is almost always true. If not, the spectrogram trace is most likely corrupted, resulting from the superposition of two or more traces, or from severe distortions [89].

Spectral Constraints

In PCGPA the pulse and gate are completely independent, the only nonlinear interaction assumed is the multiplication of the pulse by the gate. How the gate is constructed is of no concern, as a result some ambiguities involving the width of the pulse and gate can occur. For example, a very slight change in the width of the pulse may be compensated for by the algorithm by a slight change in the width of the gate without changing the RMS error significantly. These ambiguities may be resolved by the addition of a spectral constraint on either the pulse or gate [92]. This constraint is applied after the intensity constraint is applied and just before the next estimate is computed; hence the trace is in the outer product form. When in this form, each column is ideally a constant (one of the elements of the gate) multiplied by the pulse field. Thus, each column is Fourier transformed and the magnitude is replaced by the square root of the measured pulse spectrum.

Because the square root can cause small fluctuations in the wings of the gate, producing artifacts in the next estimate for the pulse, instabilities may occur in the algorithm. This can be remedied by applying the square root to only well-defined portions of the gate. Where the gate is not well defined, the intensity (and phase) of the pulse is used. To ensure the gate field is preserved, the area of the intensities before and after the spectral constraint is applied are kept equal. To prevent artifacts from appearing in the wings of the trace, the spectral constraint may only be applied to portions of the trace that has an integral above some predetermined level.

2-D Phase Retrieval Algorithm

The power method implementation of the PCGP algorithm is outlined below and illustrated in Figure 3.24. An inverse of the outer-product-to-time-domain transform is applied.

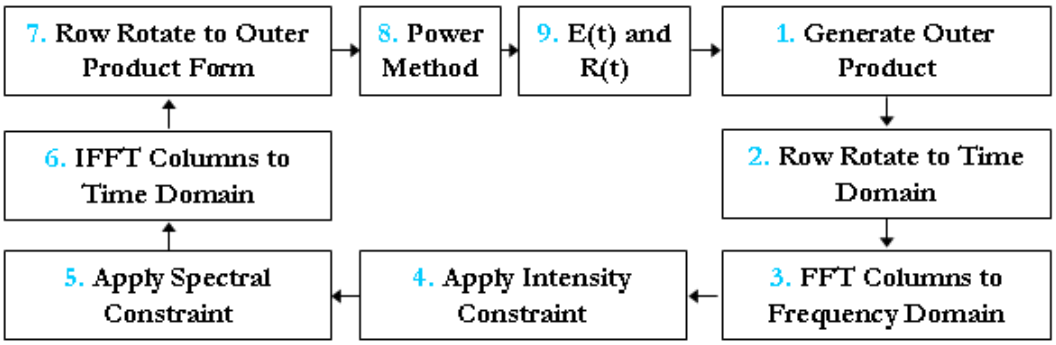

Figure 3.24: Schematic of PCGP Algorithm. Transformations from the outer product to the time domain trace (and vice versa) may be accomplished via simple permutations (rotations) of each row.

1. Initial estimate of random noise modulated by a broad Gaussian for the pulse and gate are used to construct the first outer product matrix.

2. A one-to-one transformation via permutations converts the outer product into time-domain spectrogram of the initial estimate.

3. The columns are Fourier transformed.

4. An intensity constraint is applied (its magnitude is replaced by the square root of the magnitude of the initial experimental trace).

5. A spectral constraint is applied.

6. The result is converted to the time-domain transform using an inverse Fourier transform by column.

7. The time-domain spectrogram is converted to the outer product form matrix by reversing the steps used to construct the time domain spectrum.

8. The outer product form matrix is decomposed into a superposition of weighted outer products by the power method.

9. The vector pair (outer product) with the largest corresponding weight is the best rank one approximation of the outer product form (in a least squares sense) hence this estimate is a projection and is used for the next iteration.

3.9 Conclusions

This chapter has introduced the semiconductor optical amplifier: the structure, characterisation parameters and the physics of the carrier dynamics within the semiconductor. The techniques for measuring the carrier dynamics of semiconductors have been outlined. The spectrographic technique, which is used to measure the SOA amplitude and phase dynamics in this thesis, has been presented in detail.

Chapter 4

Amplifiers in Passive Optical Networks

Section 2.5 introduced Passive Optical Networks, a point-to-multipoint optical network architecture in which numerous end users can be served by a single optical fibre. This concept may be improved by extending the reach of the network. This is a desirable development to the telecommunication operators as it can reduce their capital expenditure and reduce the unit bandwidth cost of the network as detailed in section 2.5.2.

Several scenarios can be considered when determining the optimal method to extend the reach of the PON. The first two options to extend the reach of the network would be to improve the performance at the OLT by using higher powered lasers to increase the launch power into the fibre or at the ONU by increasing the sensitivity of the detector. The impediment of these options is that the signal levels are already established in the published standards and even if the standards were to be changed, the possible gain increase is relatively small. In order to attain an increase of 20dB or more a mid-span repeater is the best option (section 2.2.3).

Recall that the GPON standard is 1.25Gbit/s at 1310nm upstream and 2.5Gbit/s at 1490nm downstream which clearly precludes erbium based fibre amplification. An OEO solution could be considered as a mid-span repeater, however this leads to preamble erosion as detailed in section 2.5.3. SOAs are therefore the most viable solution to extend the reach of PONs. The material composition of an InGaAsP SOA active layer can be adjusted to amplify signals in the region of 1200 – 1650nm thus these devices can be designed to serve either direction of travel of

this standard.

This chapter reviews the opportunities for SOAs to extend the reach of GPON. The requirements for an SOA specification in this context are reviewed. Modelling results are presented to identify the parameters affecting the mass fabrication of high gain SOAs suitable for serving GPON. A high gain SOA with low polarisation dependence is designed, fabricated and experimentally measured to show a record margin improvement in a Passive Optical Network with the inclusion of an SOA. The SOA is shown to have gain modulation sourced ISI (patterning) effects at high power which limits the performance in the PON scenario.

4.1 SOAs for Extended Reach GPON

An amplifier in a PON is normally placed between the OLT and the splitter, as shown in Figure 2.12 and Figure 4.1, as this scenario maximizes the power budget improvement [5]. However this may not always be possible depending on the availability of a power source at this point. The optimum position is a trade off between the trunk fibre loss and the splitter loss. An SOA can be considered to operate as a booster amplifier, as an in-line (mid-span) amplifier, or a preamplifier, as denoted by positions 1, 2 and 3 respectively in Figure 4.1.

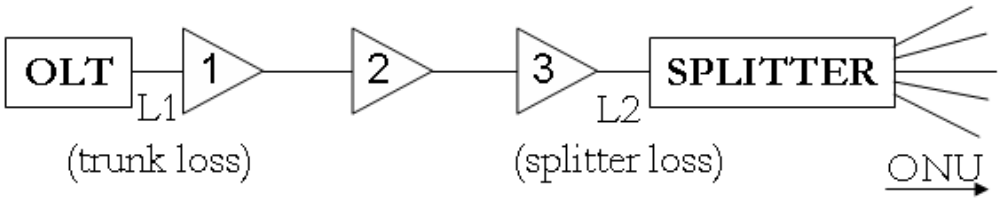

Figure 4.1: Varying SOA position in Passive Optical Network.

Figure 4.2 shows the range of powers over which the SOA would ideally work. At one extreme, where L1 is zero, the power into the SOA is high, thus it is operating as a booster (shown by the blue line), and the additional margin is that of the maximum output power of the SOA over the transmitter launch power. At high input powers, i.e. low L1 values, the achievable post amplification transmission distance is limited by the maximum power which can be launched into the amplifier. This in turn is limited by the maximum saturation output power, P_{sat}, of the SOA. In an SOA, P_{sat} is generally in the region of 13dBm

although higher powers are attainable. In this case an SOA with medium gain (about 10dB) is desirable.

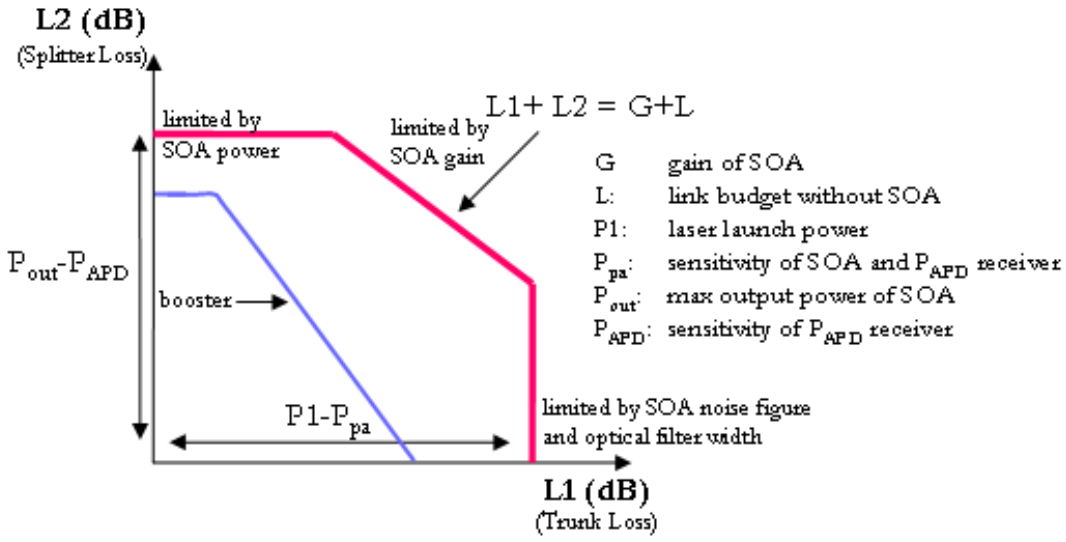

Figure 4.2: SOA in a PON link from [5].

At the other extreme where the SOA is being used as a preamplifier, L1 is high and L2 is zero, the additional margin is that of the sensitivity of a preamplified receiver over the receiver alone. The point of interest is the maximum loss that can be tolerated before a BER of $1x10^{-9}$ is no longer achievable. Here the amplifier compensates for all systems losses (splitter and trunk) and so an amplifier with high gain and low noise figure is desirable. All other cases can be considered as in-line amplification.

In addition to inserting an amplifier with high gain, the link budget can be improved by increasing the P_{sat}, decreasing the NF and / or increasing the length of the SOA. The bandwidth of the optical filtering also has an impact on the sensitivity. As Figure 4.2 implies, the maximum margin increase occurs when both L1 and L2 are large and under these circumstances the SOA gain can be the limiting factor in the margin increase.

The following section gives an overview of the characteristics of existing commercially available SOAs and details the requirements of SOAs to be useful in a GPON application.

Manufacturer	Centre λ (nm)	Gain (dB)	PDG (dB)	NF (dB)	Psat (dBm)	FWHM (nm)	Active Region
Alphion	1490	26	1.5	8	9	30	Bulk
CIP	1310	22	0.5	6.5	N/A	N/A	MQW
InPhenix	1310	22	0.5	7	10	45	Bulk or MQW
InPhenix	1550	20	0.5	9	10	45	Bulk or MQW
Kamelian	1310	18	0.5	6	8	30	Bulk
Kamelian	1550	20	0.5	6	11	34	Bulk
Thor Labs	1550	20	1	9	9	34	Bulk

Table 4.1: Summary of the main characteristics of commercially available SOAs.

4.1.1 Commercial SOA Characteristics

The characteristics of commercially available devices from five SOA manufacturers at both wavelengths of GPON operation are presented to identify their adequacy and limitations for GPON applications and are summarised in Table 4.1. CIP Photonics advertise a 'high-gain SOA' with an MQW active region. It has a gain of 22dB, polarisation dependence of 0.5dB and noise figure of 6.5dB; the details of the saturation output power and bandwidth are not available.

The InPhenix 1310nm SOA has comparable performance characteristics with the same gain and PDG as the CIP device, but has a higher noise figure of 7dB. The saturation output power for the InPhenix SOAs at both wavelengths are published as 10dBm and the bandwidth of both devices is 45nm. The InPhenix 1550nm SOA has a reduced gain of 20dB and a even higher noise figure of 9dB.

The Kamelian devices have the lowest noise figure of all the SOAs presented (6dB at both wavelengths). The Thor Labs SOA is only available at 1550nm and has a higher PDG that the previous devices of 1dB. The Alphion device has the highest gain of 26dB, polarisation dependence of 1.5dB, higher noise figure of 8dB and a bandwidth of 30nm.

In these devices the choice of the high gain Alphion SOA, with higher PDG and NF, is at a trade off to the lower gain but improved PDG and NF of the other devices.

4.1.2 SOA requirements for GPON

As illustrated in Figure 4.1 the SOA can be located in three positions in the PON network, each of which has a limiting factor as detailed in section 4.1. The

position of the SOA in the system will be determined by the availability of a power supply which will vary for each link. The ideal scenario therefore is to have an SOA which can be used in all locations of the span.

SOAs are commercially available to operate as boosters and in-line amplifiers. High gain (>20dB), low noise figure SOAs require to be developed to operate as preamplifiers. However increasing the gain of an SOA increases the difficulty in controlling the polarisation dependent gain of the device. In order to amplify the GPON network as a preamplifier the SOA will be placed after a long transmission link, thus a minimum PDG value is necessary to minimise possible performance degradation due to the drift in input signal polarisation state. This leads to the question of how reliably can a high gain device be fabricated? PDG impinges the signal and the SNR at high power and so it is desirable to develop an SOA capable of maximising the link budget whilst maintaining PDG below 1dB. Section 4.2 is a study into the fabrication tolerances required for a high gain, polarisation insensitive SOA.

4.2 Modelling Fabrication Tolerances for Polarisation Insensitive, High Gain SOAs

As introduced in section 3.3.5, polarisation independence in optical components is critical in their design and operation. In general, a fibre carrying a signal will not be polarisation maintaining thus the signal launched into a device will have an unknown polarisation state. There are several design parameters in SOAs that can be altered in order to optimise their polarisation insensitivity without compromising the device performance. This section models the polarisation dependent gain of a buried heterostructure, strained bulk active region SOA as a function of active region (mesa) width, active region thickness, separate confinement heterostructure thickness, active region refractive index and waveguide dispersion.

In order to model the strain of the SOA, empirical data is required. This data was only available at 1550nm therefore the modelling was carried out at this wavelength. However the tolerances will still be applicable to SOAs at the upstream wavelength (1310nm) of the GPON standard.

4.2.1 Polarisation Dependence in Active Waveguides

The modal confinement factor (Γ) can be defined as the fraction of the optical power which travels in the waveguide core. If the waveguide is sufficiently narrow it will only support a single transverse mode, transverse electric (TE) where the electric field is polarised along the active region plane or transverse magnetic (TM) where the magnetic field is polarised along the active region plane. Generally the TE confinement (Γ_{TE}) is greater than the TM confinement (Γ_{TM}). Tensile strain (section 3.3.5) can be introduced into the active region to increase the TM material gain relative to that of TE. It is possible to balance the two gain differences by applying the correct amount of strain thus improving polarisation independence.

These two parameters are related by the confinement factor ratio (Γ_{ratio}), shown in Equation 4.1, which is typically in the range 1.1–1.9. The larger the confinement factor ratio, the larger the value of tensile strain required to achieve polarization independence.

$$\Gamma_{ratio} = \frac{\Gamma_{TE}}{\Gamma_{TM}} \tag{4.1}$$

4.2.2 Polarisation Dependent Gain

Recall Equation 3.7 gives the SOA optical gain, G:

$$G = \frac{P_{out}}{P_{in}} = exp((\Gamma g_0 - \alpha)L) \tag{3.7}$$

where Γ is the modal confinement factor, g_0 is the material gain coefficient, α is the waveguide loss coefficient and L is the length of the device. Equation 3.7 shows that the gain and the length of an SOA are directly proportional thus increasing the length of the SOA will increase the gain. Neglecting polarization dependent losses, the influence of gain on the PDG can be described as:

$$PDG = \frac{G_{TE}}{G_{TM}} = exp((\Gamma_{TE} g_{TE} - \Gamma_{TM} g_{TM})L) \tag{4.2}$$

This shows that PDG is largely dependent on the confinement factor and the material gain of the TE and TM modes. Taking the inverse of the exponential of Equation 4.2 gives:

$$ln(PDG) = (\Gamma_{TE} g_{TE} - \Gamma_{TM} g_{TM})L \tag{4.3}$$

which shows that the rate of change of PDG with gain is constant and has an offset. A specific value of PDG (e.g. 1dB) can therefore be maintained by tightly controlling the SOA design and fabrication parameters. SOAs designed for high-gain applications, such as mid-span amplifiers in GPON, will require close control of the fabrication parameters which define the confinement factor.

Polarisation independence is achieved for this SOA design by optimising the active region strain value in an empirical manner [93]. Once this value has been set, it is possible to model the variation of the PDG caused by the variations in fabrication parameters. This is achieved by calculating the variation in the confinement factor ratio as a function of these fabrication parameters in the context of sensitivity to manufacturing tolerances and so its effect on the overall device PDG can be studied.

4.2.3 Device Design

The SOA modelling in this section has been carried out on an adaptation of a commercial device design in order to determine what the critical design parameters are in fabricating a high yield of high gain polarisation insensitive SOAs. A Kamelian SOA was modified to have improved gain by increasing the cavity length. The SOA modelled was a 0.1μm thick InGaAsP active region with a refractive index of 3.58 which was designed to operate in the 1550nm wavelength window (Q1.55), the minimum attenuation in optical fibre and that used for long haul transmission. Surrounding this are 0.1μm InGaAsP separate confinement heterostructure (SCH) layers. These are thin layers of material above and below the active region which have a refractive index value less than the active region but greater than that of the substrate (Figure 3.7) with an emission wavelength of 1100nm (Q1.1) and refractive index of 3.28. The confinement factor ratio can be controlled through variation of the SCH index and thickness resulting in the possibility of utilising lower active region tensile strain values while still achieving polarisation independence. InP blocking layers are modelled on either side of the active region to help maximise the current confinement to the active region; p-type refractive index 3.162, n-type refractive index 3.158.

The device is modelled to include 80μm long lateral tapers to maximise coupling to the input and output optics. These have an initial width of 1.4μm and a final width 0.4μm as illustrated in Figure 4.3.

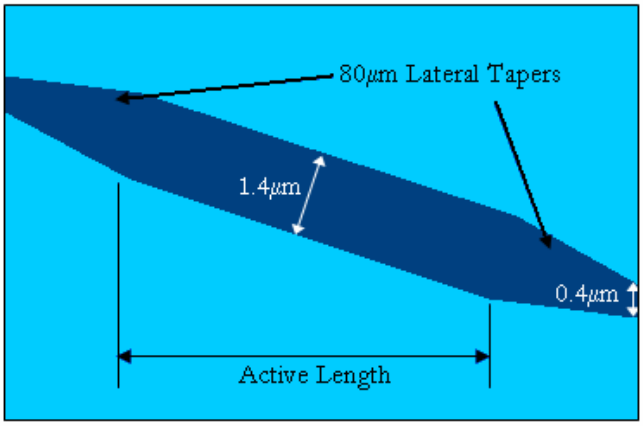

Figure 4.3: Top view of angled facet SOA with lateral tapers to provide mode-size control.

4.2.4 Modelling Setup

Figure 4.4 shows the setup for the SOA modelling in the commercial full vectorial mode solver software FIMMWAVE. The active region (Q1.55) is surrounded by SCH layers (Q1.1) and InP blocking layers to maximise the modal confinement. The influence of the growth thickness (active region and SCH layer), the control of the lithography (in the consistency of the waveguide width), and the refractive index (carrier injection) are modelled. Table 4.2 summarises the parameters varied in the modelling.

	Material	Index	Width	Thickness
Mesa Overgrowth	InP p-type	3.162	5μm	1μm
Blocking Structure	InP n-type	3.158	5μm	0.5μm
Blocking Structure	InP p-type	3.162	5μm	0.5μm
Substrate	InP n-type	3.158	5μm	3μm
Active Region	InGaAsP	3.5 - 3.6	0.4μm - 1.4μm	0.08μm - 0.12μm
SCH	InGaAsP	3.28	0.4μm - 1.4μm	0.08μm - 0.12μm

Table 4.2: FIMMWAVE Modelling Parameters

4.2.5 Modelling Results

The electric field profiles are shown in Figure 4.5 for TE (top row) and TM (bottom row) polarisation for the various stages (widths) along the taper: 0.4μm (the taper end point), 0.9μm (a point along the taper length) and 1.4μm (the

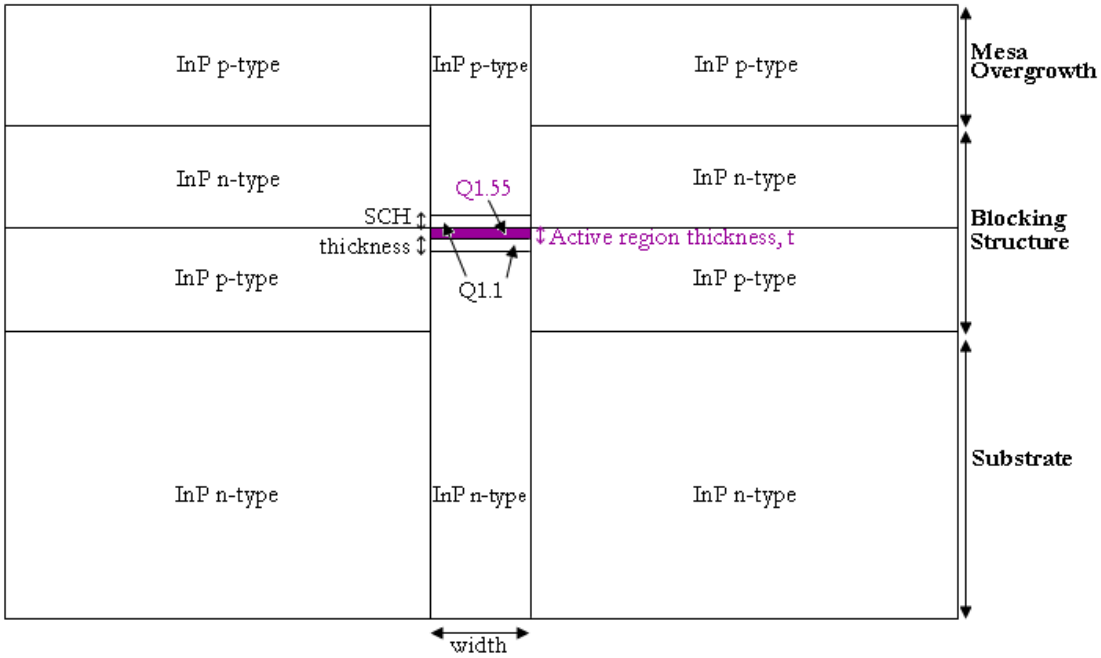

Figure 4.4: FIMMWAVE Modelling Setup.

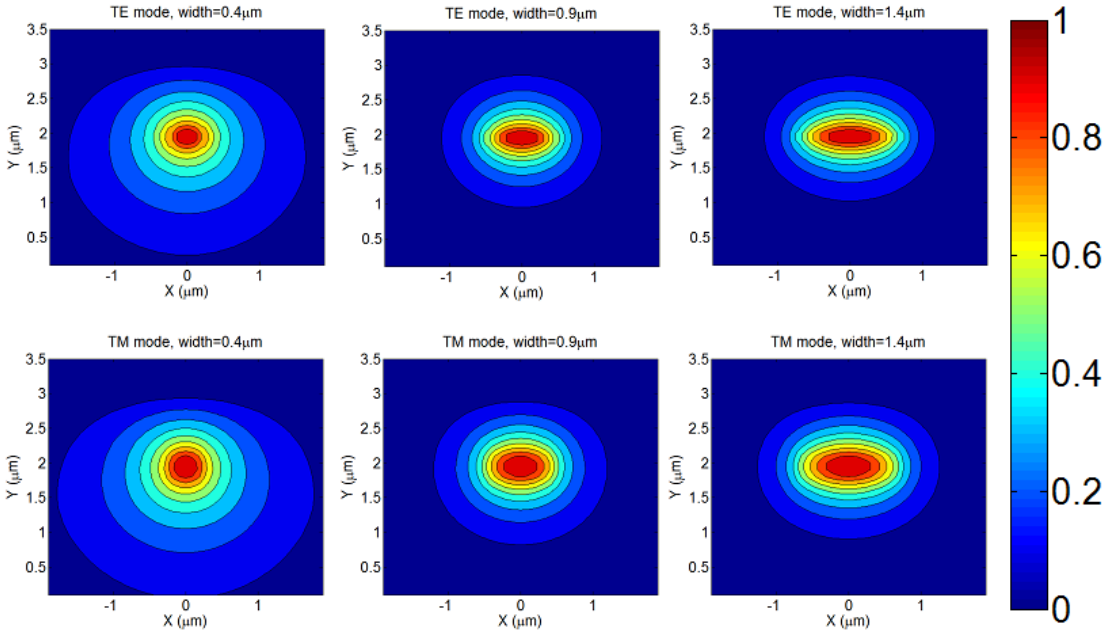

Figure 4.5: TE (top) and TM (bottom) mode confinement at various stages along the SOA taper (reproduced in RSoft).

central active waveguide width) for active region thickness and SCH thickness of 0.1μm. The mode can be clearly seen to expand with the lateral taper. The contours plot the energy density of the mode with the peak normalised to one. The interval between each contour in Figure 4.5 represents a ten percent decrease in energy density.

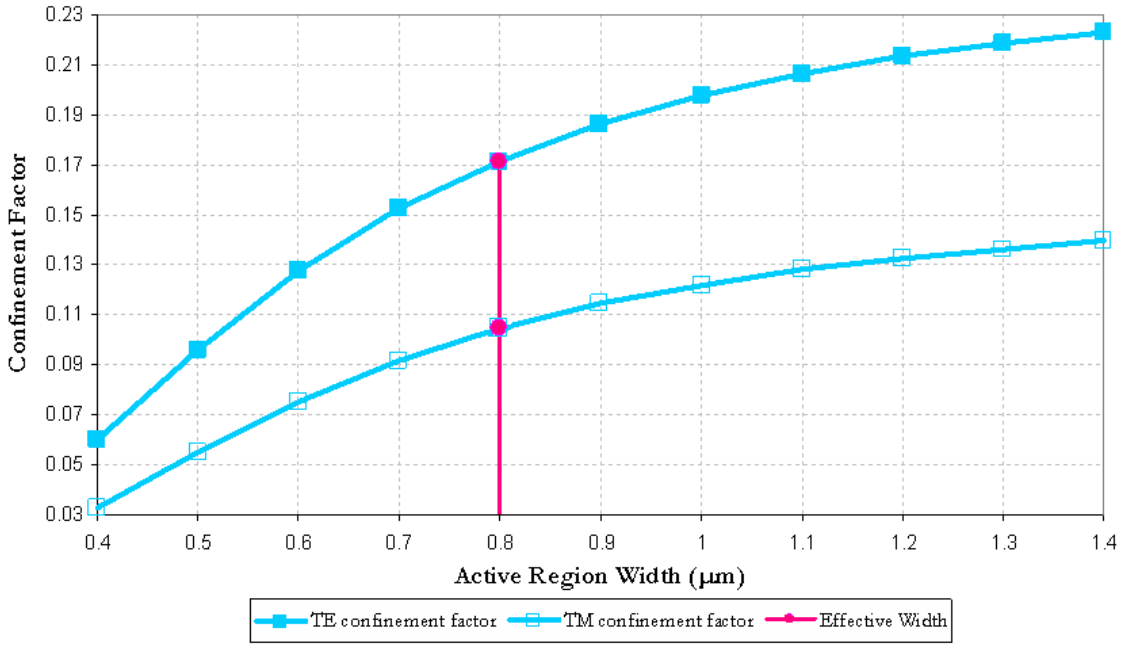

Figure 4.6: Confinement factor variation for taper region.

The variation of confinement factor along the taper is shown in Figure 4.6 for both polarisation states. The effect of the taper region is shown to reduce the confinement factor from 0.223 to 0.060 for TE polarisation. For an SOA with a constant gain it can be deduced from Equation 4.2 that PDG is influenced by variations in waveguide width through lithography precision. The variation in confinement factor with active region width, shown in Figure 4.6, can be approximated using a polynomial fit to the curves shown as:

$$\Gamma_{TE}(w) = 0.1257w^3 - 0.5188w^2 + 0.7605w - 0.1694 \tag{4.4}$$

$$\Gamma_{TM}(w) = 0.0704w^3 - 0.3035w^2 + 0.4648w - 0.1095 \tag{4.5}$$

In order to calculate the PDG variation for the device, an effective confine-

ment factor, Γ', and effective width, w', are calculated to account for the change in confinement factor from the active region along the taper length. Γ' is calculated for the taper region by integrating the contribution each element of the taper makes along the taper length:

$$\Gamma' = \int_{w1}^{w2} \Gamma(l) dl \tag{4.6}$$

This gives Γ'_{TE} as 0.17 and Γ'_{TM} as 0.105. The effective width for these confinement factors can be taken from Figure 4.6 as 0.81μm which is the equivalent width for the taper approximating to a straight waveguide with the confinement factor of Γ'.

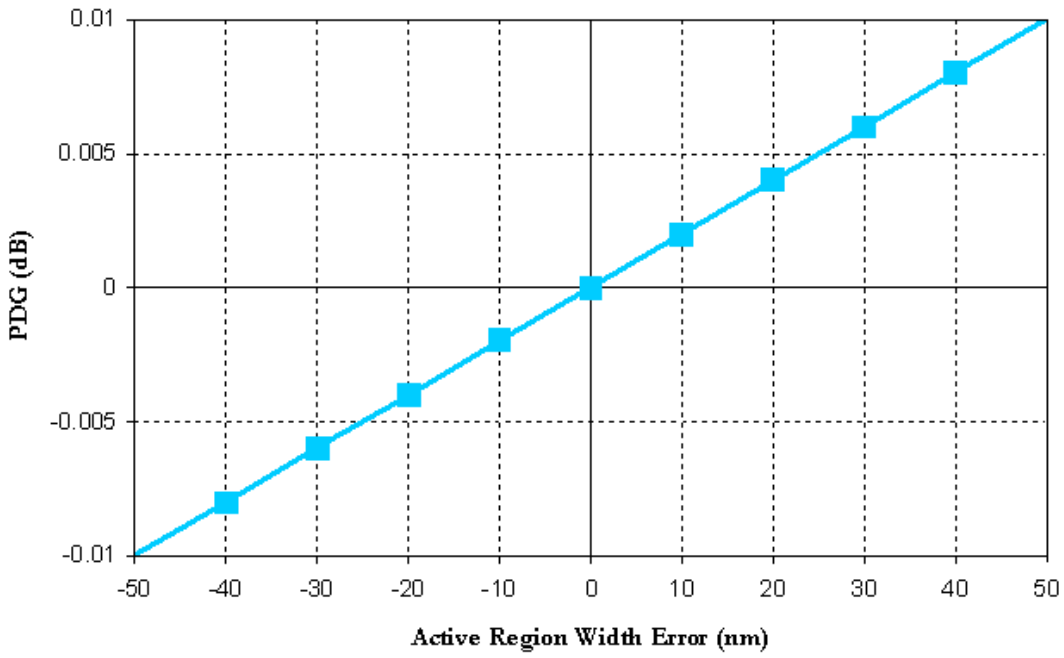

Figure 4.7: PDG Sensitivity to Width Error.

Figure 4.7 shows the calculated PDG dependence on the width of the active region mesa for an SOA with 25dB gain. This is calculated from Equation 3.7 around a target width error of 0nm, taking into account the effective confinement factor for both tapers and the actual confinement factor for the waveguide active length of 840μm. Lithographic fabrication tolerances are <5nm, thus from Figure 4.7 it can been deduced that waveguide width fabrication error has a negligible

effect on the PDG (<0.01dB).

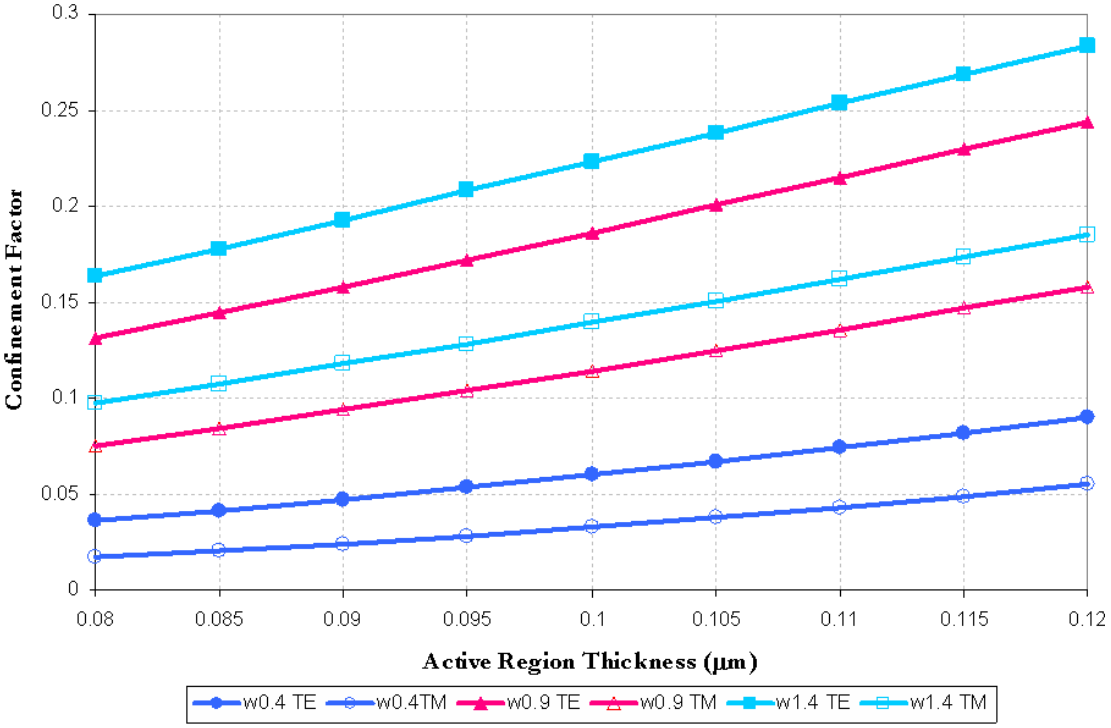

Figure 4.8: Variation in confinement factor with growth thickness.

Figure 4.8 depicts, for the three widths representing the taper, how the confinement factor varies for both TE and TM modes as a function of waveguide active region thickness control. The confinement factor is strongly influenced by the active region (growth) thickness, t, over the entire length of the taper. Γ is greatest for the TE mode at the widest part of the taper so it can be assumed that this will dominate the PDG performance of the SOA. The confinement factor sensitivity to variations in the growth thickness, $d\Gamma/dt$, increases as the active region thickness increases. It can also be observed in Figure 4.9 that there are greater confinement factor differences between the relative TE and TM modes as the active region thickness decreases.

Figure 4.10 shows the PDG versus active region growth control for deviations around the target growth thickness of 100nm for an amplifier of 25dB gain. The limiting factor in these calculations is that the effective confinement factor has been calculated for a constant active region thickness of 100nm and so the same Γ' has been used for all points on this curve.

The SCH layer contributes to the waveguiding properties and so it will have

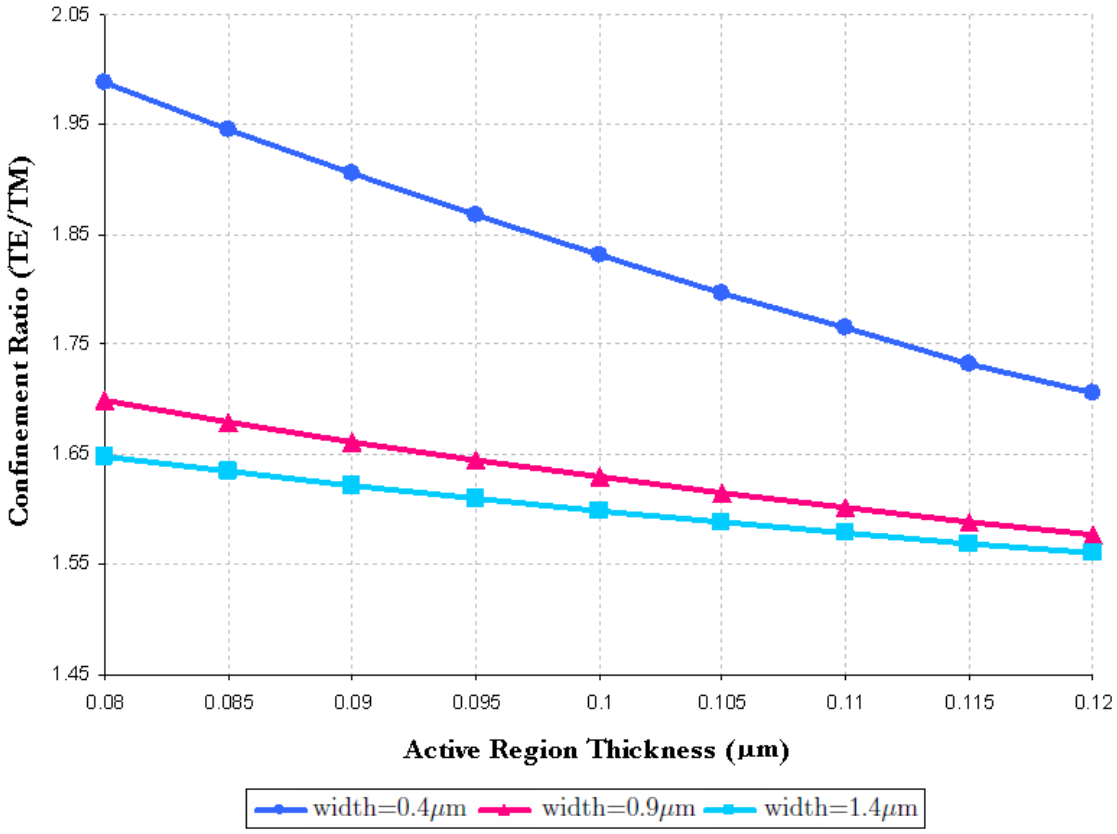

Figure 4.9: Confinement factor ratio as a function of thickness.

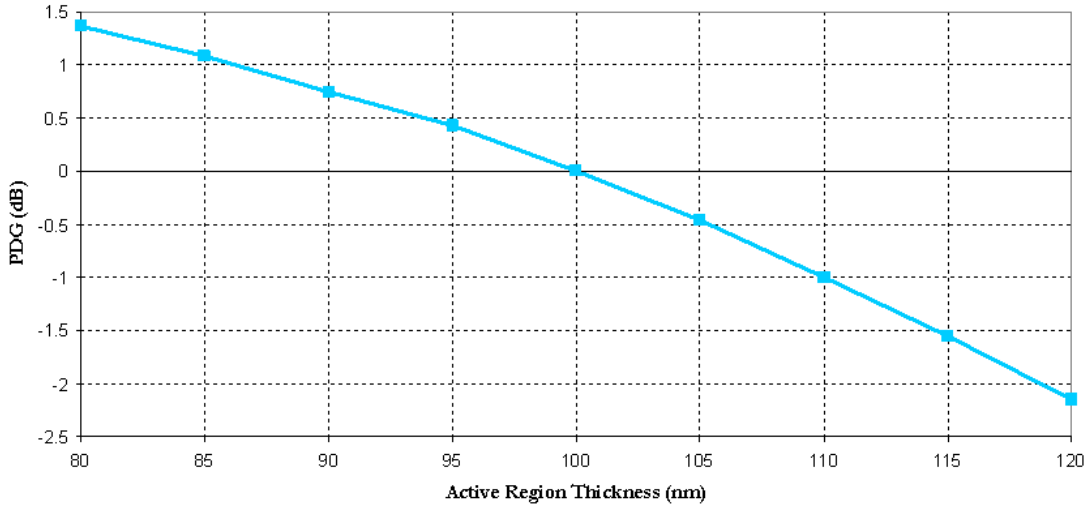

Figure 4.10: PDG variation with Active Region Growth Thickness.

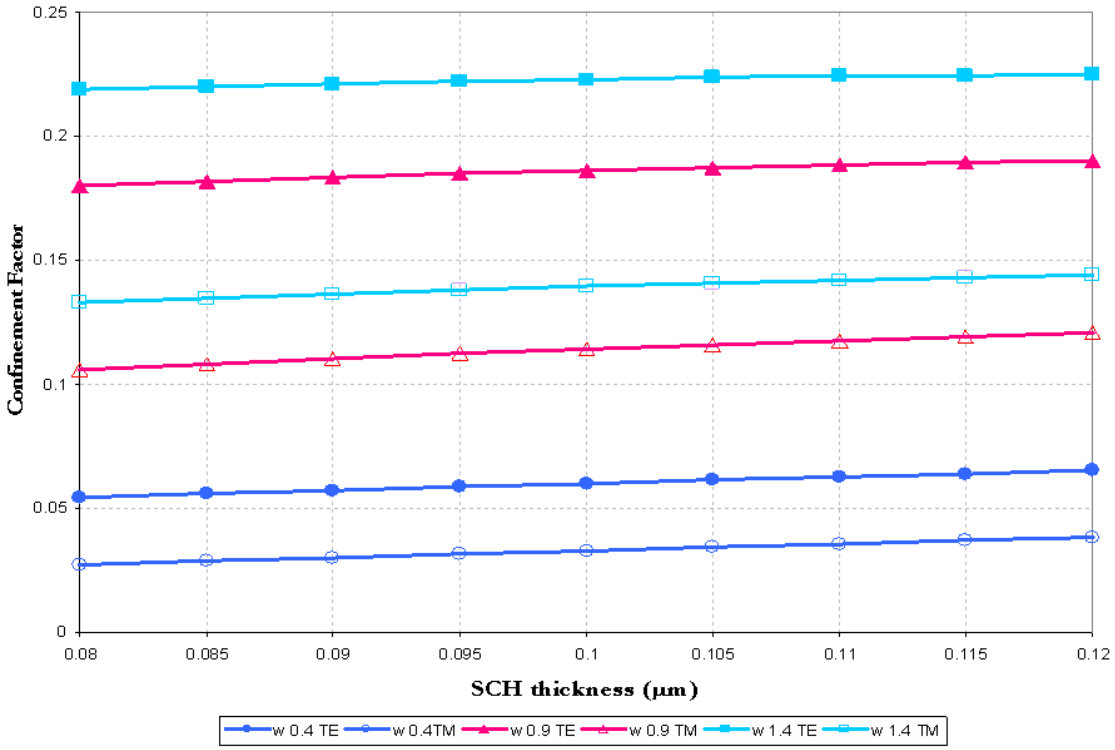

Figure 4.11: Confinement factor variation with SCH thickness.

an influence on PDG. Examining the variations in confinement factor with changes in the SCH thickness can be seen in Figure 4.11 and Figure 4.12. Figure 4.12 was calculated in a similar manner to that of Figure 4.10 for a SOA with a gain of 25dB. The effect is relatively small compared to the active region thickness, for a fabrication tolerance of ±5nm the PDG contribution of SCH is only 0.13dB compared to 0.46dB for the active region thickness.

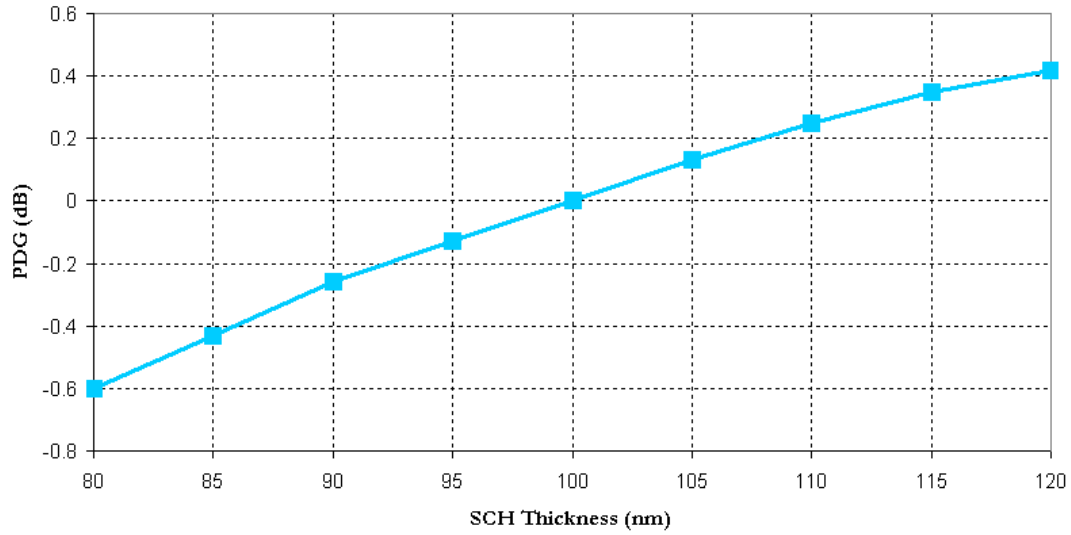

Figure 4.12: PDG Variation with SCH Thickness Growth.

Figure 4.13 plots the variation of confinement factor with change in active material refractive index (due to carrier injection) and the impact this has on PDG as shown in Figure 4.14. The variations in PDG for the SOA design shows clearly that the modal index influences the behaviour in a similar manner to the active-region thickness.

From [94], values for the change in refractive index with carrier density in bulk material are -1.34 x $10^{-20} cm^{-3}$. This means that, for typical carrier densities up to ∼5 x 10^{18}, there will be a refractive index reduction of up to ∼0.06 in the active region. While this effect appears significant, the strain optimization process takes place at high drive currents, resulting in low PDG with the variation occurring at lower gain values where the tolerances to these effects are higher.

Figure 4.15 shows the PDG variation with waveguide dispersion over the C-band (1530 - 1565nm). The dispersion across the wavelength range introduces a maximum penalty of 0.24dB.

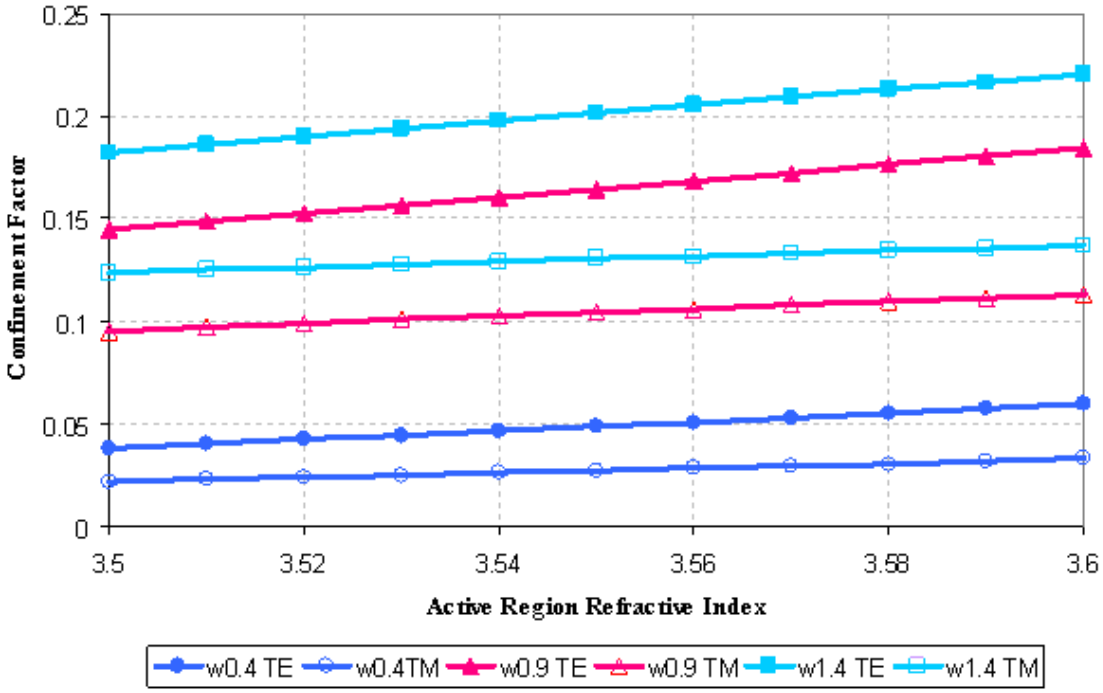

Figure 4.13: Confinement factor ratio variation with active-region index.

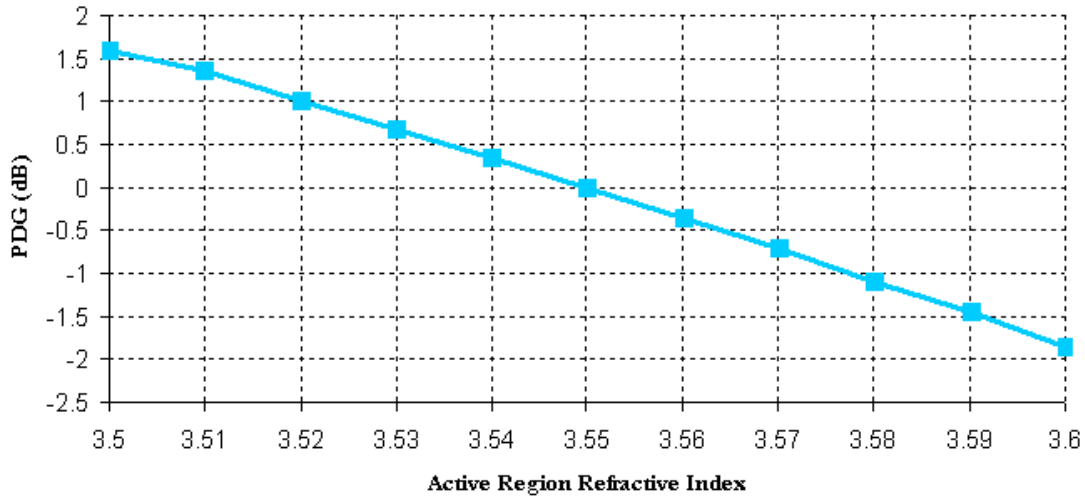

Figure 4.14: PDG Variation with Active Region Refractive Index.

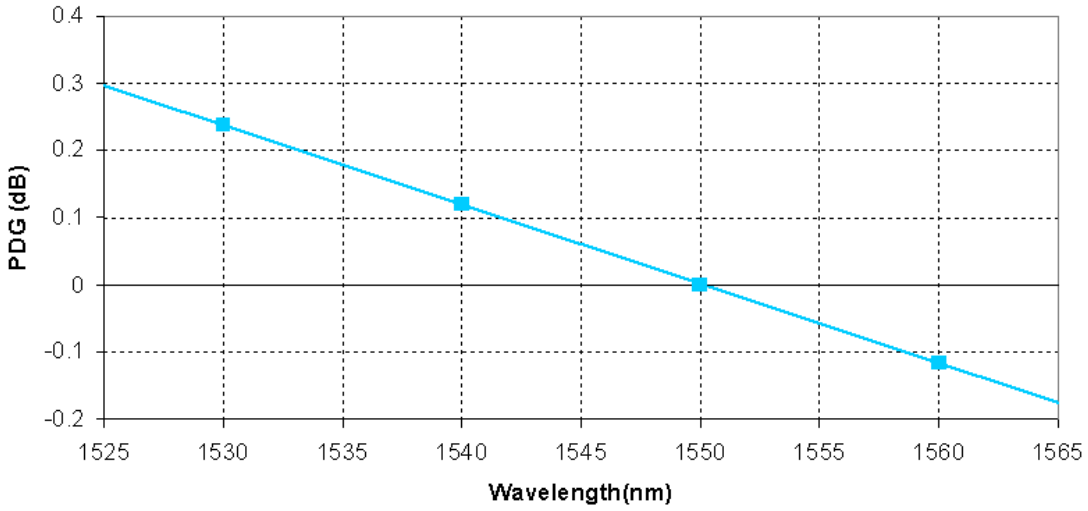

Figure 4.15: PDG Variation resulting from waveguide dispersion.

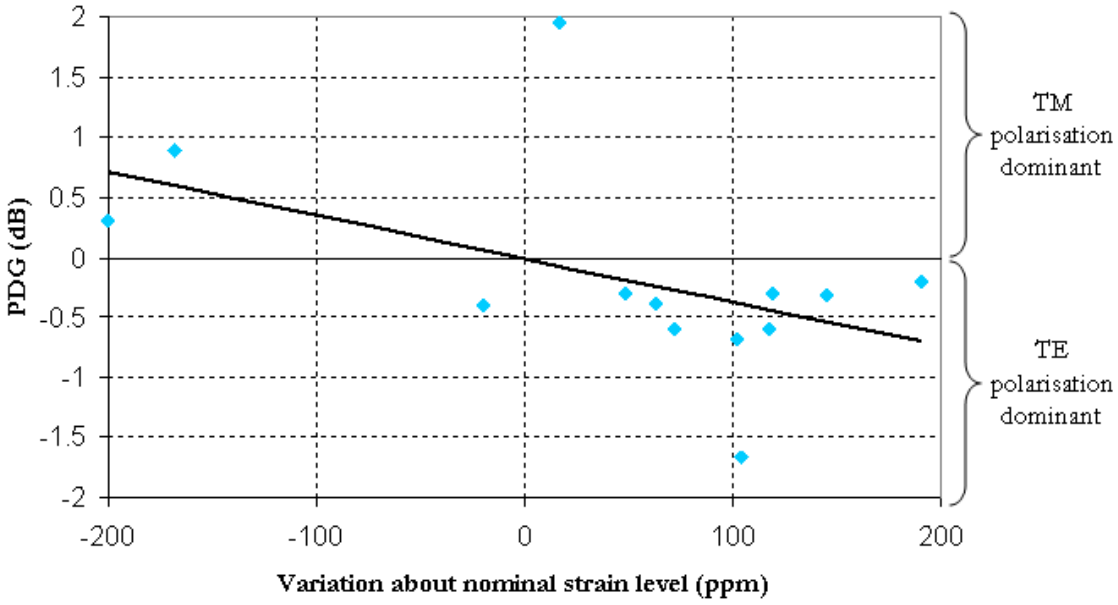

Figure 4.16: PDG variation with change in wafer strain about nominal level.

	PDG Value
Width (lithography)(±100nm)	0.1dB
Active Region Thickness (±5nm)	0.46dB
SCH Thickness (±5nm)	0.13dB
Waveguide Dispersion (C-band)	0.24dB
Wafer Strain (±50ppm)	0.19dB
PDG TOTAL (MAX)	1.12dB

Table 4.3: Summary of PDG Contributions

The modelling results presented in this section describe the contributions to PDG within an SOA. As introduced in section 3.3.5 strain can be introduced in the wafer to compensate for the PDG. To determine the PDG sensitivity to strain, values were provided pertaining to the average relative gain of TE and TM modes from a selection of wafers with the same design and different strain values. The strain and PDG measurement accuracy was approximately 25 ppm and 0.15 dB, respectively. Figure 4.16 shows how this value varies with strain at 1550 nm with positive values of PDG indicating that TM polarisation is dominant and negative values indicating that TE polarisation is dominant. The scatter in the results is due to process variations. It can be observed that where the wafer has high tensile strain TM polarisation is dominant and where the strain value is low the PDG is TE dominant. The sensitivity to strain is approximated from a linear fit to the sampled range of measurement points as -0.0039 dB/ppm, which, for a wafer specification of 50 ppm, leads to a PDG sensitivity of 0.19 dB.

The analysis in this section describes and quantifies the origin of the major contributions to PDG within an SOA and the results summarised in Table 4.3. To establish initial bounds on what might be practically achieved in terms of PDG performance, the individual contributions can be summed. In practice, this will produce an overestimate as not all of these factors will add cumulatively. In practice better performance can be achieved, as shown in Table 4.1 as low as 0.5dB is commercially available.

Ensuring tight control over all aspects of the manufacturing process will allow SOAs with excellent gain, NF, P_{sat}, and PDG performance to be produced in high volume. The PDG results in variable power into the receiver, but also results in a reduced signal to ASE ratio due to more ASE being generated in the strong polarisation state. This is of particular importance when using avalanche

photodiodes (APD) with wide filters and can limit the sensitivity at low input powers to the SOA. The analysis presented shows the greatest contributing factor to PDG variation is the active region thickness error with tolerances in the required region of ±5nm to maintain PDG of ∼0.5dB which is difficult to achieve in bulk production; a tolerance of ±10nm is a realistic expectation for repeatability. A PDG of 0.5dB - 1dB is consistent with commercially available devices with a gain of ∼20dB (see Table 4.1). Further work on this has been published in [95] where PDG has been experimentally measured versus gain and drive current.

4.3 Optimised Gain, Polarisation Insensitive SOA in a PON Link

As introduced at the start of this chapter the inclusion of an SOA into GPON is desirable to increase the reach of the network. To increase this link budget as much as possible the preferred SOA will have high gain, low noise figure and low polarisation dependence. In this section an optimised gain, polarisation insensitive SOA has been designed and experimentally measured to demonstrate the possible improvement to the reach of a PON.

The following section describes an SOA with a comparably high gain to those presented in Table 4.1 with high saturation output power, improved polarisation dependence and low noise figure which is applicable for improvement of a GPON.

4.3.1 High Gain SOA Details: Fabrication and Characteristics

The SOA designed for the GPON margin improvement experiments was an InP-based buried heterostructure with 1.2μm wide and 0.2μm thick InGaAsP tensile strained bulk active region orientated at 10° to the cleavage plane. The device was 800μm in length and the active region has been tapered linearly in the lateral direction from 1.2μm to approximately 0.45μm over 80μm approaching the facet to optimize the coupling to fibre. Antireflection coatings were deposited on each facet of the device before they were hermetically sealed in a butterfly package. The device was designed for amplification around 1300nm as illustrated by the ASE spectrum shown in Figure 4.17. SOA gain ripple, caused by residual reflections

from the SOA facets, can be observed in this graph.

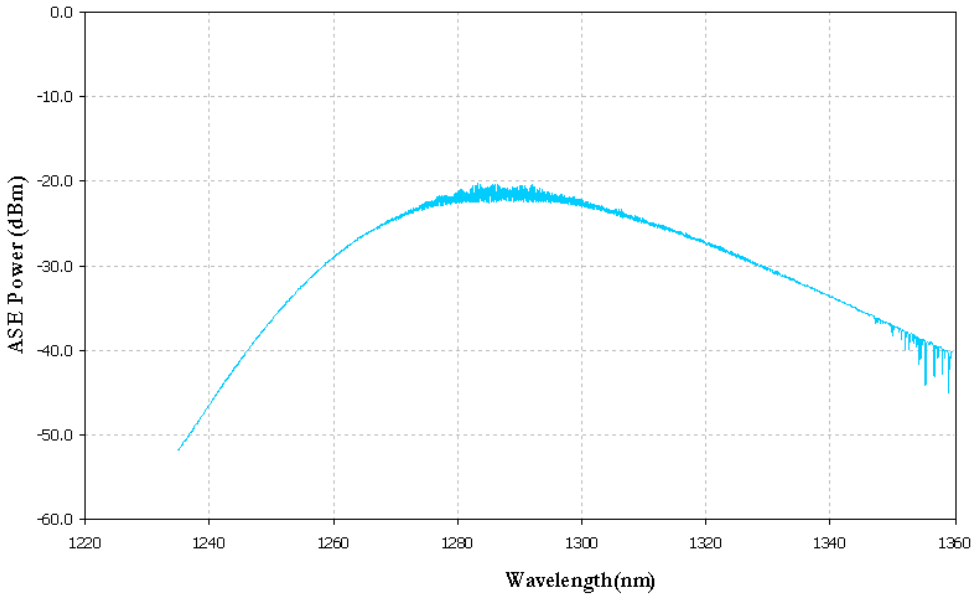

Figure 4.17: High Gain InGaAsP SOA: Amplified Spontaneous Emission Spectrum.

Figure 4.18 shows that between the wavelengths of 1300nm and 1320nm the device has a minimum gain of 24.5dB at an operating current of 200mA. Figure 4.19 shows the P_{sat} value of the device is 13dBm and noise figure (including fibre coupling issues) is less than 7dB and the polarisation dependent gain less than 1.75dB as shown in Figure 4.20. Specifically at the GPON upstream wavelength of 1310nm the device has a gain of 28dB, polarisation dependence of 1.06dB and noise figure of 6.7dB. This SOA has been designed to produce high gain and to have a low polarisation sensitivity as analysed in section 4.2 and [95].

4.3.2 Receiver Modelling

A receiver for a PON should have a high sensitivity to the emission wavelength range of the light signal, minimise the addition of noise to the signal and have a fast response speed. Both PIN and APD receivers are suitable detector types for PONs (see section 2.2.4). The sensitivity is defined as the minimum acceptable average received power level to achieve a BER of $1x10^{-9}$. This sensitivity does not include power penalties caused by any optical path effects, these are specified separately in GPON standard of being a maximum of 1dB.

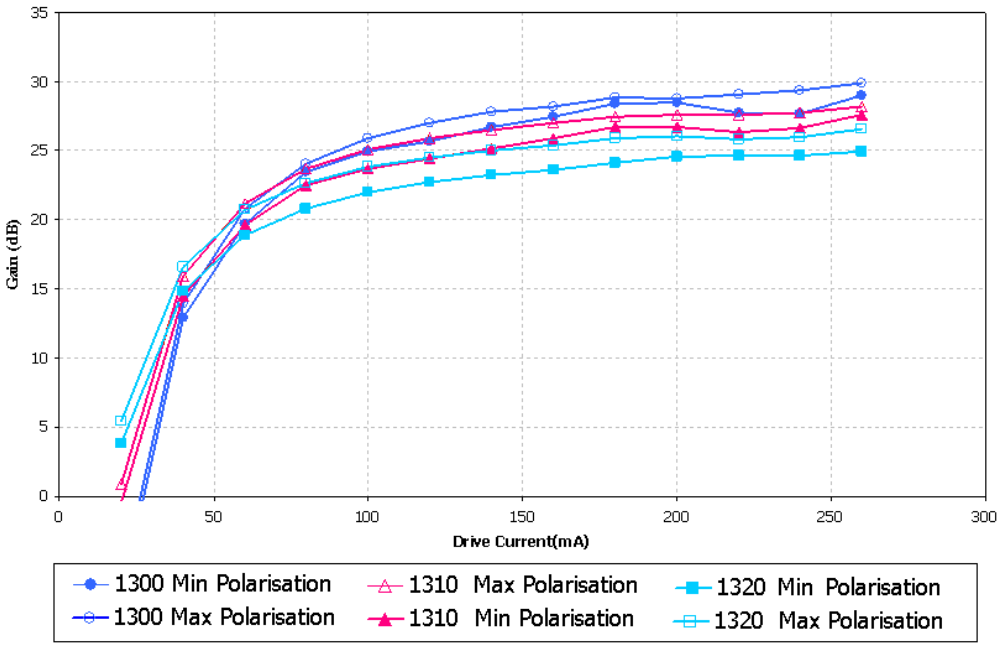

Figure 4.18: High Gain InGaAsP SOA: Gain versus Current.

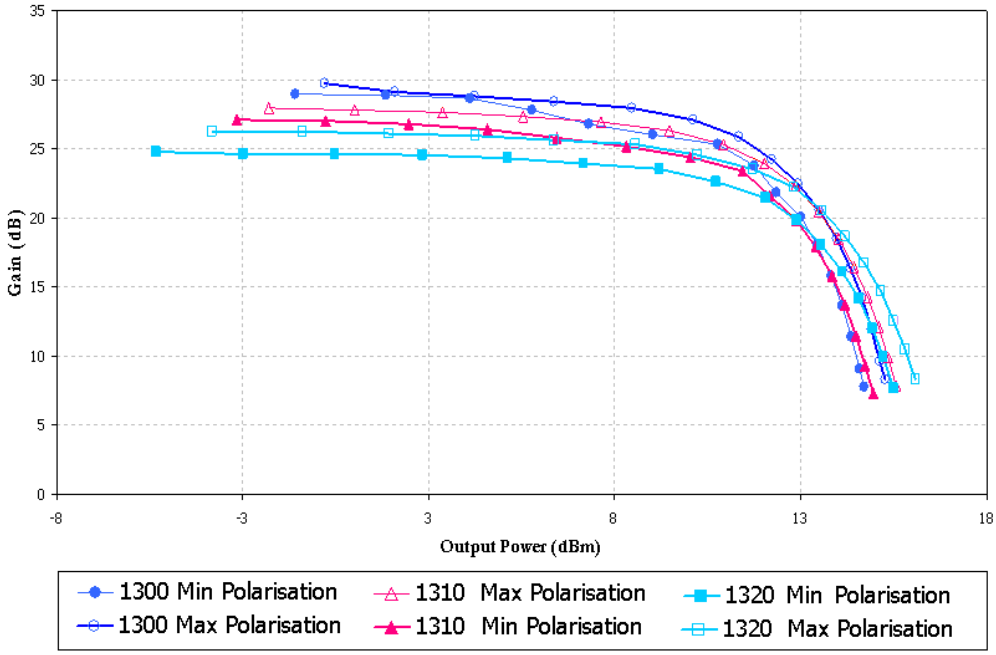

Figure 4.19: High Gain InGaAsP SOA: Gain versus Output Power.

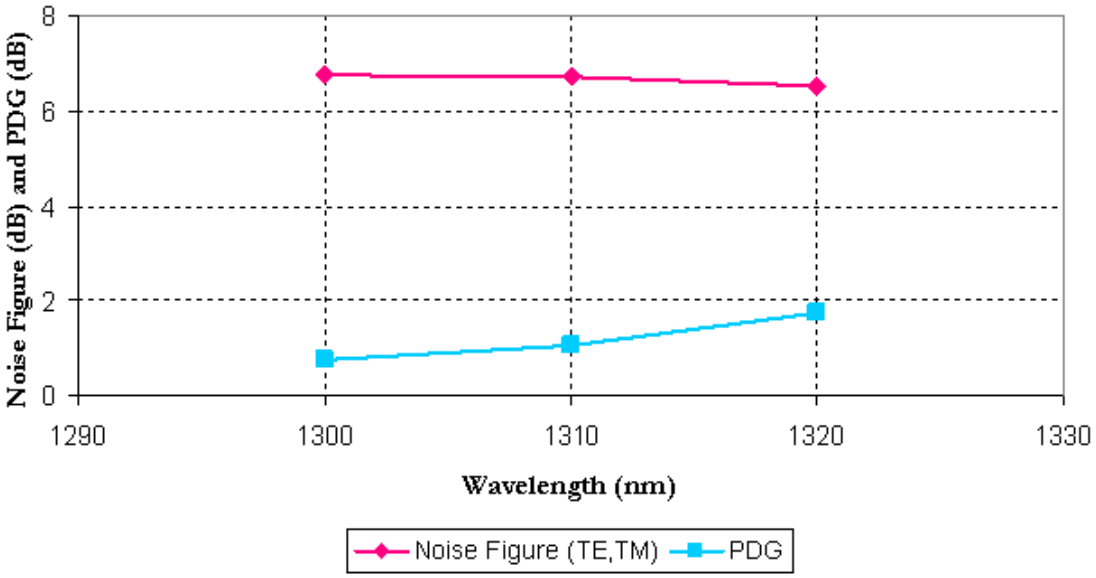

Figure 4.20: High Gain InGaAsP SOA: Noise Figure and PDG Characteristics at 160mA.

The influence of amplification on a PIN and an APD receiver have been modelled in [6]. This is shown for the received power and extinction ratio for various filter widths in Figure 4.21. As the filter width increases the ASE has a greater influence on the extinction ratio as it will contribute significant energy to the 'zeros' in the transmission, i.e. a DC offset. In a high gain (>20dB) amplifier this can be more than 0dBm.

In the case of GPON, where a filter width of 20nm is specified in the standard, the benefit accrued through optical amplification has been reduced by between 7dB–8dB versus that with a narrow filter width of 1nm. A clear correlation between degradation in performance and reduction in extinction ratio is evident.

Yin et al. [96] experimentally compared the sensitivity of an APD and PIN receiver and reported a 15dB improvement of the APD sensitivity over the PIN receiver. This can be translated to a 10km longer link with the APD receiver than the PIN assuming fibre attenuation of 1.5dB/km. The experiments in this section use an APD receiver to gain additional link margin over that achievable using a PIN receiver termination.

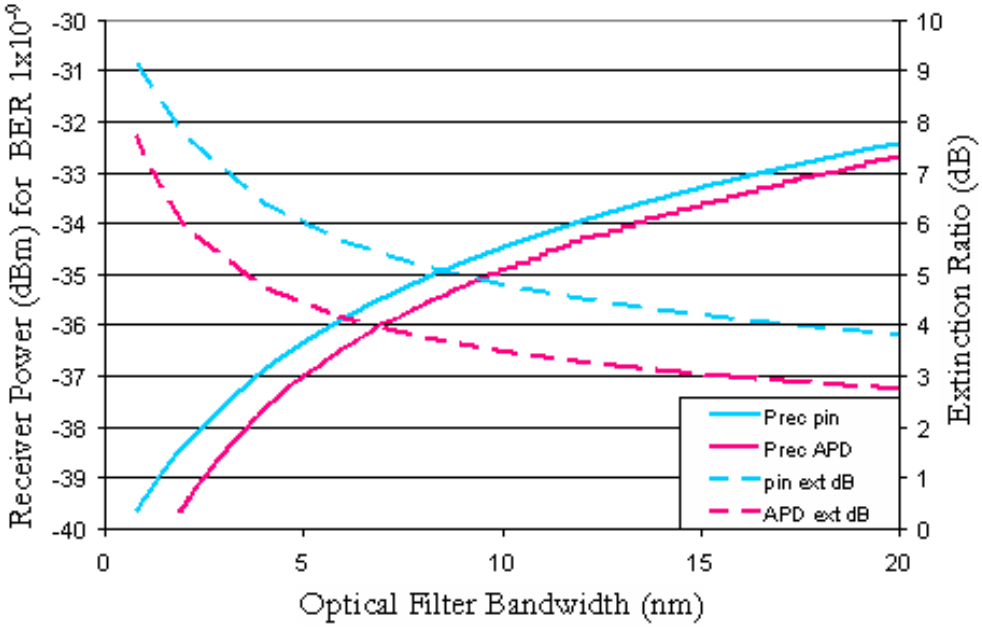

Figure 4.21: PIN VS APD from [6].

4.3.3 Systems Experiments

GPON specifies different bit rates at different wavelengths for upstream and downstream transmission, 1.25Gb/s at 1310nm and 2.5Gb/s at 1490nm respectively. The results presented are solely measured at the appropriate bit rate at 1310nm due to the limitation in available detection equipment at 1490nm.

To obtain an accurate benchmark of performance the back to back (BTB) receiver sensitivity is measured. The ideal BTB measurement has a sensitivity of -28dBm to mimic the maximum loss of the standard [97]. Figure 4.22 illustrates the experimental setup for the BTB measurement. The system characterisation at 1.25Gb/s is shown in Figure 4.23 which yielded a -28dBm receiver sensitivity without the SOA. This Figure also shows the influence of optical bandwidth on receiver sensitivity, the experimental arrangement for this measurement is also shown in Figure 4.22. As the filter bandwidth decreases, the average power hitting the receiver decreases also as the ASE power to the receiver is increasingly filtered out. The extinction ratio will therefore increase and so overall performance can be seen to be improved. The current GPON filter standard is 20nm bandwidth however a power improvement of 4dB can be seen through the introduction of the 10nm filter over the BTB power. This echoes the relationship shown in Figure 4.21.

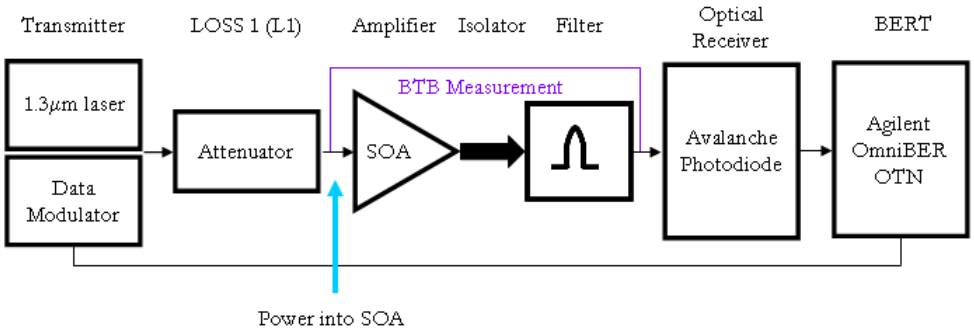

Figure 4.22: Experimental Method for BTB and Sensitivity Measurements

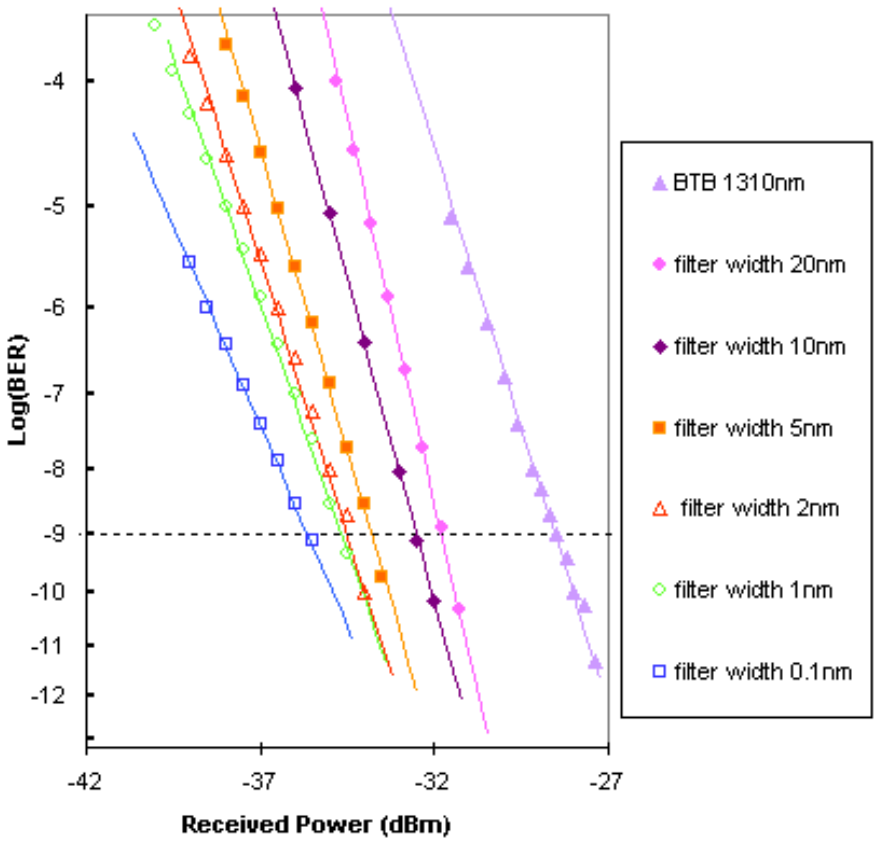

Figure 4.23: Back to Back sensitivity of system at 1310nm with a bit rate of 1.25Gb/s and the influence of various filter widths on the system.

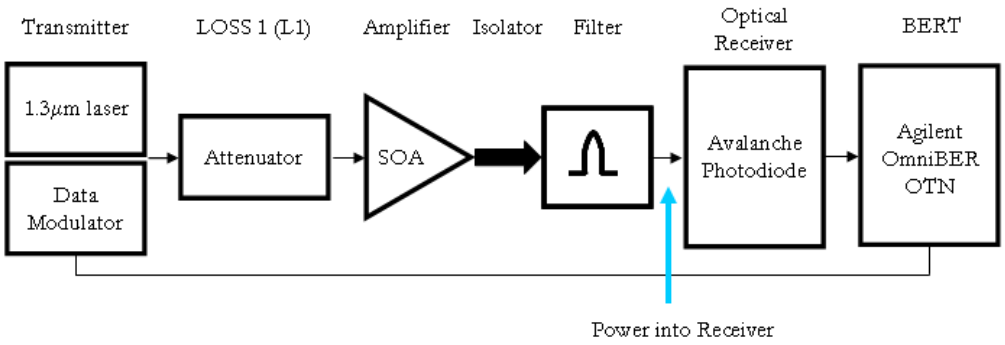

Figure 4.24: Experimental Method for BER Measurements for varying SOA input powers.

Figure 4.25 shows the measurements of the system for various powers injected into the SOA with a filter width of 20nm. The experimental arrangement for this is shown in Figure 4.24. The SOA with an input power of -15dB produced a BER of $1x10^{-9}$ with a received power of -22.5dBm, showing a power penalty of 9.3dB. An improvement on this can be seen by increasing the SOA input power to -20dB (-27dBm) and -25dB (-28dBm). The SOA launch power of -29dB however has a sensitivity of -25dBm producing a penalty of 6.8dB over the filtered system value. As shown in Figure 4.23 insertion of a smaller filter into the system would improve the sensitivity further. The effect of the increasing attenuation on system margin is discussed in the following section.

Figure 4.26 shows a schematic of the SOA testbed which was used to mimic a PON link. L1 represents the attenuation incurred before the amplifier; such as trunk fibre loss from the OLT to the splitter. L2 denotes the losses incurred after the amplifier; related to splitting losses and fibre attenuation to the terminating premises. A 20nm bandpass filter is included, in accordance with the filtering in a GPON network, to allow for manufacturing tolerances and the effects of temperature drift on carrier wavelength.

In order to measure the increased reach of the PON with the addition of an SOA into the network, a test system was setup to measure the maximum margin for a bit error rate (BER) of $1x10^{-9}$ while varying the losses experienced by the 1310nm, 1.25Gbit/s signal before and after the SOA, which was biased at 150mA. The testbed consisted of a tunable 1.3μm laser combined with an external data modulator as the transmitter. This signal was then attenuated to represent L1 before insertion to the SOA. The signal was transmitted through an optical

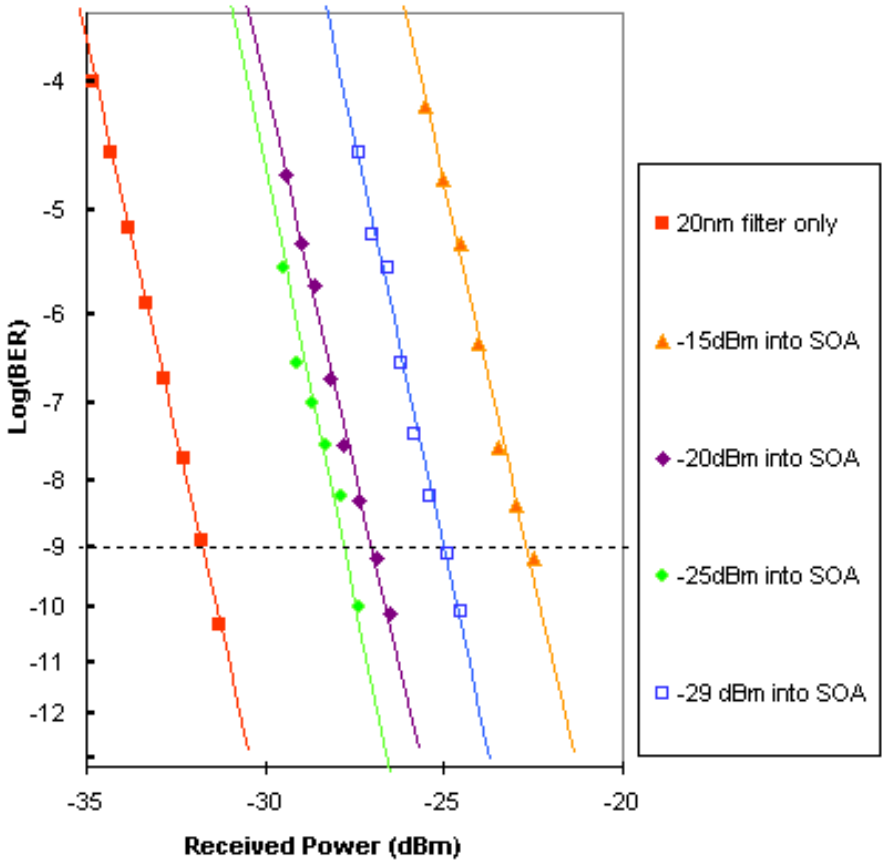

Figure 4.25: BER curves plotted as a function of received power at 1310nm with a bit rate of 1.25Gb/s with a drive current of 200mA and a 20nm filter for varying SOA input powers.

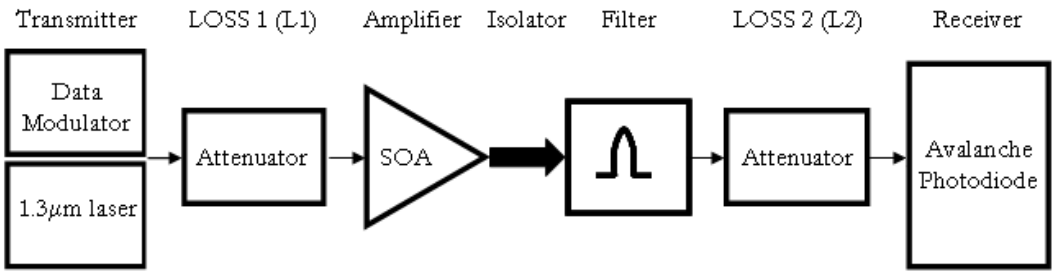

Figure 4.26: Modelling and Experimental Arrangement.

isolator and filtered before being attenuated again after the SOA to mimic L2 and received by an APD. This enabled both the post amplification dynamic range and the power penalty associated with amplification to be measured.

The maximum power that could be delivered into the SOA was limited to around -6dBm as the experiments were conducted using a combination of a laser plus external modulator as a transmitter and the modulator insertion loss was around 6dB. The maximum power that could be delivered into the receiver was -9dBm.

4.3.4 Effect of Optical Filtering and Varying Attenuation on System Margin

Figure 4.27 shows eye diagrams of the device output at input powers of a) -29dBm, b) -19dBm and c) -9dBm. The increase in intersymbol interference (ISI) can clearly be observed with increasing input power. Figure 4.27(a) has a low input power and so the extinction ratio is small, Figure 4.27(b) has a higher input power, greater extinction ratio with initial signs of overshoot and Figure 4.27(c) has high input power, even greater extinction ratio but shows a large signal distortion. It can also be observed that the 'zero' line is moving further away from the ground line for increasing input power; this is due to the increase of ASE in the system.

As the input power increases the ISI increases as can be clearly seen in both the 'zero' and 'one' lines in Figure 4.27(c). This increases the probability of bits being detected erroneously.

PON systems include optical filters at the ONU. The width of these filters can affect the noise on the receiver due to the ASE bandwidth collected from the amplifier. The ASE contributes significant energy to the 'zero line' in the transmission and so it has been investigated how the filter width effects the system extinction ratio.

Figure 4.28 shows the power measured incident upon the receiver for matching the losses for a BER of $1x10^{-9}$ with three different optical filter widths. Using the experimental setup shown in Figure 4.26 the power into the SOA (L1) was set for each point on the x-axis while the second attenuator after the filter (L2) was also varied for each point on the x-axis until the power incident upon the receiver was a BER of $1x10^{-9}$.

L1 could not be measured below 6dB as this is the modulator insertion loss

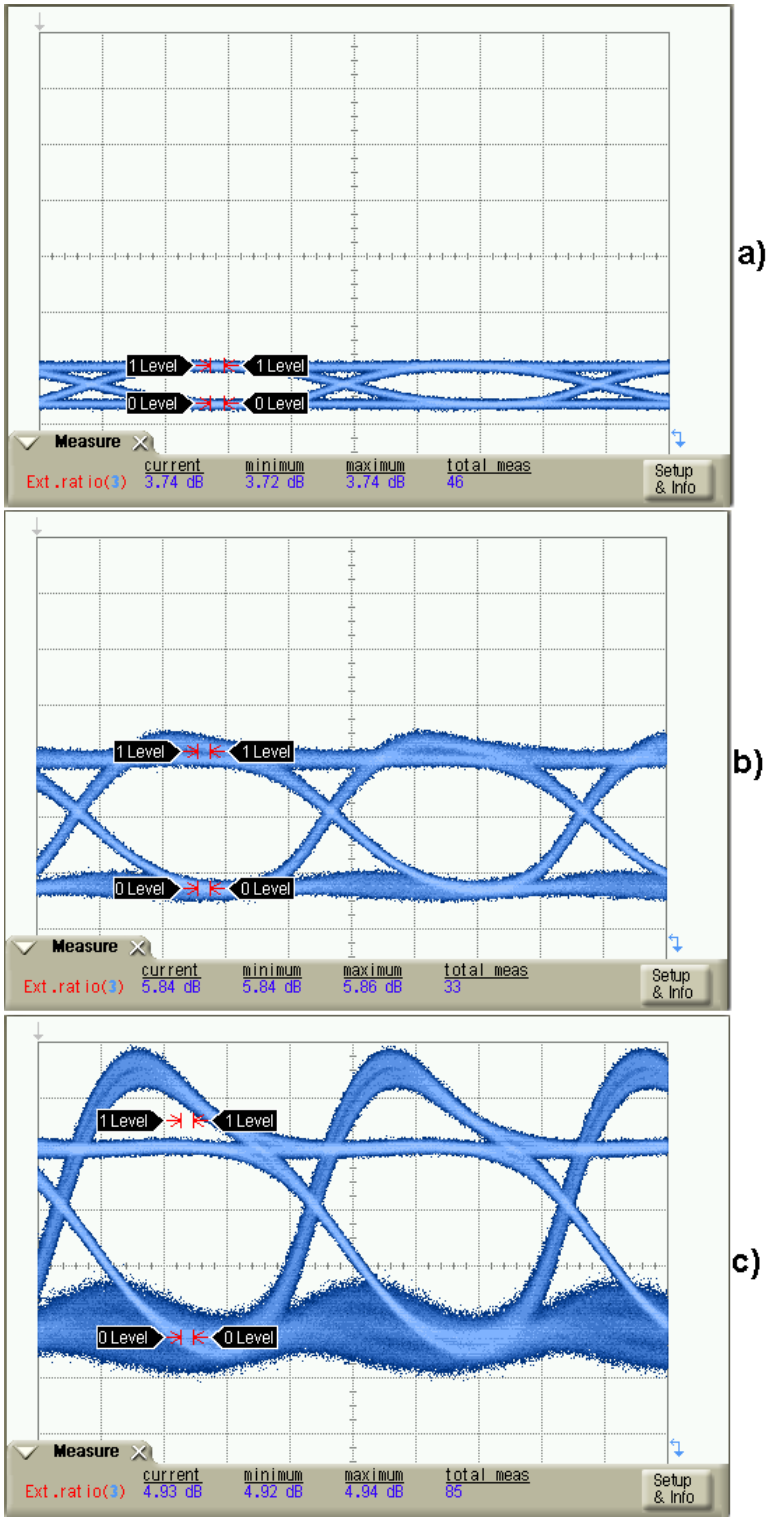

Figure 4.27: Patterning effects for various input attenuation at 1.25Gb/s on Figure 4.29: (a) high input attenuation: Pin = -29dBm, (b) medium input attenuation: Pin = -19dBm, (c) low input attenuation: Pin = -9dBm.

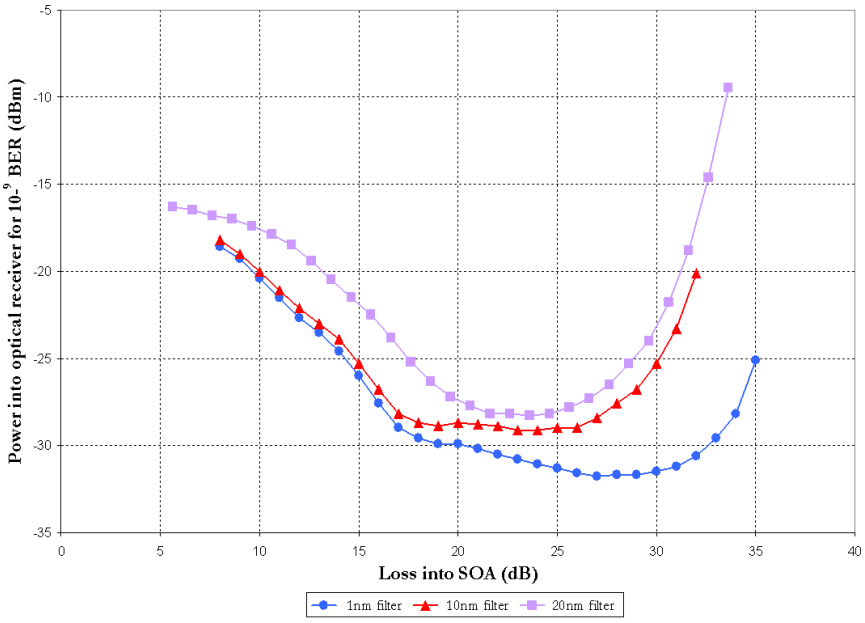

Figure 4.28: Power onto the APD receiver for BER of 1x10^{-9} for three optical filter bandwidths.

and the maximum power that can be measured onto the optical receiver (L2) is -9dBm as this is the APD maximum value. As expected the narrower the filter width allows for an improved sensitivity as it reduces the ASE beat noise components and also reduces the DC offset that ASE can produce. The 1nm, 10nm and 20nm filters produce maximum sensitivities of -32dBm, -29dBm and -28dBm respectively, with the performance at high input powers converging as at this point the system is not noise limited. At high input attenuation to the SOA the 1nm filter shows vastly improved performance over the wider filters as this filter will block out more of the system noise.

4.3.5 System Margin Improvement Results

Figure 4.29 shows the variation of the loss before (x-axis) and after (y-axis) the SOA for a measured BER of 1x10^{-9} and the power measured onto the APD receiver for these losses. The results on this graph are restricted by the modulation insertion loss (6dB) and the maximum power to the APD receiver (-9dBm). The green dashed line is the unamplified system margin of 28dB.

In the case where the amplifier is acting as a booster there is high power

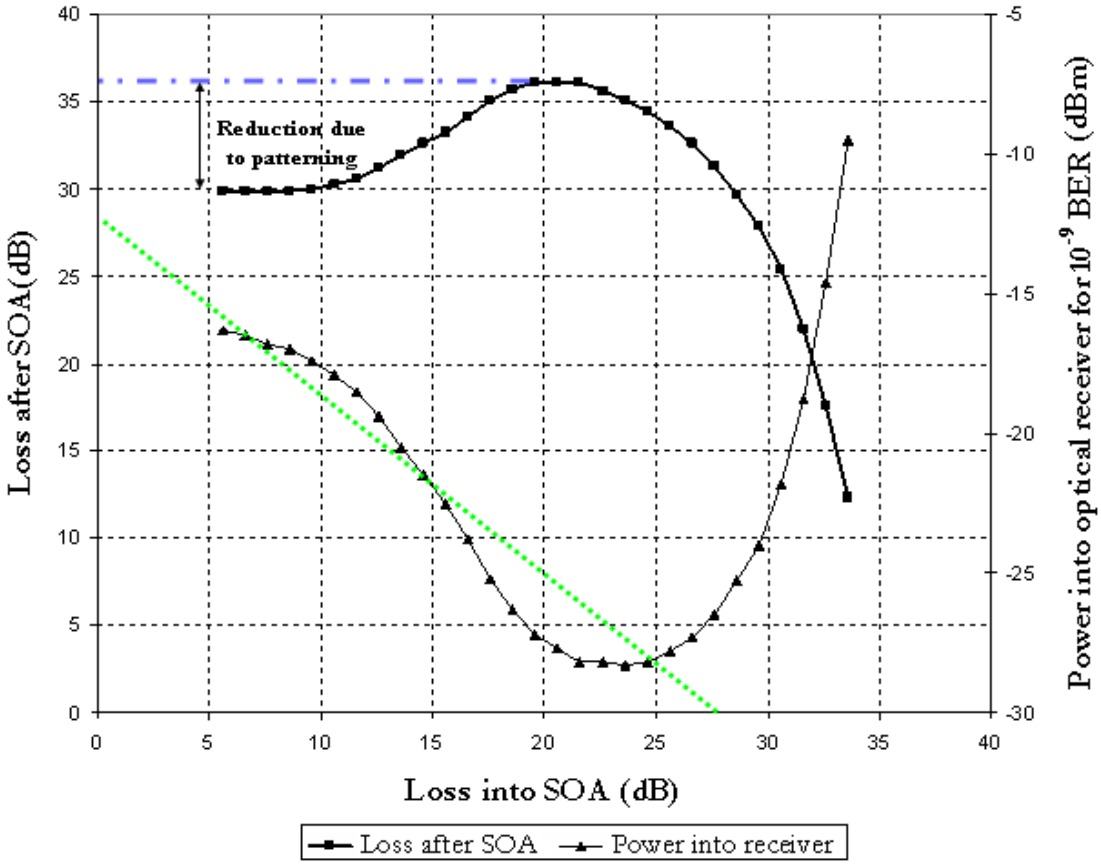

Figure 4.29: PON System Margin Experimental Investigation.

and small input losses to amplifier, the loss that can be compensated using the SOA is limited by the P_{sat} of the SOA. The reduction from the maximum value is due to the fact that the system performance in this region is dominated by the amplifier dynamics associated with gain recovery (patterning) as was illustrated in Figure 4.27(c).

In the other extreme of operation when the SOA is operating as a preamplifier, the maximum loss that can be tolerated into the SOA equates to around 33dB. In this scenario, the benefit that is derived from amplification is limited to around 5dB (the difference in sensitivity between the APD and the amplified APD). The post amplifier loss that can be tolerated here falls off very sharply in the region 32–34 dB input loss. This is because the extinction ratio has degraded to the point where the power penalty increases asymptotically and the addition of amplification brings no further benefit. In this mode of operation the output power must be carefully controlled in order to protect the APD from damage due to excessive power. Operation in this region can be considered to be less stable as the system is highly sensitive to small changes in input power as can be seen from the steep roll off of the system margin. The rapid degradation of extinction ratio, as a consequence of the significant ASE power on the zeros, explains the origin of this rapid loss of margin. This can be improved with tighter optical filtering but this is not accommodated within the GPON specification. When the SOA is operating in a mid-span position the pre- and post- amplification losses are balanced out.

It can be seen that the diagram has the general form as anticipated in Figure 4.2 with the margin increase being maximized at high values, >20dB, for L1 and L2. The main difference is the introduction of a power penalty when the SOA input power is high; gain modulation results in ISI. Due to the very high device gain, the system margin is reduced at low values of L1. The impact of amplification position is shown more clearly in Figure 4.30 where the difference between an unamplified PON and amplified PON of Figure 4.29 is plotted as a function of the loss that precedes the amplifier input. The performance enhancement of the booster is low due to the patterning effect. Thereafter, as the loss increases, greater benefit from amplifying the signal is seen, rising to the point where the system margin increase is equivalent to the amplifier gain. A total system margin of 56dB was achieved due to the high gain SOA. This corresponds to a record margin increase of 28dB from the unamplified system. The benefit drops sharply

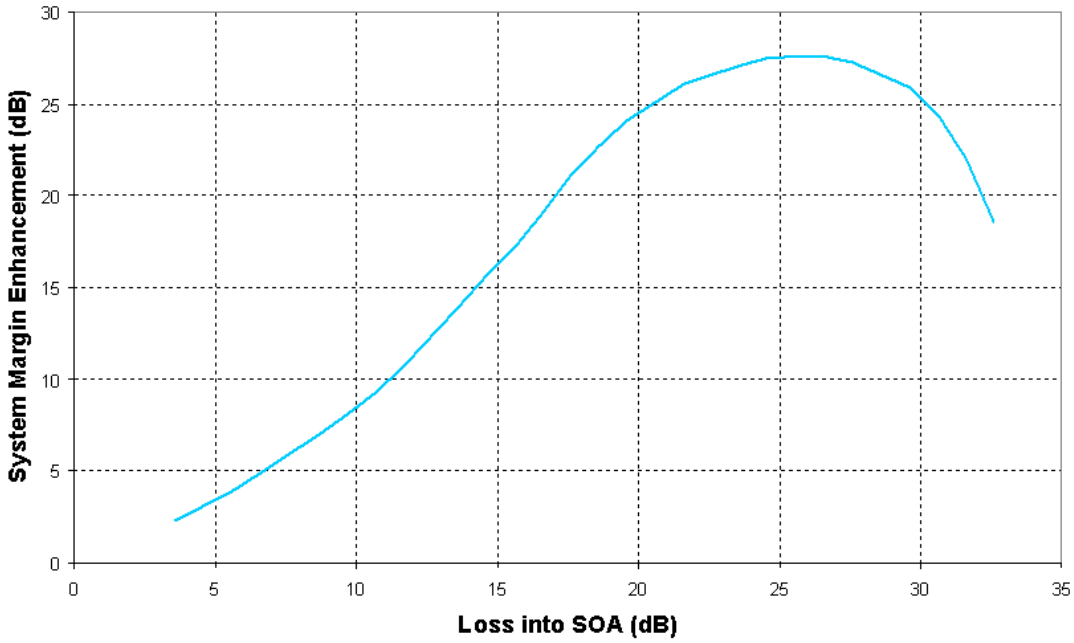

Figure 4.30: System margin enhancement due to amplification.

as the losses increase to the point where the extinction ratio diminishes.

In order to reduce this effect, the designed gain of the SOA can be reduced to increase the saturation input power by decreasing the cavity length or reducing the confinement factor. Alternatively, quantum dot devices have been shown to be less prone to patterning and may reduce this power penalty [98, 99]. Another option is to consider SOAs with the capability to provide adjustable gain-clamped operation [100]. Another option is the addition of attenuation in the extender box but this must be designed with care and is undesirable from a cost perspective. A total system margin of 56dB was achieved due to the high gain SOA. This corresponds to a record margin increase of 28dB from the unamplified system.

4.4 Conclusions

In this chapter the requirements for SOAs to extend the reach of PONs have been defined and the parameters of commercially available SOAs have been presented. Following this a series of modelling was undertaken to determine the viability of mass production of low PDG SOAs with high gain as per the requirements for PONs. Polarisation dependent gain impinges the signal to noise ratio

in high gain devices thus it is desirable to manufacture high gain devices with low PDG. The greatest contributing factor to PDG variation is shown to be the active region thickness error which in bulk production needs to be grown to a tolerance of ±10nm to maintain PDG of ∼1dB; consistent with commercially available devices.

A high gain, polarisation insensitive SOA has been designed, fabricated and experimentally tested in the context of improving the margin and hence the reach a PON link. A device with high-gain should be located mid-span; if positioned as a preamplifier or as a booster a high gain device will degrade the system. The SOA was positioned as a mid-span amplifier in the link and was shown to improve the margin by a record 28dB.

Also it has been shown that the power transmitted during a 'zero' produces significant effect and that the extinction ratio of the received signal is considerably degraded where limited optical filtering is employed. In a typical PON with a filter width of 20nm, this will produce a performance penalty due to the additional noise terms and also due to the loss of extinction ratio. The overall power penalty can be in the region of 8–9dB.

Gain modulation sourced ISI is shown to limit performance of the SOA at high input powers. To further improve the margin of a PON link, high gain SOAs which are less prone to patterning can be considered, such as those with different active region materials or those with the capability to provide adjustable gain-clamped operation. Quantum dot SOAs have been reported to be less susceptible to patterning and so the carrier dynamics of these can be investigated to evaluate their possible benefit to a GPON system.

Chapter 5

SOA Gain and Phase Measurements

Section 4.1.2 specified the requirements of an SOA to extend the reach of a passive optical network. The ideal scenario is to develop an SOA optimised to operate at all locations in the link. The previous chapter presented measurements on bulk InGaAsP SOAs. These were shown to be susceptible to gain modulation sourced ISI (patterning) which introduced a power penalty thus limited their performance at high input powers. Chirp due to gain modulation can also degrade the performance of the SOA. The reduced performance of the SOAs limit the capacity for reach extension of GPON and 10G-PON (10Gbit/s downstream and 2.5Gbit/s upstream).

SOAs with an active region under quantum confinement such as Multiple Quantum Well (MQW) and Quantum Dot (Qdot) are reported to be less susceptible to patterning due to their higher saturation power and shorter carrier lifetimes, respectively. This chapter investigates carrier lifetime and patterning in bulk, MQW and Qdot SOAs to further improve the margin of GPON.

This chapter reports the origin of patterning in SOAs and reviews the reports in literature of Qdot SOAs overcoming patterning. The launch power in the experimental scenario is evaluated in order to mimic the GPON system. Experiments using the spectrogram technique compare the amplitude and phase recovery times and the α-factor values of bulk, quantum well and quantum dot SOAs. Conclusions are reported in the context of reducing or eliminating patterning to extend the reach of GPON through the introduction of amplification with reduced dimen-

sion active region SOAs.

5.1 Optical Gain Saturation

It has been shown previously that at high input powers SOAs exhibit a waveform distortion which can restrict their operation (sections 2.4.3 and 4.3.4). This is a particular issue in optical networks with high bit rate applications. If the time between the input pulses to the SOA is shorter than the carrier recovery time of the SOA then the gain will not be able to recover completely, resulting in carrier depletion thus reduced optical gain at high input powers. The gain of a given pulse is dependent on the pattern of the pulse train entering the SOA i.e. it leads to patterning effects. This is known as gain saturation and is illustrated in Figure 5.1.

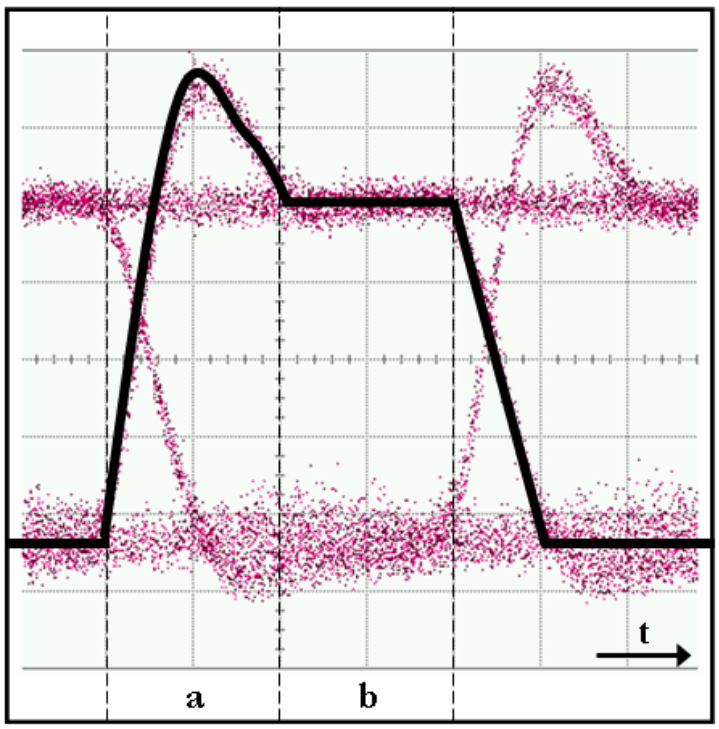

Figure 5.1: Measurement of a distorted pulse from bulk 1300nm SOA at high input power.

If the bit rate is lower than the gain recovery, the leading part of the pulse (Figure 5.1, (a)) is amplified with unsaturated gain, and the output of the trailing part subsequently decreases as the SOA gain saturates (Figure 5.1, (b)). At high

bit rates the amplifier gain does not return to the unsaturated value and even the leading part is amplified with a partially saturated gain value [101].

Uskov et al. [102, 103] state the patterning effect that occurs in conventional SOAs (bulk or quantum well) when operated in the gain-saturation regime can be overcome using quantum dot SOAs. At high pump currents the Qdot ground state is filled and large carrier populations are accumulated in the Qdot upper levels and wetting layer (WL) i.e. the upper states work as carrier reservoirs [68]. If sufficient carriers are accumulated in the WL then carrier depletion is no longer an issue and the patterning effect is minimised. This has been defined as 'Pattern-effect-free' (PEF) amplification and the possibility of high bit rate amplification under gain saturation without patterning has been proposed [99].

PEF amplification is explored further showing interferometers containing QDot SOAs could be effective for ultrafast optical processing with low pattern dependence [98]. The advantage of Qdot SOAs is shown to be the decoupling of gain and refractive index modulation mechanisms in the gain-saturation regime due to the carrier accumulation in the wetting layer. Experimental results in [104] show that the relaxation of the wetting layer carrier density has a strong effect on the phase dynamics and a weaker effect on the gain dynamics reiterating the possibility of PEF amplification utilising Qdot SOAs.

Literature is enthusiastic regarding the opportunities for Qdot SOAs in ultrafast optical processing however it is difficult to gauge if it will be possible to mass produce these devices for commercial purposes. Fabricating polarisation insensitive bulk active region SOAs has been shown to be difficult involving several inter-related parameters. This is even more difficult in Qdot and MQW SOAs as detailed in section 3.3.5.

The ideal comparison for amplification in GPON applications would be the bulk InGaAsP SOAs from Chapter 4 with Qdot and MQW SOA devices operating at 1300nm. However these were not available for the experiments and so bulk 1300nm devices were measured and are compared to bulk 1550nm devices. The 1550nm bulk devices are then compared to Qdot and MQW SOAs at 1550nm.

5.2 Device Structures and Characteristics

There are two bulk InGaAsP SOAs measured in this chapter: one designed to amplify at 1300nm and the second at 1550nm. These are shown in Figure 5.2 and are of similar structure to that described in section 4.3.1, both with InGaAsP tensile strained bulk active region however these were not sealed in a butterfly package in order to be measured in the experimental setup. The 1550nm device is 900μm long with an active region 1.4μm wide and 0.1μm thick. The 1300nm SOA has an active region that is 1.2μm wide and 0.2μm thick and the device is 800μm in length. The 1300nm device does not have SCH as this was not required for confinement at this wavelength.

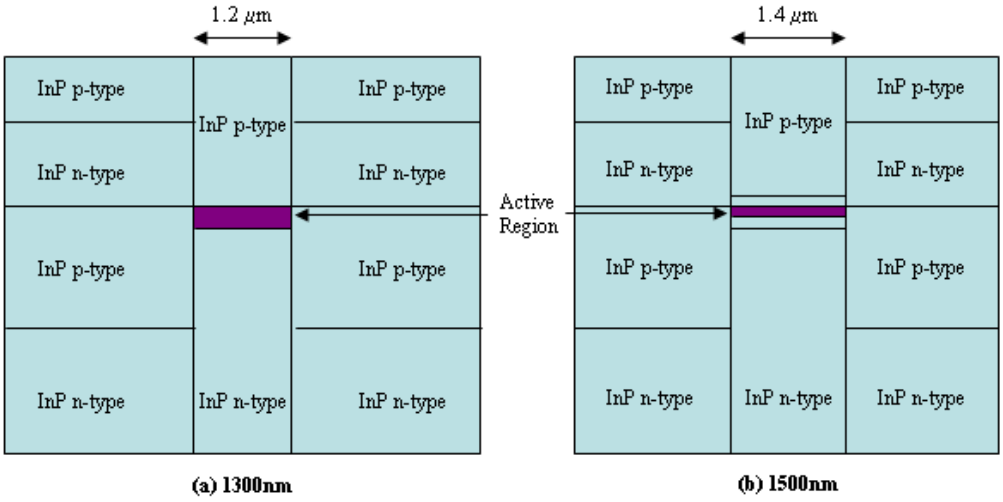

Figure 5.2: Bulk 1300nm and 1550nm structures.

Also measured are a quantum well SOA and a quantum dot SOA that were fabricated in the semiconductor growth facilities in the Institute of Microstructural Sciences, Canada. The MQW and Qdots are very similar in structure to each other as illustrated in Figure 5.3. These are 2μm wide ridge-waveguide devices on InP cladding layers both 1mm long and with antireflection coated facets. The Qdot has a core consisting of five stacked layers of SK-grown InAs dots embedded in $In_{0.805}Ga_{0.195}As_{0.405}P_{0.595}$ 1.15-μm-band-gap barrier layers. The MQW SOA has a core consisting of five $In_{0.805}Ga_{0.195}As_{0.8}P_{0.2}$ compressively strained quantum wells.

Figure 5.4 shows the amplified spontaneous emission spectra of the 1300nm bulk SOA for bias currents increasing in steps of 20mA. At low bias of 10mA the peak is at 1335nm however as the bias is increased the gain peak wavelength

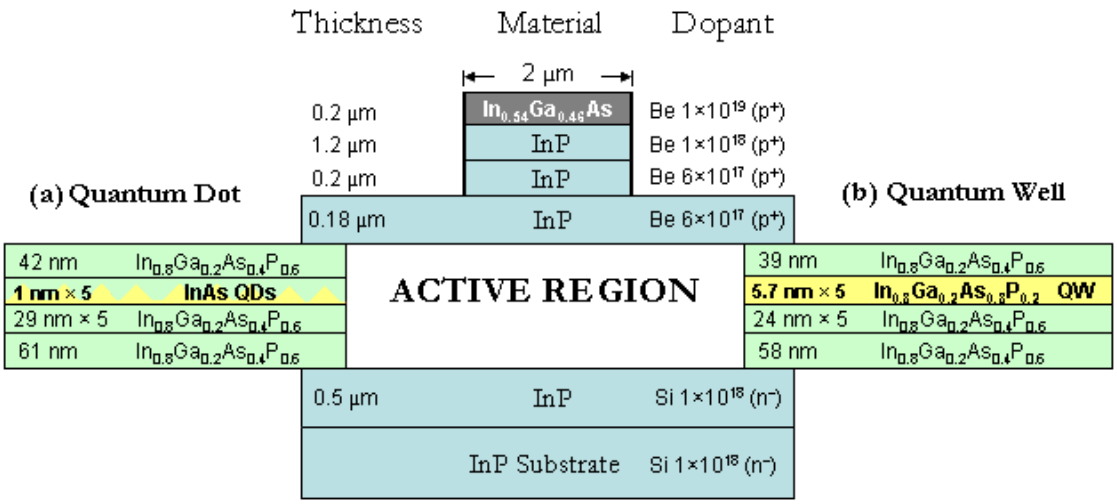

Figure 5.3: Qdot and MQW SOA structures.

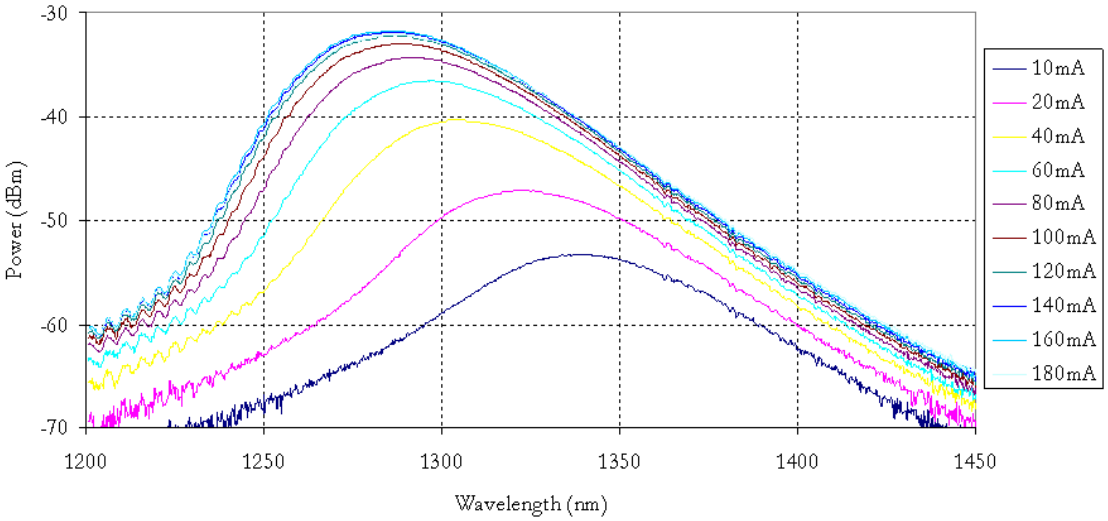

Figure 5.4: 1300nm bulk SOA amplified spontaneous emission spectra varying the injection current.

shifts towards the shorter wavelengths and the spectrum peaks at 1287nm at maximum bias of 160mA. The bulk SOA spectrum has a full-width at half-maximum (FWHM) of 150nm. The ASE for the 1550nm bulk SOA is shown in Figure 5.5. The spectrum can be seen to peak at 1515nm with a FWHM of 150nm when the applied bias is 160mA.

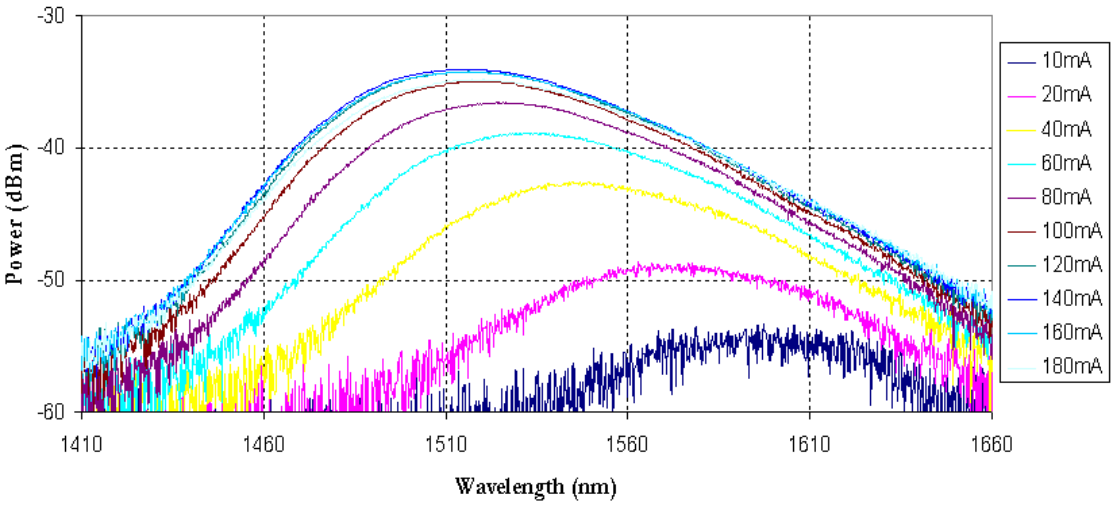

Figure 5.5: 1550nm bulk SOA amplified spontaneous emission spectra varying the injection current.

The ASE spectra emitted from the two quantum confined samples under maximum applied bias are shown together in Figure 5.6. It should be noted that the maximum applied bias of the MQW in the experiments was 50mA, not 100mA as shown in Figure 5.6. The MQW spectrum peaks at 1575nm and the Qdot at 1620nm. The Qdot SOA spectrum has a full-width at half-maximum (FWHM) of 164nm and the MQW has a much narrower FWHM of 72nm. The Qdot emission spectrum should be significantly narrower than the MQW spectrum (see section 3.2.2), but can be attributed to being a series of delta functions at the dot energies that are both homogeneously and inhomogeneously broadened by the dot size distribution [62]. Lower wavelength spectral features at ∼1620 nm, ∼1580 nm, and ∼1540 nm can be observed, which is indicative of a 0D density of states composed of a ground state at 1655nm and three excited states at the lower wavelengths.

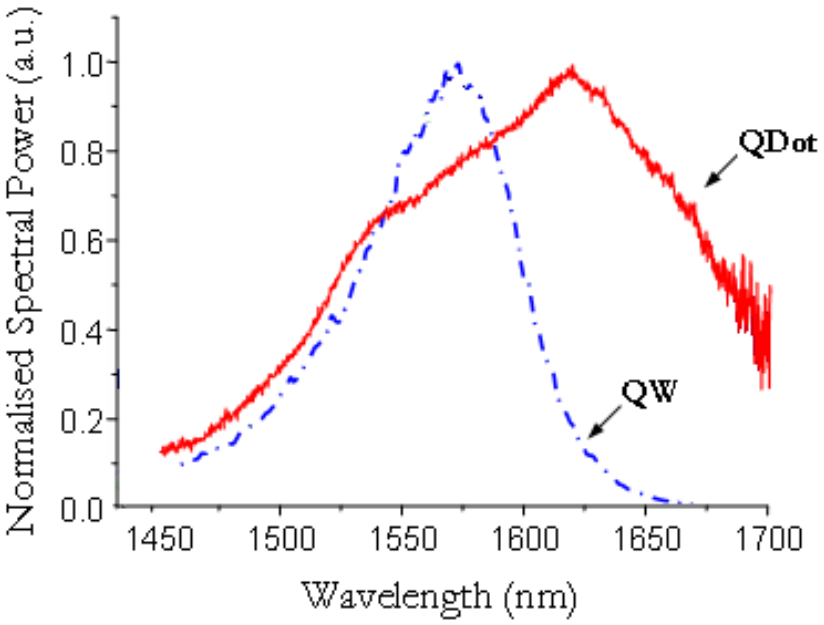

Figure 5.6: Amplified spontaneous emission of MQW SOA at 100mA and Qdot SOA at 150mA.

5.3 Launch Conditions and Optimisation of Power for Measurements in GPON Context

A series of measurements were taken to identify the optimum difference in power between the pump and the probe and the optimum launch power into the device for the pump. These measurements were carried out on a 1550nm bulk InGaAsP SOA using the pump-probe technique.

The generic setup of a pump-probe system outlined in section 3.6.1 is made specific for the setup with wavelength to be used as the discriminator between the pump and the probe, illustrated here in Figure 5.7. An Optical Parametric Amplifier (OPA) that produces 200fs pulses that can be tuned from 930-2300nm at a repetition rate of 100kHz is used as the master pulse source. The required pump and probe signals are obtained by filtering the broad 70nm FWHM spectrum of the OPA pulses with two 3nm bandwidth tunable optical filters as shown in Figure 5.8. Figure 5.9 shows the unfiltered pulse width has been measured to be 600fs. Due to chromatic dispersion (see section 2.2.2) in the fibre of the system, the pulse duration increases to 1.2ps when they reach the test device.

The path of the probe is varied through an automated stepping stage. The

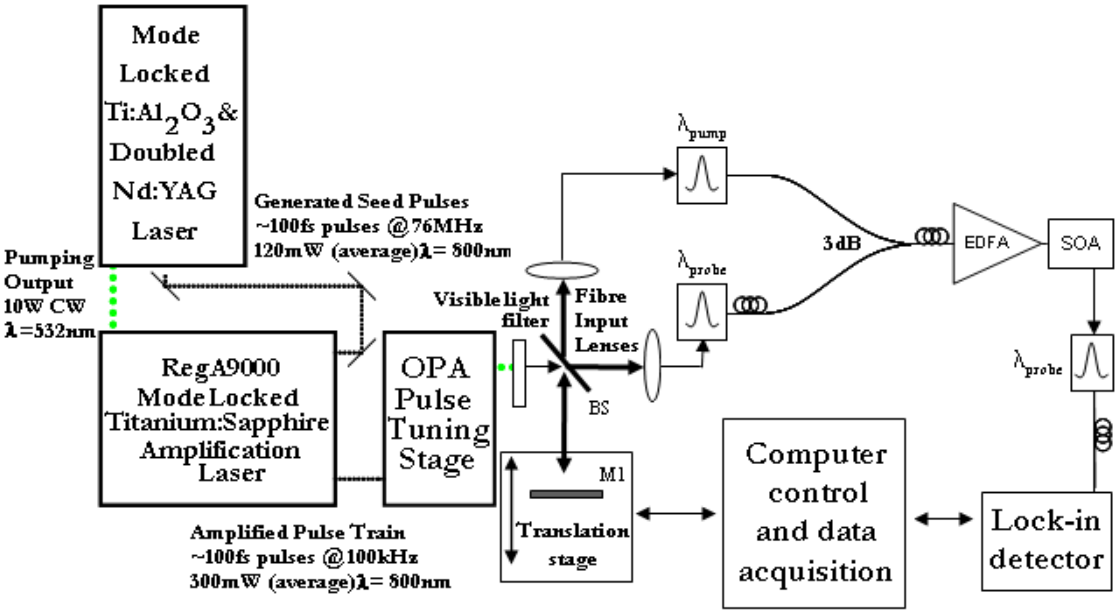

Figure 5.7: 1550nm ultra short pulse generation system and fibre components of the wavelength discriminated pump-probe testbed

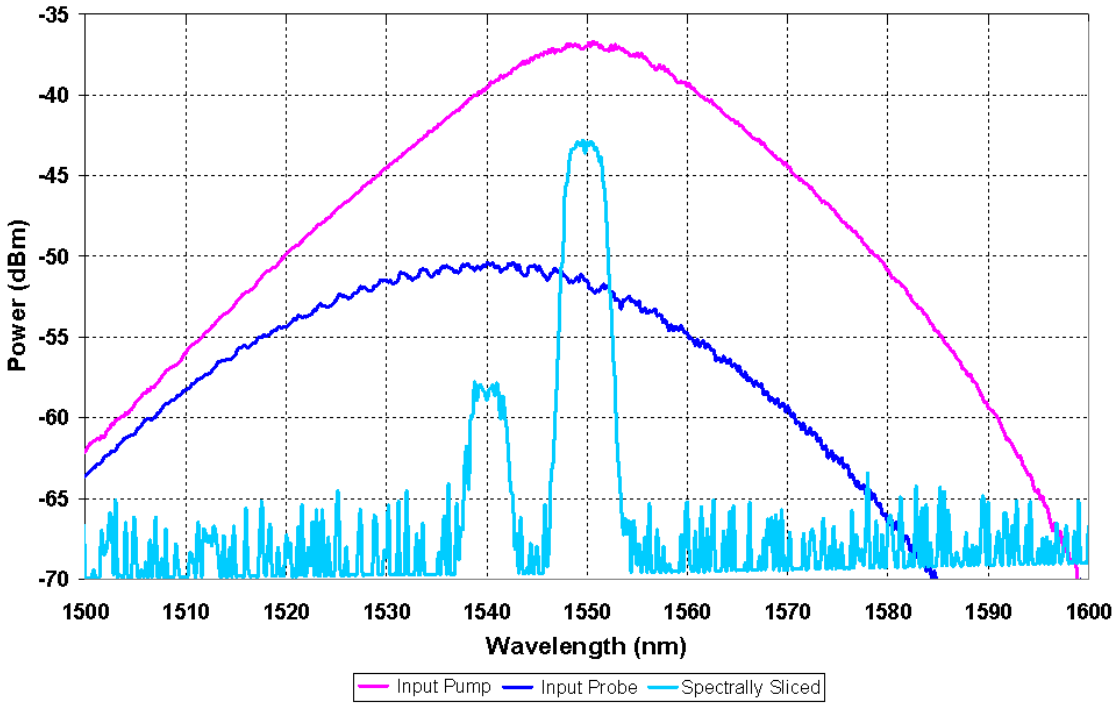

Figure 5.8: Spectra of pulses coupled into fibre and after the slicing stage

probe is selected for detection through wavelength discrimination using the filters. The pulses are then combined using a 3dB coupler, amplified using an EDFA and launched into the test device. On exiting the test component the signals are filtered by a third tunable filter which is used to remove the pump wavelength pulse and pass the probe signal. At each pump-probe delay setting, the modulation of probe transmission is measured by phaselock detection of the probe through the lock-in amplifier. Polarisation controllers are used to correctly orient the polarisation of the signals in the device. In these measurements the pump wavelength was set at 1550nm and the probe wavelength was 1540nm.

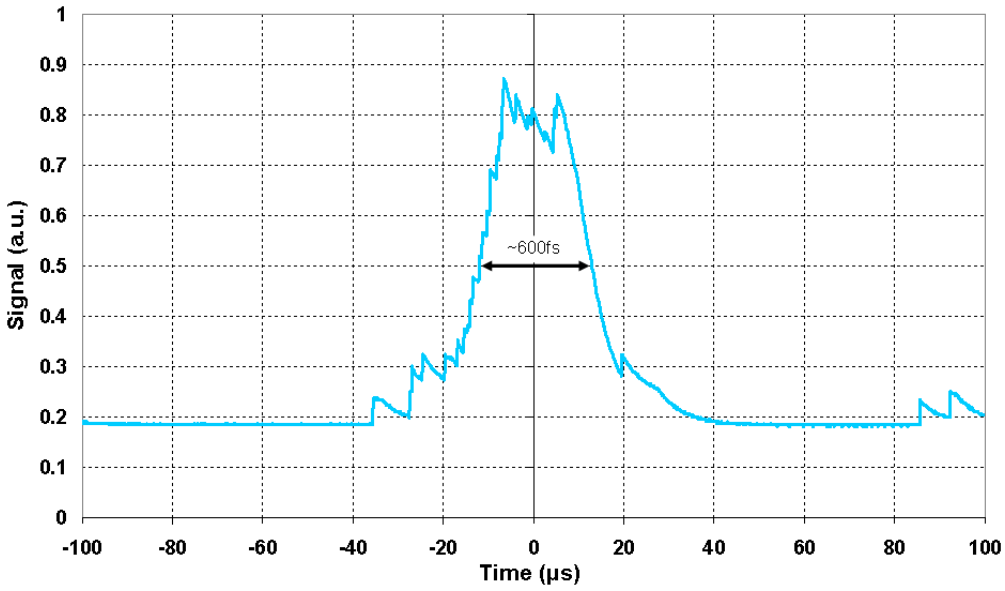

Figure 5.9: Autocorrelation trace of unfiltered pump pulse

Figure 5.10 shows an example amplitude recovery trace in the gain regime. For the purposes of determining a recovery time, the data sets are truncated at approximately 20ps thus removing the coherent artefact and any ultrafast processes, allowing a simple exponential curve fit to determine band filling based recovery rates.

Figure 5.11 shows the effect on carrier lifetime recovery of increasing the difference between the pump (constant at -22dBm) and the probe. The device was biased at 150mA and had a constant input pump power of -40dBm after filtering corresponding to a pulse energy of 1pJ entering the SOA. The probe was varied from -40dBm to -58dBm, the signal was too weak to be resolved below -58dBm. The figure of merit (mean-squared error to the fitting equation) remains

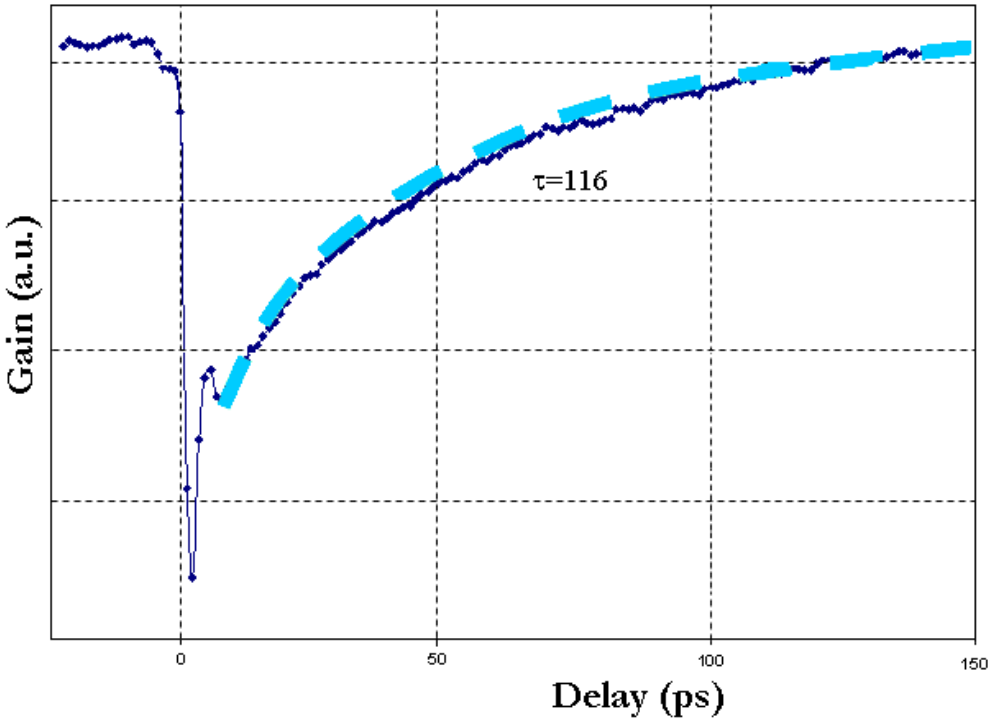

Figure 5.10: Curve-fitting of amplitude pump-probe measurement to find carrier lifetime on a 1550nm bulk InGaAsP active region SOA at 100mA.

insignificant for probe powers above -52dBm, and rises to 4.5% at -56dBm. There is a significant drop of 15ps recovery time for a probe power of -50dBm, which is 10dBm below the pump power. At this launch power it is thought that the probe will be low enough that it will not saturate the device. Following this the power of the probe pulse in future measurements is set to be 10dBm less than that of the pump pulse to ensure that the probe pulse has a minimal effect on the SOA dynamics (unless it is specifically being measured).

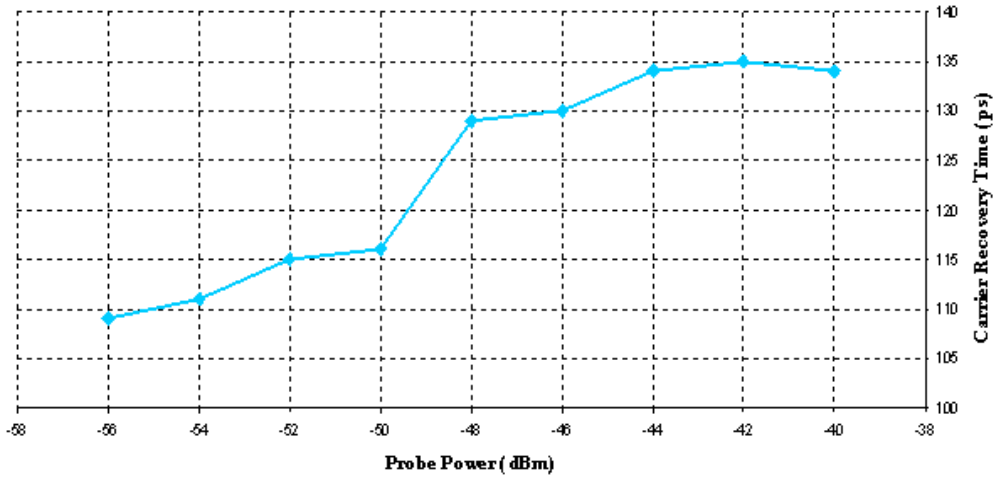

Figure 5.11: Carrier lifetime launch power dependency for constant pump power (-40dBm) and decreasing probe power.

Figure 5.12 shows the effect of reducing the pump power into the device using an attenuator thus keeping 10dBm difference between the pump and probe. This is shown for two different device currents of 100mA and 150mA. The carrier lifetime remains constant for increasing attenuation of up to 5dB as the high pump power is saturating the device. For attenuation greater than 5dB the carrier lifetime decreases considerably, for SOA bias of 100mA, from around 115ps for attenuation of 5dB to 95ps and to 65ps for attenuation of 10dB and 15dB respectively. It is worth noting that the figure of merit increases significantly from 2% at 10dB attenuation to 8% at 15dB attenuation. These results show that it is possible to reduce the carrier lifetime by reducing the launch power; with too much power the probe saturates the device and reduces the carrier density resulting in a larger carrier lifetime, i.e. moving to the left of Figure 3.15.

These results show that future measurements should be taken with lower launch powers to achieve shorter carrier recover times.

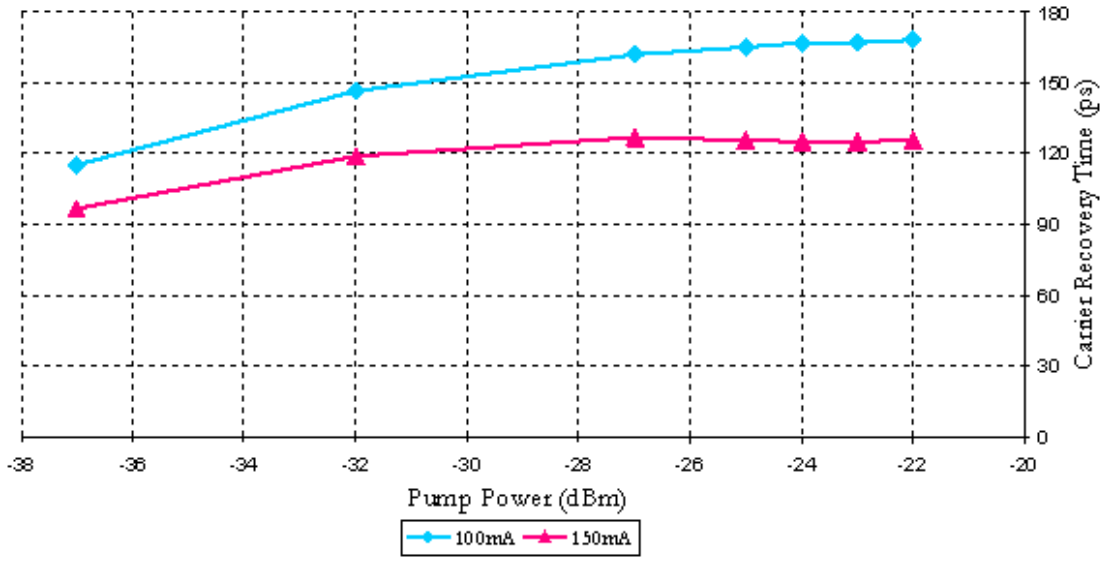

Figure 5.12: Carrier lifetime launch power dependency for constant pump probe ratio of 10dBm.

In these experiments the pulse energy into the SOA generated from the OPA was in the order of 1pJ. This is too high for GPON context and so the measurements to calculate the amplitude and phase recovery times of the SOAs were taken on a more stable system with a higher repetition rate as this results in an improved SNR for the same pulse peak power.

5.4 Spectrographic Experimental Method

The laser source used for the spectrogram measurements is a Ti:sapphire-pumped optical parametric oscillator (OPO), producing a pulse train with 150-fs pulses at a repetition rate of 76.6 MHz. The output of the OPO is tunable from 1200nm to 1700nm utilising different non-linear crystals thus is suitable for the measurements at both wavelengths of interest. Figure 5.13 shows the OPO output with a resolution bandwidth of 0.5nm tuned to two different wavelengths, 1550nm and 1620nm. A spectrographic technique which simultaneously obtains both the temporal amplitude and phase of the SOA optical impulse response similar to that demonstrated by Kang et al [105] was implemented. This technique has been explained in great detail in section 3.8 and makes use of a short intense pump pulse to excite the optical impulse response of each SOA. A weak probe pulse is

then temporally scanned to sample the SOA response.

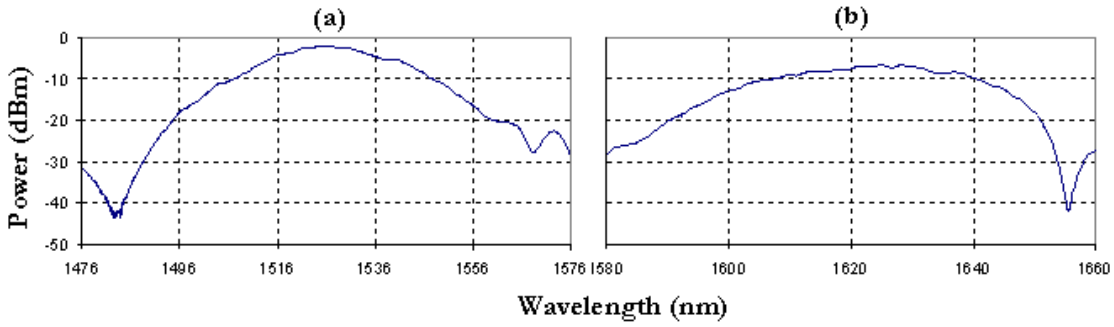

Figure 5.13: Output of the Optical Parametric Oscillator centred at (a) 1550nm and (b) 1620nm

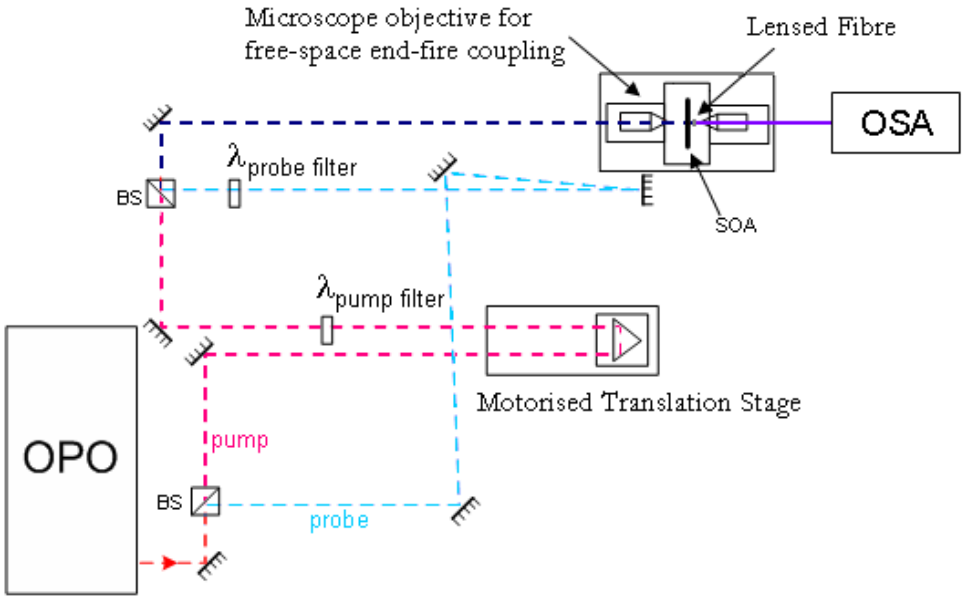

Figure 5.14: Schematic of spectrographic pump probe measurement setup used to characterise of the optical impulse response of the SOAs.

The generic setup of a pump-probe system introduced in section 3.6.1 is made specific for the setup with wavelength used as the discriminator between the pump and the probe, illustrated here in Figure 5.14. The output of the OPO is split into two beams, the pump and the probe, by a beamsplitter (BS). The path of the pump is varied through a 60cm motorised translation stage controlled by the PC so that the pump pulses are delayed an adjustable time, τ, with respect

to the probe pulses. The pulses are then recombined collinearly and coupled into the SOA device under test using a microscope objective. The input power to the SOA device was varied between 100μW and 300μW. On exiting the test component the signal is entered into an optical fibre and input to the optical spectrum analyser (OSA) to record the output at each τ. The probe is selected for detection through wavelength discrimination using the OSA. The spectrogram is obtained by measuring the spectrum of the probe pulses using the OSA as a function of the relative delay between the pump and the probe pulses. The temporal amplitude and phase of both the SOA response and the probe pulse are then simultaneously retrieved from the measured spectrogram using an iterative numerical algorithm [90] as explained in section 3.8.1 thus a phase reference is not required.

5.4.1 Filter Characterisation

As wavelength is the discriminator in this spectrographic technique, two glass bandpass filters were used to select the required wavelengths of the pump and the probe. Figure 5.15 shows the unfiltered pump input to the device and the characterisation of a 1300nm filter. 1250nm and 1280nm were selected for the wavelengths of the probe and pump respectively when measuring the 1300nm bulk SOA. Figure 5.13 shows the output of the OPO tuned to 1550nm and 1620nm for characterisation of the MQW and Qdot devices. Figure 5.16 shows the effect of the 1550nm filters through the MQW device where the pump wavelength is 1545nm and the probe 1535nm. Figure 5.17 shows the 1600nm filters through the Qdot device for varying pump wavelengths (1600 - 1610nm) and the probe constant at 1640nm.

5.5 Gain and Phase Recovery Dynamics

The recoveries of the pump-pulse induced carrier density returning back to the equilibrium state is the critical characteristic that determines an amplifier's temporal response to saturation which has been shown to be a limitation of extending GPON with SOAs.

Based on the previous dynamics reports summarised in section 3.4.5, the gain recovery (g(t)) is expected to be on the order of a few hundred picoseconds

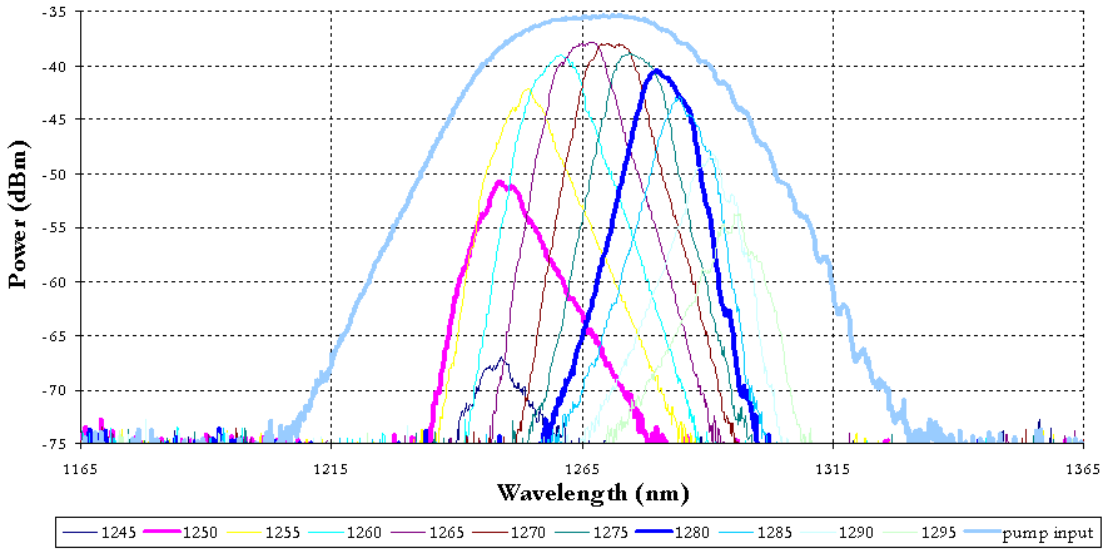

Figure 5.15: 1300nm filter characterisation with OPO input only.

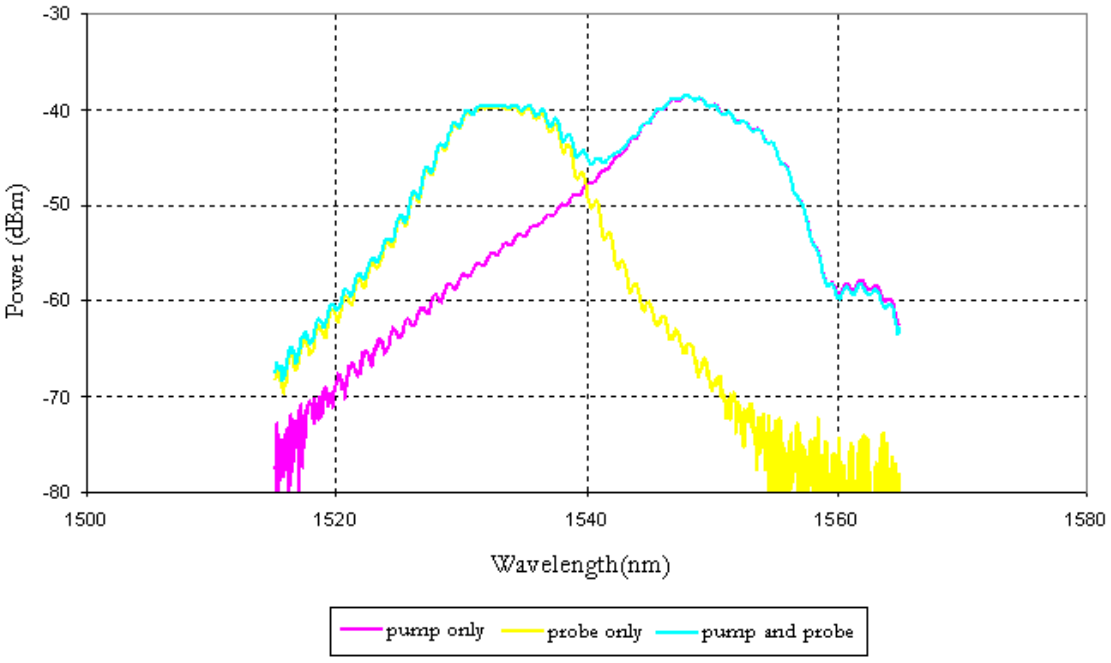

Figure 5.16: Characterisation of the 1550nm filters through the MQW device.

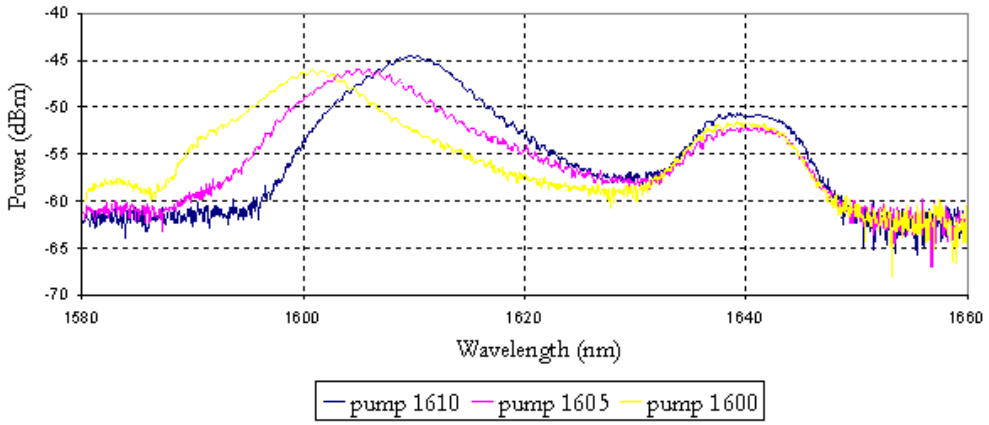

Figure 5.17: Characterisation of the 1650nm filters through the Qdot device.

in MQW and bulk SOAs and less than 100ps in GaAs-based Qdots and the phase recovery ($\phi(t)$) expected to be on the order of one nanosecond in MQW and bulk SOAs.

The results presented in this thesis are the first to compare the gain and phase recoveries of a MQW, Qdot and bulk amplifier together.

Recall the multi-exponential equations used to fit the data for the gain and phase dynamics:

$$g(t) = [a_0 e^{-t/\tau_0} + a_1 e^{-t/\tau_1} + a_2 e^{-t/\tau_2} + a_3 \delta(t)] \otimes I_p(t) \tag{3.20}$$

$$\phi(t) = [\frac{\alpha_0 a_0}{2} e^{-t/\tau_0} + \frac{\alpha_1 a_1}{2} e^{-t/\tau_1} + \frac{\alpha_2 a_2}{2} e^{-t/\tau_2} + \frac{\alpha_3 a_3}{2} \delta(t)] \otimes I_p(t) \tag{3.21}$$

Figure 5.18 shows a screenshot of the Matlab program that was used to to retrieve the results presented below. The 'Experimental Spectrogram' is the aggregation of the measured spectra recorded from the OSA for each step on the translation stage. The 'Retrieved Spectrogram' is the corresponding matrix following the manipulation of the data using the PCGP Algorithm. The horizontal ripple that can be observed on these is due to the ripple on the spectrum which can be observed in the 'Spectral Marginal' box. The vertical colour change that can be observed on both spectrogram measurements is due to the change in intensity when the pump crosses the probe, this can be seen to correspond to the drop in intensity in the 'Temporal Marginal' box. The calculated error between the measured and

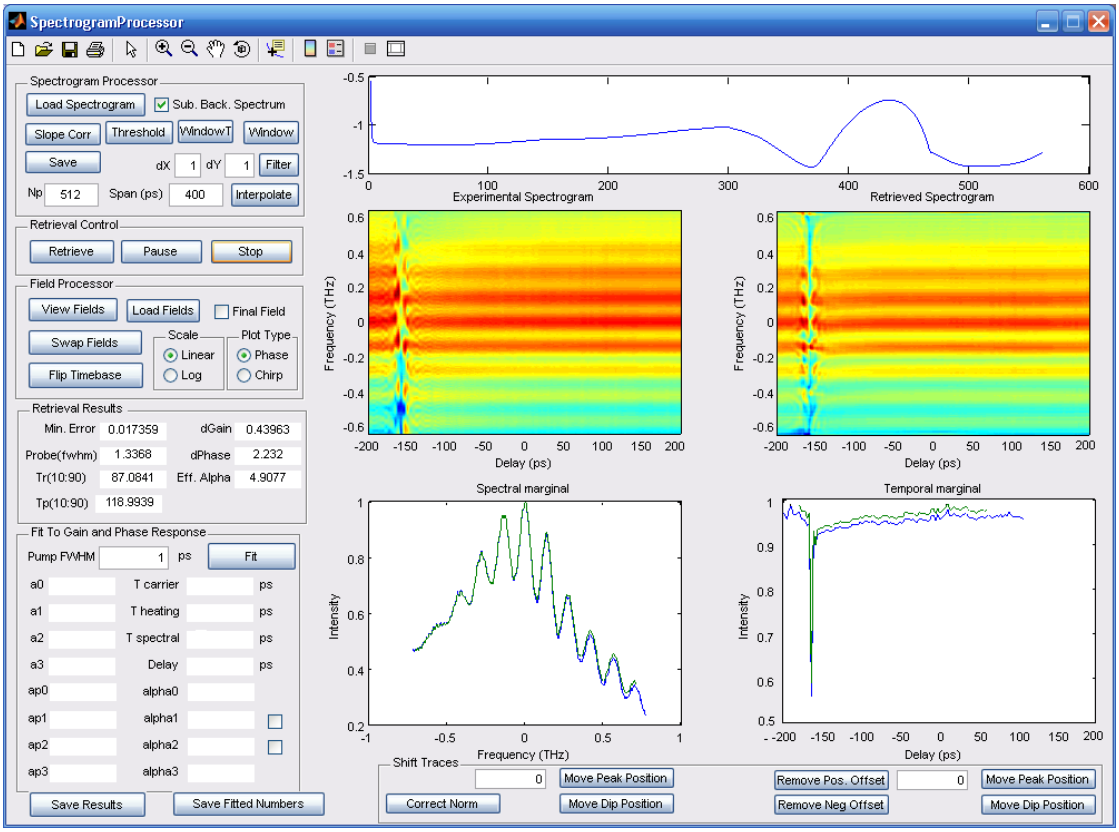

Figure 5.18: Matlab retrieval program screen shot.

retrieved spectrogram has been limited to a maximum of 2%. Figure 5.19 shows an example of an extracted amplitude trace and the calculated gain recovery and Figure 5.20 is an example of a phase measurement from the experiment and the fit curve from the software. The time constants obtained from the amplitude and phase traces are normalized to the transparency current. This section studies and compares the amplitude and phase recoveries of bulk, MQW and Qdot amplifiers.

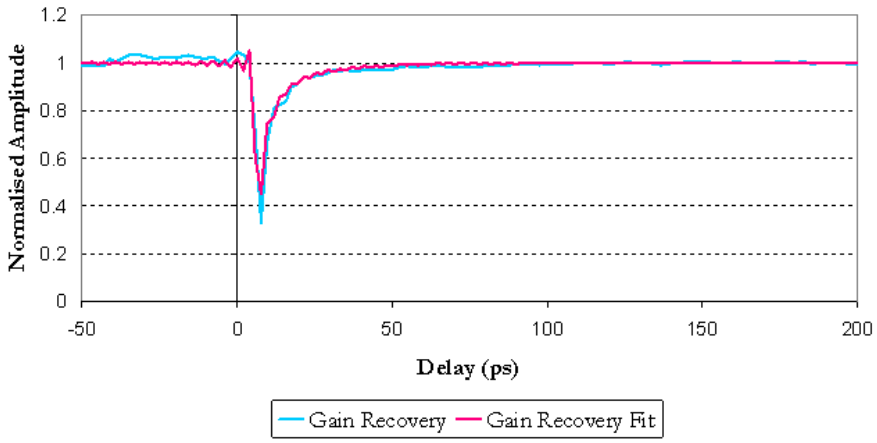

Figure 5.19: Example measured amplitude spectrogram trace (blue line) and gain recovery fit (pink line).

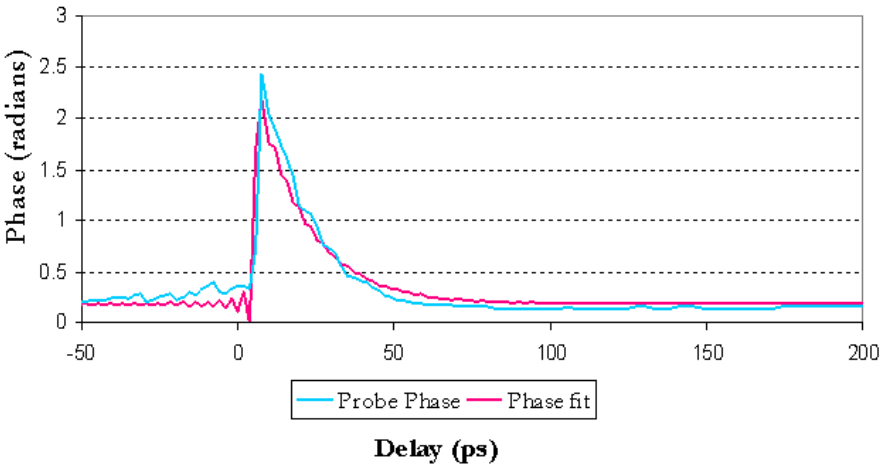

Figure 5.20: Example measured phase spectrogram trace (blue line) and phase recovery fit (pink line).

Figure 5.21 is a log plot of the amplitude recovery trace of the Qdot SOA at varying bias at which 10mA is in absorption, 50mA is near transparency and

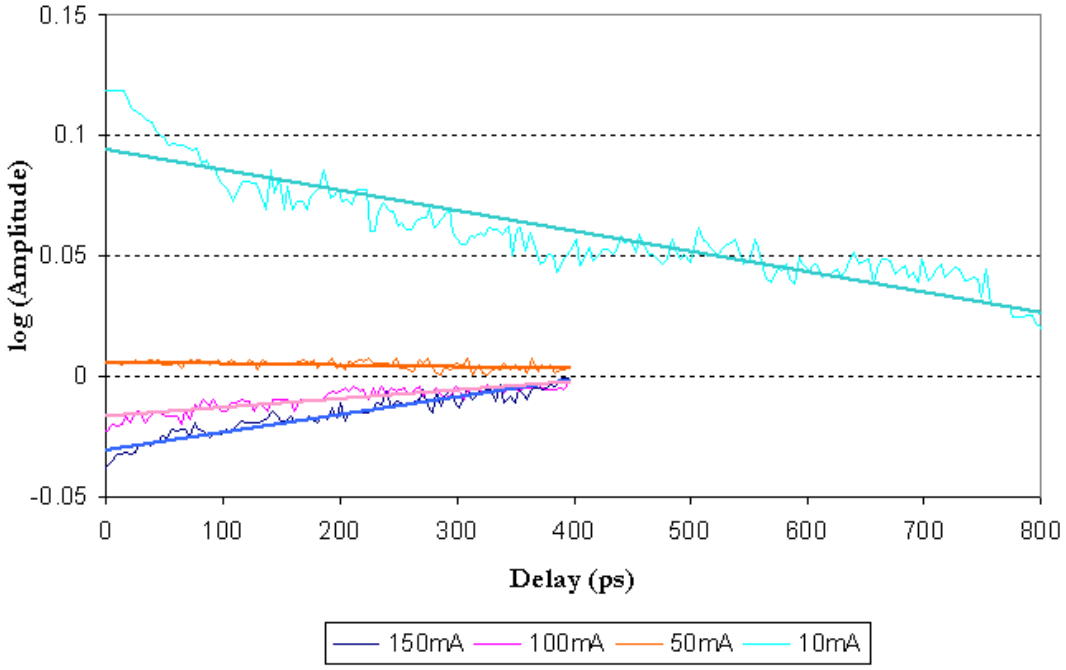

Figure 5.21: Log plot of the amplitude recovery trace of the Qdot SOA at varying bias.

100mA and 150mA are in the gain regime. Each plot has a linear trend meaning that the variability is explained by a single time constant recovery. This implies that the intraband effects of carrier heating, spectral hole burning and two photon absorption have not been resolved in the long-delay scans and only the interband effects τ_0 are retained in fitting the curves. This is as anticipated as the 3ps step size cannot resolve microscopic phenomena.

It is critical to ensure the gain can fully recover before the next pulse arrives at the receiver thus the slower interband recovery time, rather than the intraband dynamics, are of interest in the GPON context as these are responsible for the reduction in waveform fidelity.

5.5.1 Amplitude Recovery Dynamics

Bulk

Figure 5.22 shows the absorption and gain recoveries of the bulk 1550nm SOA with varying bias for high input power (300μW), obtained from pump-probe delay scans over 2ns, facilitated by the long 60cm translation stage in the pump-probe

setup. The device can be seen to be operating in the absorption regime at 20mA above which it passes through transparency into the gain regime as can be seen in the 40mA and 140mA measurements. The absorption and gain recovery of the amplitude is as expected by theory (see section 3.4.5). When the pump energy is greater than the bandgap energy, absorption dominates over stimulated emission and so the carrier density increases due to the presence of the pump. This results in a step increase in amplitude transmission as observed in Figure 5.22. In the gain regime the pump-induced stimulated emission reduces the carrier density and so the probe pulse experiences a reduction in gain. This results in an initial step reduction in amplitude transmission which recovers as the carrier density returns to its unperturbed equilibrium state exponentially with the carrier recovery time.

The absorption recovery time was measured to be 719ps (outwith the range of this graph) and the gain recovery time is minimised at 81ps at high bias (140mA).

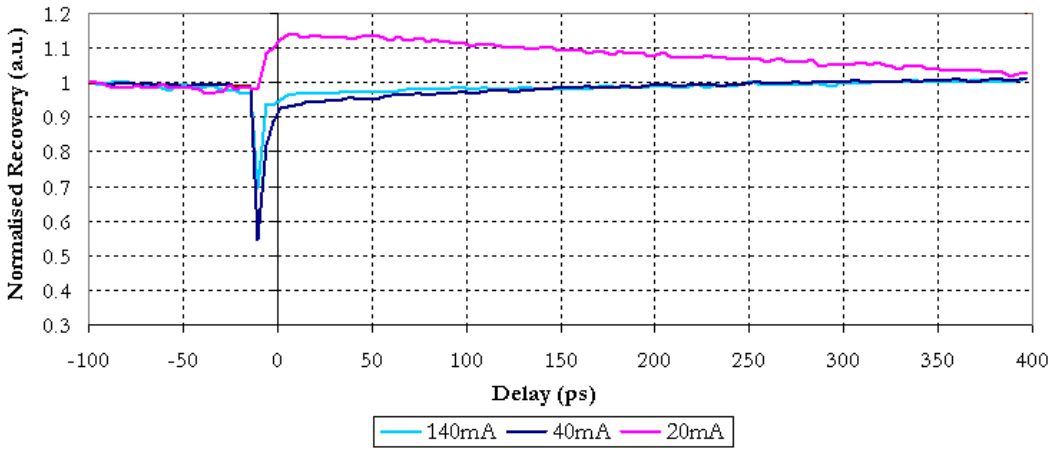

Figure 5.22: Amplitude (g(t)) dynamics for both absorption and gain regime bias currents in the 1550nm bulk SOA obtained from pump-probe scans over 2ns at an input power of 300μW.

Quantum Well

Figure 5.23 shows the measured spectrogram traces of the MQW SOA with varying bias and an input power of 300μW. Figure 5.24 shows the measurements for highest bias (50mA) and lower input power (200μW) and the results are shown for varying probe power. The fastest recovery is for the probe 10dB less than the pump which confirms the conclusions in section 5.3. The fastest gain recovery time is 435ps and in the absorption regime the recovery time is 1260ps.

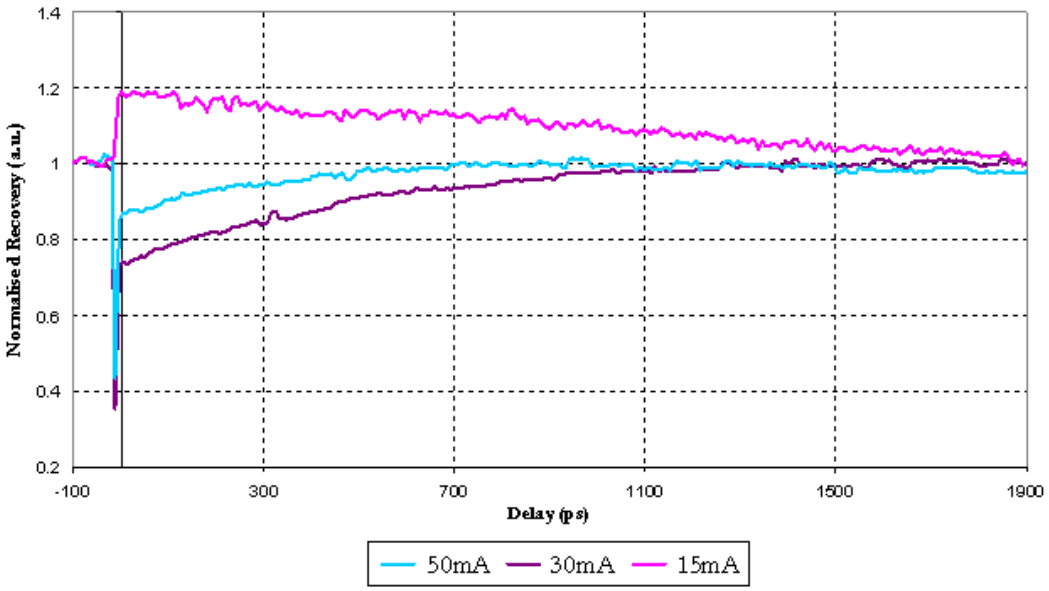

Figure 5.23: Amplitude (g(t)) dynamics for both absorption and gain regime bias currents in the MQW SOA obtained from long-range pump-probe scans over 2ns at an input power of 300μW.

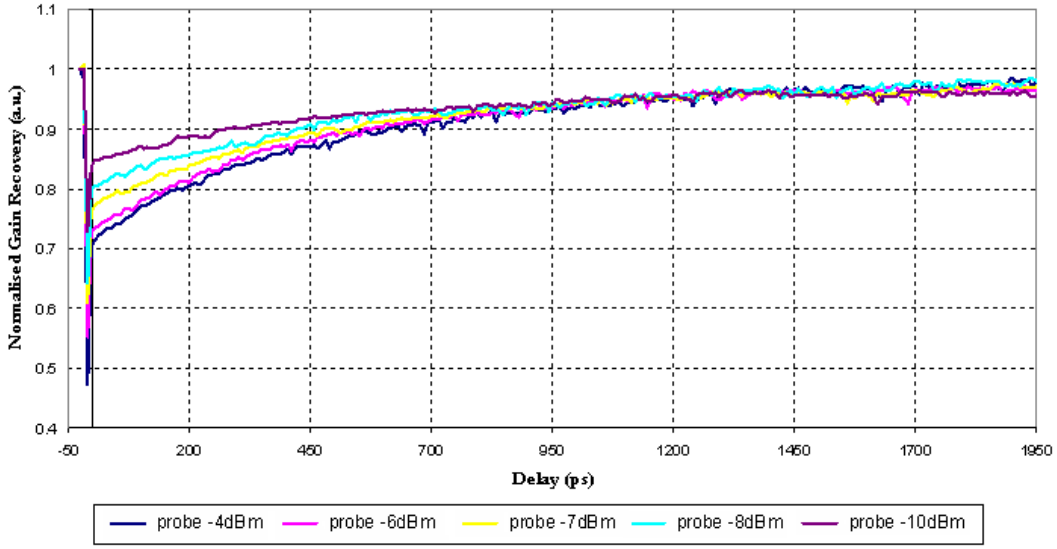

Figure 5.24: Amplitude (g(t)) dynamics for gain recovery in the MQW SOA varying the probe power for constant pump power of 200μW and bias of 50mA.

Quantum Dot

Figure 5.25 shows the measured absorption and gain spectrogram traces of the Qdot SOA with varying bias for low input power (100μW). The device can be seen to be operating in the absorption regime at below 40mA (absorption recovery time of 480ps) above which it passes through transparency (∼50mA) into the gain regime. The Qdot device in Figure 5.26 shows the measured gain spectrogram traces of the Qdot SOA with high bias (150mA) for varying input power (with the probe constant difference from the pump). The carrier recovery time of 54ps was measured for low pump power (100μW).

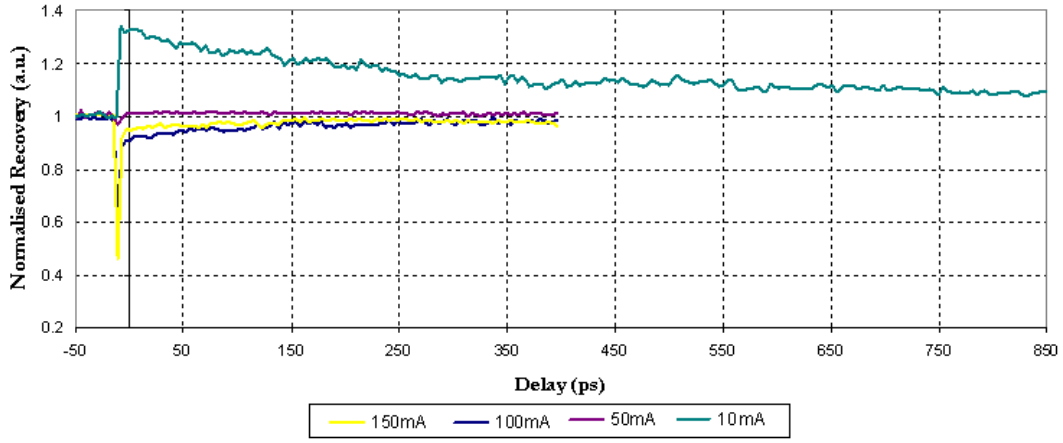

Figure 5.25: Amplitude (g(t)) dynamics for both absorption and gain regime bias currents in the Qdot SOA obtained from pump-probe scans over 2ns.

5.5.2 Comparison of Amplitude Recovery Measurements of 1300nm and 1550nm Bulk SOAs

Figure 5.27 shows the carrier recovery time for the 1300nm bulk SOA and the 1550nm SOA at low input power (100μW). The results for the 1300nm and 1550nm bulk SOAs are very similar and so it is reasonable to consider the 1550nm results for all devices as in the context for GPON applications.

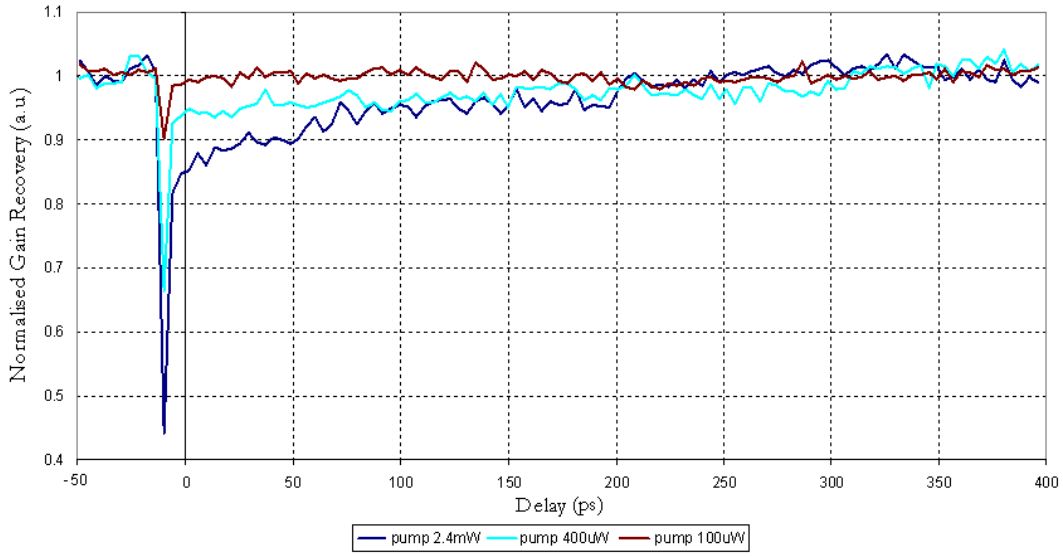

Figure 5.26: Amplitude (g(t)) dynamics in the Qdot SOA at high bias for varying input power obtained from pump-probe scans over 500ps.

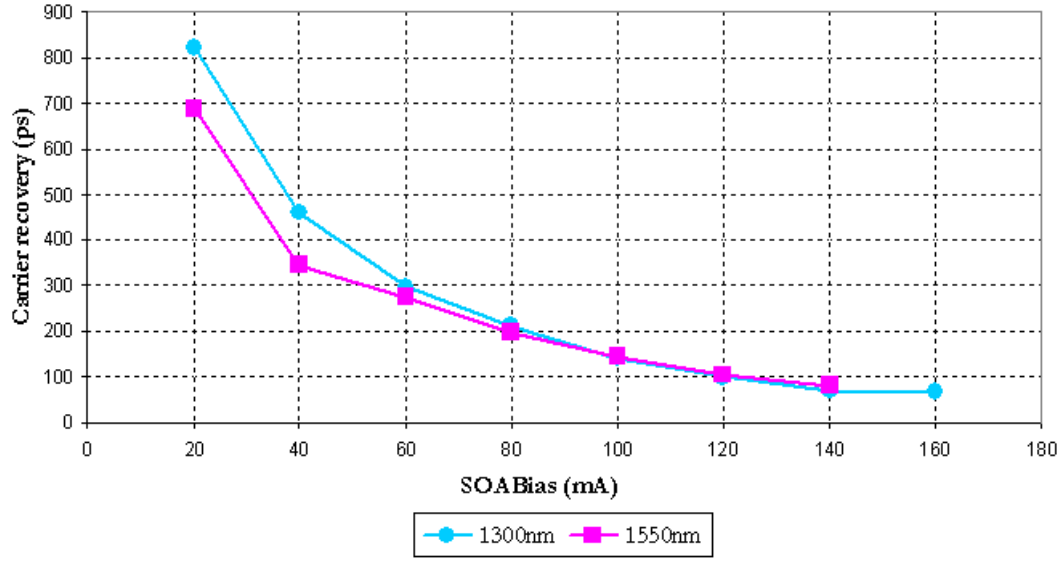

Figure 5.27: The carrier recovery time of 1300nm bulk SOA and 1550nm bulk SOA at low input power (100μW) for varying SOA bias.

5.5.3 Comparison of Amplitude Recovery Measurements of 1550nm Bulk, MQW and Qdot SOAs

Figure 5.28 compares the carrier recovery time of the three C-band SOAs against SOA bias. As expected the Qdot SOA has the fastest recovery time, less than 120ps for all drive currents. The bulk SOA is slower with the recovery times in the range 95ps to 380ps for increasing bias at high input power (300μW). The MQW SOA is the slowest with recovery times ranging from 478ps to 604ps. Note that transparency in the Qdot SOA is 75mA and is 30mA in the MQW SOA; the maximum operating bias of the MQW SOA is 50mA. It can be speculated that there was an issue with the contact resistance of the MQW which reduced the maximum operating bias significantly.

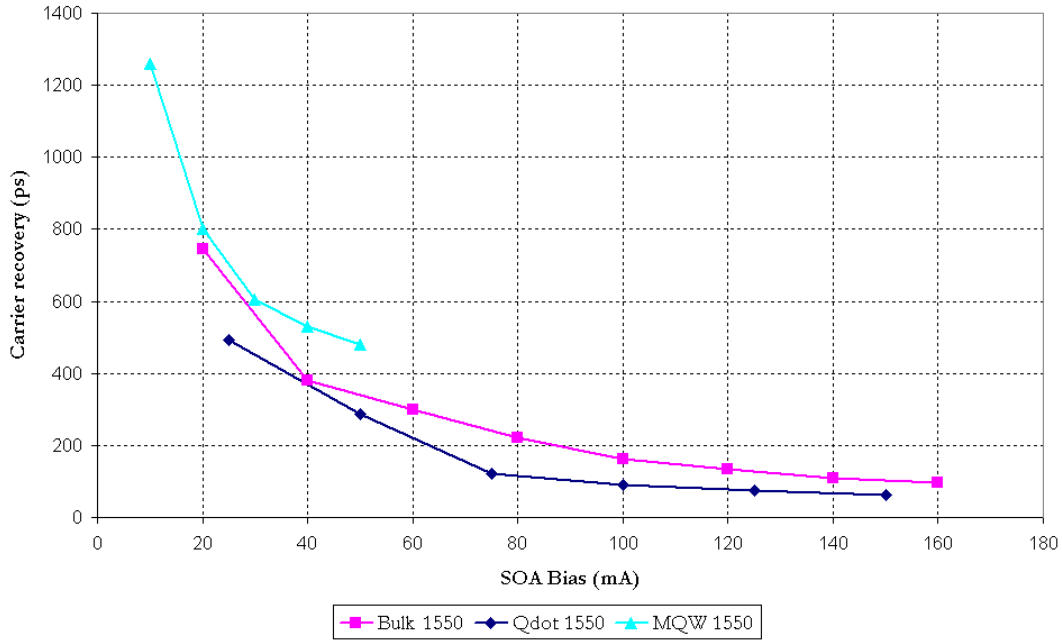

Figure 5.28: The carrier recovery time of the 1550nm bulk SOA at 300μW and the MQW and Qdot SOAs, both at 200μW, for varying SOA bias.

5.5.4 Analysis of the Amplitude Recovery Measurements

The minimum carrier recovery times in the absorption regime are 480ps for the Qdot SOA, 688ps for the bulk SOA and 1260ps for the MQW SOA. The Qdot SOA recovery is approximately three times faster than the MQW SOA of identical

structure. This is due to the carriers in the ground state escaping to the wetting layer rather that participating in radiative recombinations.

In the gain regime the spontaneous recovery times are shorter than the corresponding absorption recovery times and are minimised at 54ps in the Qdot SOA, 80ps in the bulk SOA and 435ps in the MQW SOA all for high bias (150mA, 160mA and 50mA respectively) and low pump power (100μW). Consider the MQW and Qdot SOAs which are of the same structure. In the MQW SOA the recovery time is influenced only by the replenishing of the entire carrier distribution occupying the well and barrier states and is largely attributed to Auger recombination as discussed in section 3.4.2. The Qdot recovery time is 1.6 times faster than the MQW recovery time at 50mA. This is attributed to the carriers occupying not only the dot states but also the wetting layer states. These wetting layer carriers act as a reservoir feeding the dot states through fast carrier capture processes. This concept has been introduced previously in section 5.1 which attributed this reason to the reduced patterning effects in Qdot devices [68].

It is expected that bulk and MQW devices have similar recovery times, which can be observed at low bias (20mA), however at higher bias (40mA) the bulk is 1.4 times faster than the recovery time of the MQW SOA. These devices are made of different material and have different structure.

The recovery of the Qdot is 1.5 times faster than the bulk SOA of similar length giving potential improvement in the PON scenario. It can be speculated that adjusting the design of the bulk SOA from Chapter 4 to include a Qdot active region could make a high gain, fast recovery SOA which could improve the margin of GPON further.

5.5.5 Phase Recovery Dynamics

The results presented in this section extend the benefit of using the spectrograph technique as the phase dynamics of the device are measured. The phase recovery ($\phi(t)$) expected to be on the order of one nanosecond in MQW and bulk SOAs. The results measured here are considerably less than this. As introduced in section 3.4.4 the gain change has an associated refractive index change (phase change) and for decreasing gain the refractive index increases and vice versa.

Figure 5.29 shows the phase recoveries of the bulk 1550nm SOA for high input power (300μW) for bias in both the gain and absorption regimes.

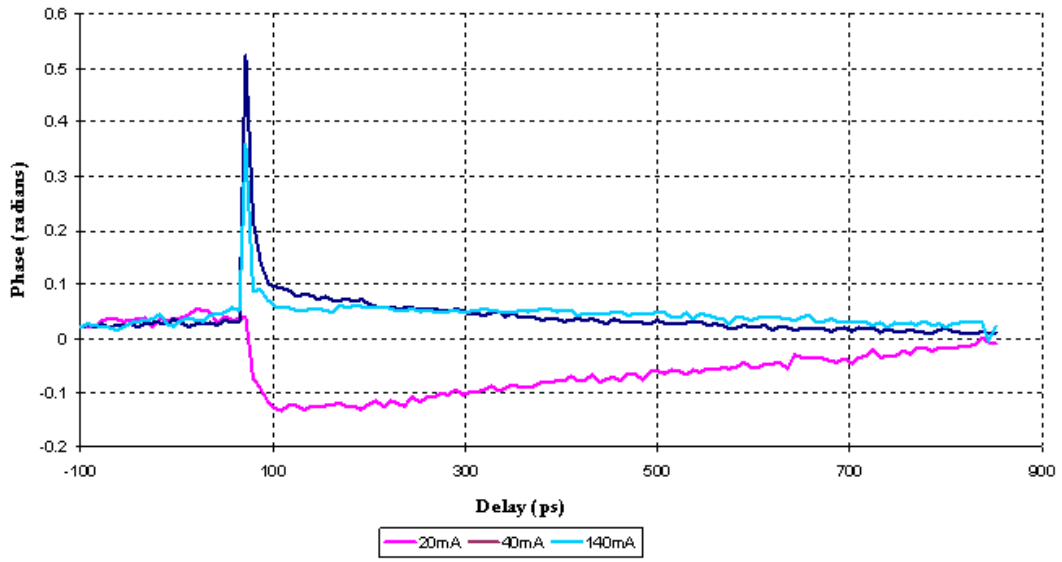

Figure 5.29: Phase ($\phi(t)$) dynamics for both absorption and gain regime bias currents in the 1550nm bulk SOA obtained from long-range pump-probe scans over 2ns.

The absorption and gain recovery of the phase is as expected by theory (see section 3.4.5). When the pump energy is greater than the bandgap energy, absorption dominates over stimulated emission and so the carrier density increases due to the presence of the pump. This results in a step increase in amplitude transmission thus a step decrease in phase (α is negative (Equation 3.18)) as observed Figure 5.29.

In the gain regime the pump-induced stimulated emission reduces the carrier density and so the probe pulse experiences a reduction in gain. This results in an initial step increase in phase transmission which decays as the carrier density returns to its unperturbed equilibrium state exponentially with the carrier recovery time.

The absorption recovery time of the phase was measured to be 719ps (outwith the range of this graph) and the phase recovery time is minimised at 102ps at maximum bias. The minimum phase recovery time at high bias is similar to that of the minimum gain recovery time.

Figure 5.30 shows the phase recoveries of the MQW SOA for varying bias. The absorption recovery time of the phase for MQW was measured to be 1439ps and the phase recovery time is minimised at 531ps at maximum bias.

Figure 5.31 shows the phase recoveries of the Qdot SOA for varying bias.

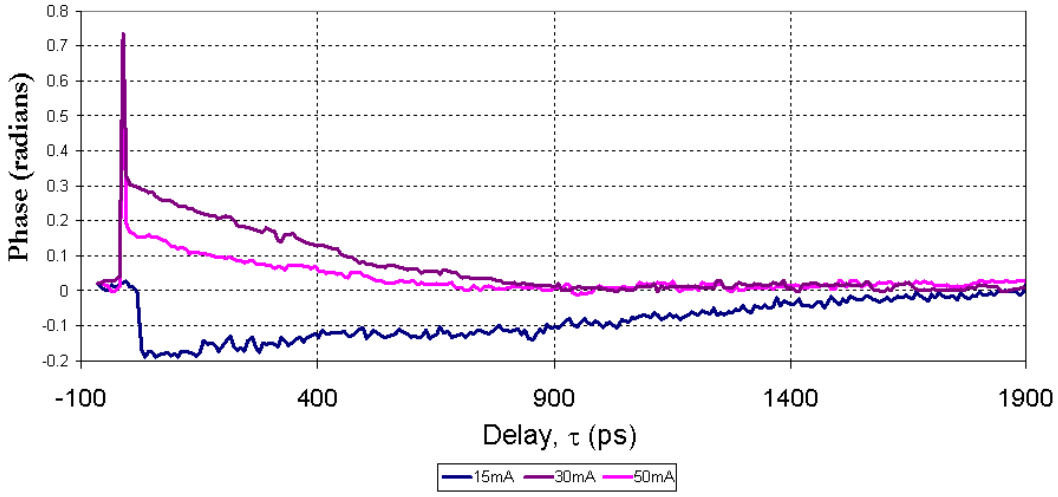

Figure 5.30: Phase ($\phi(t)$) dynamics for both absorption and gain regime bias currents in the MQW SOA obtained from long-range pump-probe scans over 2ns.

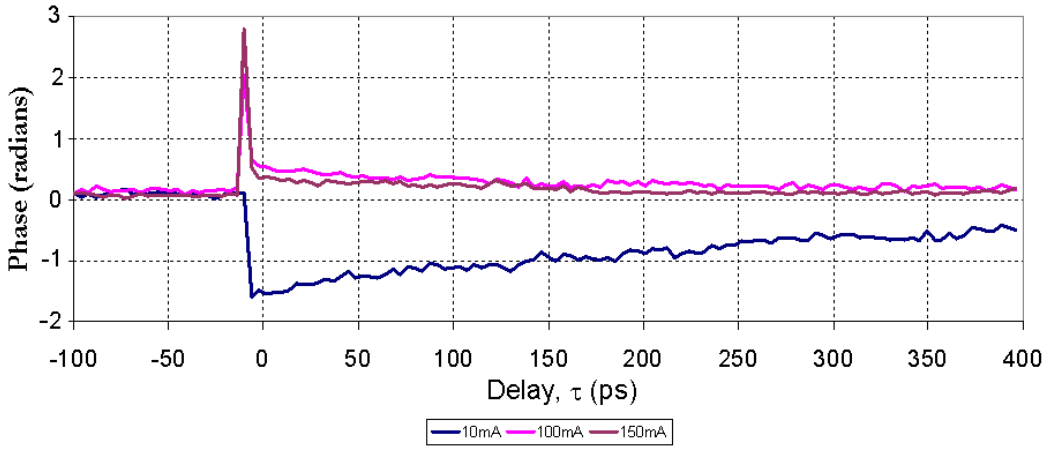

Figure 5.31: Phase ($\phi(t)$) dynamics for both absorption and gain regime bias currents in the Qdot SOA obtained from pump-probe scans over 2ns.

The absorption recovery time of the phase for Qdot was measured to be 922ps and the phase recovery time is minimised at 140ps at maximum bias.

5.5.6 Analysis of the Phase Recovery Measurements

Figure 5.32 compares the phase recovery time of the three C-band SOAs for increasing SOA bias. A clear correlation can be observed between the SOA bias and the phase recovery time. The minimum phase recovery times in the absorption regime are 1439ps for the MQW SOA, 922ps for the Qdot SOA and 719ps for the bulk SOA. The phase recovery times in the gain regime are minimised at 102ps in the bulk SOA, 120ps in the Qdot SOA and 531ps in the MQW SOA all for high bias and low pump power (100μW). Unlike like the amplitude recovery, it can be observed that the bulk SOA has marginally faster phase recovery time than the Qdot SOA. The phase dynamics of the Qdot SOA are influenced by the dynamics of the higher-lying states, thus leading to the slower recovery of the phase to equilibrium.

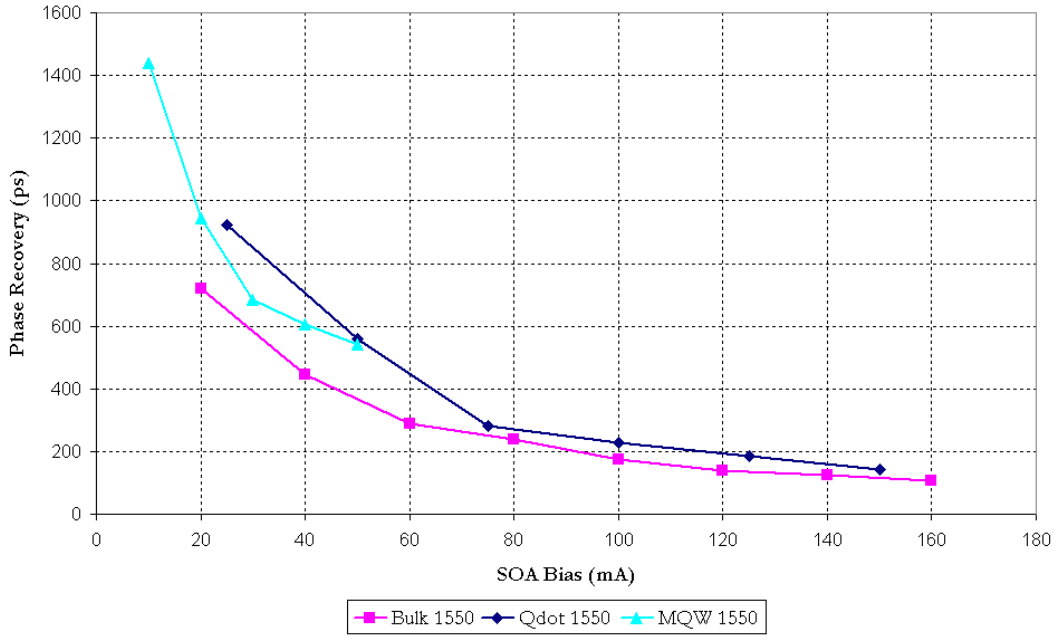

Figure 5.32: The phase recovery time of the 1550nm bulk SOA at 300μW input power and the MQW and Qdot SOAs, both at 200μW, for varying SOA bias.

5.5.7 Summary of Gain and Phase Measurements

The phase recovery times have been shown to be longer than the corresponding amplitude recovery times and are summarised in Table 5.1 and Figure 5.33. The greatest difference is observed in the Qdot SOA where the phase recovery time is approx 2.5 times greater than the amplitude recovery time. The gain recovery time is reduced as the wetting layer carriers act as a reservoir feeding the dot states through fast carrier capture processes.

Active Region	Min Gain Recovery	Min Phase Recovery
Bulk	80ps	102ps
MQW	435ps	531ps
Qdot	54ps	120ps

Table 5.1: Summary of Minimum Gain and Phase Recovery Measurements

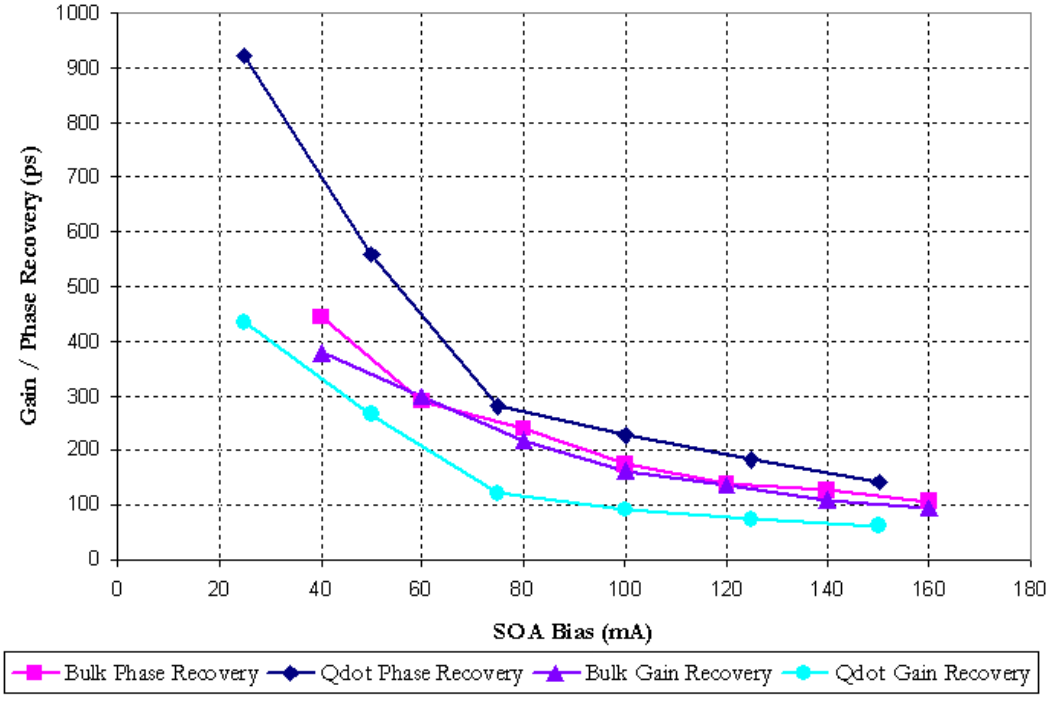

Figure 5.33: Comparison of Gain and Phase recovery times of the bulk and Qdot SOAs.

It can be observed in Figure 5.33 that the gain and phase recovery times of the bulk SOA are very similar with increasing bias; unlike the measurements for the Qdot device in which the gain recovery time is consistently around twice

as fast as the phase recovery for increasing bias density. Table 5.2 provides comparative insight on the differences measured at 100mA and Figure 5.34 illustrates the ratio of phase to amplitude recovery for the bulk (ratio around 1) and Qdot (ratio between 2 - 2.5). These observations are in agreement with the theoretical predictions [103] and the slow processes measured on 1300nm InAs/GaAs Qdot SOA by Vallaitis et al. [106] in which the gain recovery is reported to be predominantly fast, while the phase recovery is predominantly slow. In the GPON context this implies that to avoid phase effects and patterning the Qdot SOA should be operated at high bias current densities with small input power levels.

Active Region	Gain Recovery @ 100mA	Phase Recovery @ 100mA
Bulk	163ps	175ps
Qdot	91ps	227ps

Table 5.2: Comparison of Bulk and Qdot Gain and Phase Recovery Measurements at 100mA

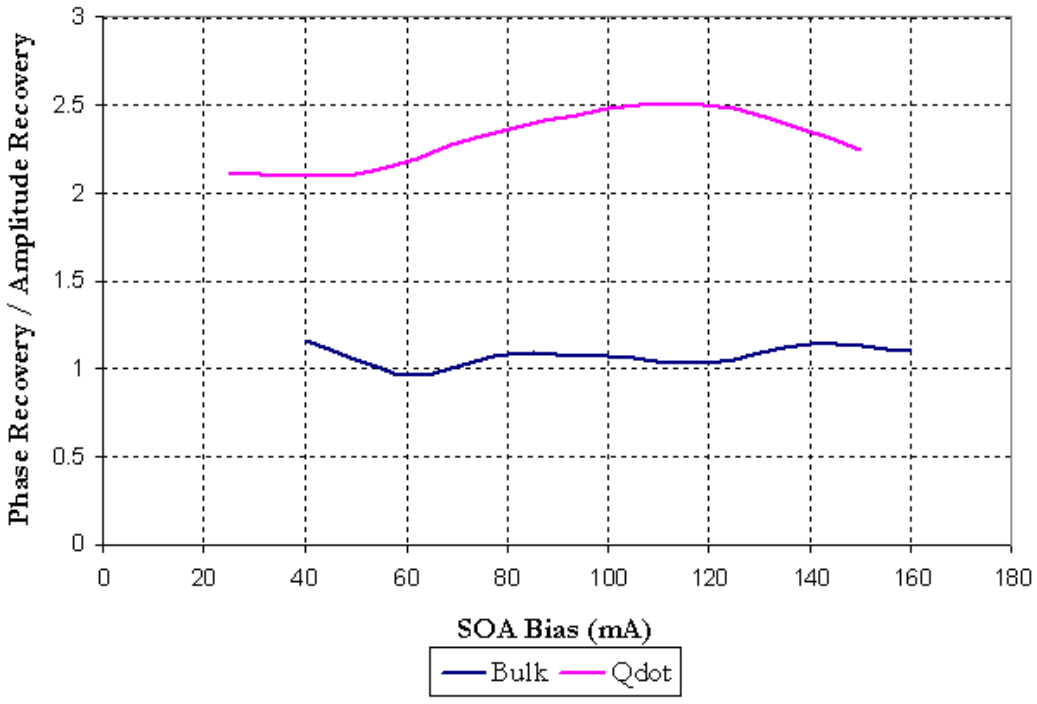

Figure 5.34: Phase to Amplitude Recovery Ratios for Bulk and Qdot

5.5.8 Alpha Factor Study

In addition to measuring the gain dynamics of the SOAs, the spectrogram measurements also resolve the phase-amplitude coupling factor, or α-factor (as introduced in section 3.4.4). This is an important parameter dictating the phase effects in SOAs in optical signal processing schemes [60]. A large α-factor may be desirable in an SOA, for example to maximize the modulation efficiency in a cross-phase-modulation based all-optical signal processing device. However in the context of GPON a low α-factor is desired for minimizing chirp and phase nonlinearities during amplification of short pulses.

The effective phase-amplitude coupling factor (α_{eff} factor) is the α-factor calculated from time-integrated gain and index changes and has been defined:

$$\alpha_{eff} = -2\frac{\Delta\phi}{\Delta ln(g)} \tag{3.19}$$

This section presents the measured α_{eff} factor in all four devices as extracted from the spectrogram measurements and is the first to compare the effective α-factor of bulk, quantum well and quantum dot SOAs.

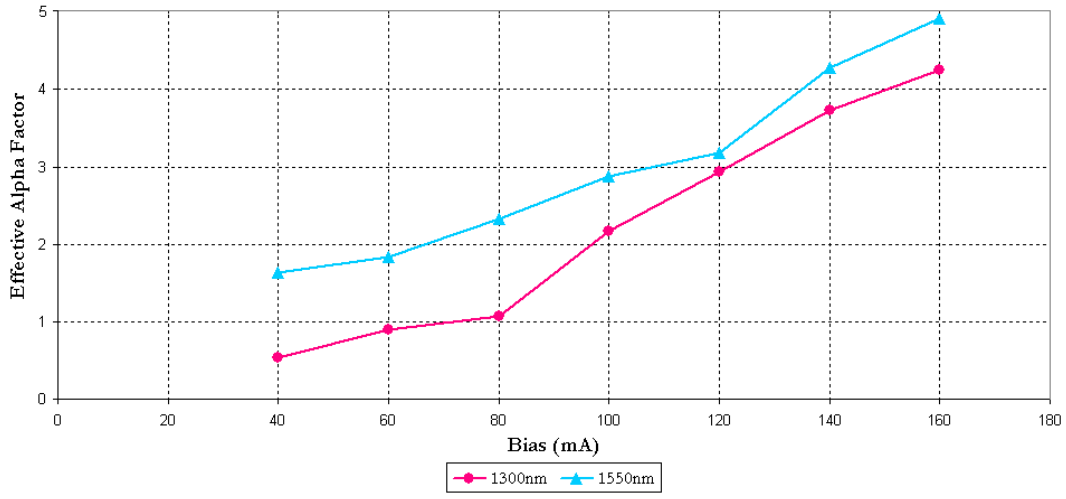

Figure 5.35: Effective Alpha Factor values of the 1300nm and 1550nm bulk SOAs for varying SOA bias.

Figure 5.35 shows the effective α-factor values of the bulk 1300nm and 1550nm SOAs for increasing bias. Increasing bias leads to an increase in the carrier density thus the α-factor values increase with bias as expected [107]. For

the bulk SOAs these range from 0.5 to 4.2 for the 1300nm SOA and 1.63 to 4.9 for the 1550nm device.

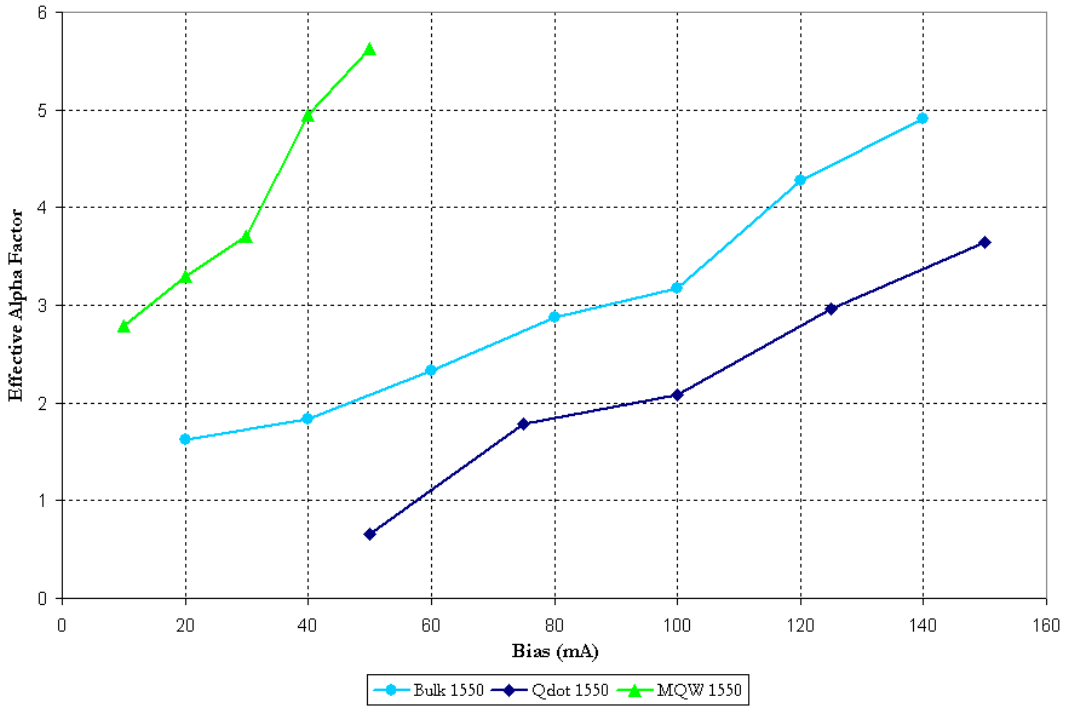

Figure 5.36: Effective Alpha Factors of the 1550nm SOA, MQW SOA and Qdot SOA for varying SOA bias.

Figure 5.36 shows the effective α-factor values of the 1550nm bulk, MQW and Qdot SOAs for increasing bias. The α-factor values increase from 0.7 to 3.6 for the Qdot SOA, 1.63 to 4.9 for the bulk SOA and 2.7 to 5.6 for the MQW SOA.

The consistent variations in effective α-factor as a function of bias current presented here emphasize that the phase effects of an SOA cannot be quantified by quoting a single α-factor. Quoting the minimum α-factor value would underestimate the chirp penalty in a system if the SOA were to be operated at a higher bias. These results indicate that lower chirp can be achieved in optical applications at 1550nm by utilising Qdot SOAs. However to identify the benefit for reducing chirp in 10G-PON further studies at different wavelengths are required.

5.6 Implications for SOAs Operating in a PON

The measurements presented on bulk InGaAsP SOAs in Chapter 4 showed that these were susceptible to patterning (Figure 4.29) which introduced a power penalty thus limited their performance at high input powers such as in the operation as a booster in a PON.

The gain of the Qdot SOA has been shown to recover to equilibrium 1.5 times faster than the bulk SOA. This indicates that it could be less susceptible to patterning in amplification at high bias current densities as it recovers from saturation more quickly; Figure 5.28 illustrated the gain recovery stabilising at lower bias. When observed under heavy saturation the Qdot device recovery slowed down which could limit the usefulness of the near-pattern-free amplification.

However, the fastest recovery times are achieved at smaller input power levels (Figure 5.11) which is inconsistent with the operation of a booster. In the GPON context the recovery time is expected to be sufficient, however for 10G-PON and 100G-PON the slower phase recovery of the Qdot SOA might not be fast enough to amplify without patterning.

The improvement of the Qdot SOA in operation at smaller input power levels could be beneficial when operating as a preamplifier however there are several disadvantages of a Qdot SOA in operation in a PON. Qdot SOAs have higher polarisation dependent gain than bulk SOAs causing inconsistent amplification across the TE and TM modes. The wide bandwidth of the Qdot SOA (Figure 5.6) could be considered to be detrimental to the amplification of a PON due to the increased ASE in the network.

The lower confinement factor of a Qdot SOA leads to an increased device length causing a higher drive current and higher power consumption. The highest reported Qdot SOA gain of 25dB [39] had a drive current of 2A which is a factor of ten higher than the drive current of a traditional (bulk) SOA [108]. This significantly increased power consumption will require an analogous increase in cooling; a parameter difficult to achieve in the desired flexibility posed in the street cabinet solution to extended reach GPON.

The nature of GPON operation in the access network alludes to a higher sensitivity to capital and operating expenditure than in a long haul network. Fabrication of a high yield of consistent performing Qdot SOAs with high gain and low power consumption will be critical to these being embraced by the telecom-

munication operators.

5.7 Conclusions

In this chapter the opportunity to improve the reach of GPON through the insertion of a quantum dot SOA has been investigated.

Gain saturation was shown to restrict the operation of SOAs at high input powers. A literature review of Qdot SOAs operating with a reduced patterning effect has been presented. This has been attributed to carriers accumulating in the Qdot upper levels overcoming the carrier depletion. In order to evaluate the possible benefit of Qdot SOAs in a GPON system the carrier dynamics of these were compared to the bulk SOA presented in Chapter 4.

The structures and emission properties of the bulk, MQW and Qdot SOAs studied in this chapter have been described. Two bulk SOAs were presented; one operating at 1300nm (from Chapter 4) and another operating at 1550nm to allow comparison with the MQW and Qdot SOAs in the experiment. The amplified spontaneous emission spectra of the four devices were demonstrated; the Qdot SOA was shown to be significantly wider than expected theoretically due to homogeneous and inhomogeneous broadening.

This chapter then identified the ideal launch conditions for an amplifier in a Passive Optical Network. It was shown that the carrier recovery time can be reduced by reducing the launch power into the SOA as with too much power the probe saturates the device and reduces the carrier density resulting in a larger carrier lifetime. A minimised carrier recovery time is required in order to allow the amplifier gain to return to its unsaturated value as quickly as possible to avoid gain saturation.

Following this the spectrogram characterisation facility used for the measurements was described and the experimental measurements presented of the gain and phase recovery dynamics. It has been shown that the carrier recovery time in all devices is dependent upon input power and bias.

The results presented for the carrier recovery of the 1300nm and 1550nm bulk SOAs were shown to be very similar allowing the 1550nm results for all devices to be considered in the context of GPON applications.

The results for the MQW SOA were limited as the maximum operating bias

was 50mA compared to the Qdot SOA of the same structure which had a maximum operating bias of 150mA; it was speculated that this could be due to an issue with the contact resistance in the MQW SOA.

The spontaneous recovery times in the gain regime decreased with increasing bias and were minimised at 54ps in the Qdot SOA, 80ps in the bulk SOA and 435ps in the MQW SOA all for high bias and low pump power (100μW). The carrier recovery time of the Qdot SOA is 1.5 times faster than the bulk SOA of similar length. This has been attributed to the wetting layer carriers act as a reservoir feeding the dot states through fast carrier capture processes. For GPON this recovery time is expected to be sufficient, however for 10G-PON and 100G-PON the recovery might not be fast enough to amplify without patterning.

As the transmission power in GPON is high it may not be possible to amplify with the shortest carrier lifetime (Figures 5.11 and 5.28) and so pattern effect free transmission may not be possible with the bulk SOA. Qdot SOAs may be preferential to bulk SOAs in this scenario as they recover from saturation more quickly as Figure 5.28 shows the gain recovery stabilising at lower bias.

The phase recovery times also decreased with increasing bias and were minimised at 102ps in the bulk SOA, 120ps in the Qdot SOA and 531ps in the MQW SOA all for high bias and low pump power (100μW).

The gain and phase recovery times of the bulk SOA were shown to be very similar with increasing bias; unlike the measurements for the Qdot device in which the gain recovery time was consistently around twice as fast as the phase recovery for increasing bias density. In the GPON context this implies that to avoid phase effects and patterning the Qdot SOA should be operated at high bias current densities with small input power levels. It was speculated that adjusting the design of the bulk SOA from Chapter 4 to include a Qdot active region could make a high gain, fast recovery SOA which could improve the margin of GPON further.

An alpha factor study was presented, in the context of GPON a low α-factor is desired for minimizing chirp and phase nonlinearities during amplification of short pulses. The α-factor values of the bulk, MQW and Qdot SOAs were compared and found to increase with increasing bias, attributed to an increase in the carrier density. The Qdot SOA was measured to have the lowest alpha factor which could be beneficial for reducing chirp in 10G-PON. Further studies at different wavelengths are required.

From a GPON perspective, Qdot SOAs are shown to be less susceptible to

patterning and could overcome the limitations in reach extension when operating as a booster as measured in Chapter 4. However there are limitations due to the higher bandwidth and higher cooling requirements related to the increased power consumption. Additionally there are expected difficulties of mass production on a commercial scale.

Chapter 6

Conclusions

This thesis investigated the opportunity to enhance the reach of Passive Optical Networks through the insertion of a semiconductor optical amplifier.

Passive Optical Networks are a point-to-multipoint network architecture which utilise the huge bandwidth potential of optical fibres to bring data at high speed and high bit rates all the way to the end user while minimising the amount of equipment within the network. They are one of the most promising solutions to the bottleneck situation within the telecommunications access network.

The maximum physical coverage of a PON is up to 20km and its logical reach can be up to 60km. There is a trade off between the PON length and its splitting capability. If an 'extender box' is included in the system it may be possible to increase the reach from 20km up to 100km thus enabling more subscribers to be served from a single termination point at the telecommunications providers' Central Office. The position of the SOA in the system will be determined by the availability of a power supply which will vary for each link. The ideal scenario therefore is to have an SOA which can be used in all locations of the span.

In order to extend the reach of a PON without degrading the signal the ideal amplifier would have high gain, high saturation output power and low noise figure. SOAs are commercially available to operate as boosters and in-line amplifiers; high gain (>20dB), low noise figure SOAs require to be developed to operate as preamplifiers. Increasing the gain of an SOA increases the difficulty in controlling the polarisation dependent gain of the device. In order to amplify the GPON network as a preamplifier the SOA will be placed after a long transmission link, thus a minimum PDG value is necessary to minimise possible performance degradation

due to the drift in input signal polarisation state.

Results from SOA modelling showed that the greatest contributing factor to PDG variation was the active region thickness error. In the context of bulk production this requires have a realistic tolerance of ±10nm to maintain PDG of ∼1dB.

To address the gap in the market a high gain, polarisation insensitive SOA was designed and experimentally tested in the context of improving the margin and hence the reach a PON link. The SOA was positioned as a mid-span amplifier in the link and was shown to improve the margin by a record 28dB.

The SOA performance was shown to be limited in performance at high input powers due to gain modulation sourced intersymbol interference, a waveform distortion which can restrict their operation. This is a particular issue in optical networks with high bit rate applications. If the time between the input pulses to the SOA is shorter than the carrier recovery time of the SOA then the gain will not be able to recover completely, resulting in carrier depletion thus reduced optical gain at high input powers.

In order to combat this the carrier dynamics of SOAs with different active region materials were investigated to evaluate their possible benefit to a PON system. Quantum dot SOAs operating with a reduced patterning effect have been reported in literature and attributed to carriers accumulating in the Qdot upper levels overcoming the carrier depletion. In order to evaluate the possible benefit of Qdot SOAs in a GPON system the carrier dynamics of these were compared to the bulk SOA previously designed and shown to improve the link margin.

A comparative study of the gain and phase recovery times of various dimensional SOAs were presented. Using the spectrogram method it was shown that reducing the input power and increasing the bias of the SOA can reduce the carrier recovery time.

A Qdot active region SOAs was shown to considerably reduce the gain recovery time: 1.5 faster than a bulk SOA of similar length. This is attributed to the wetting layer carriers act as a reservoir feeding the dot states through fast carrier capture processes. For GPON this recovery time is expected to be sufficient, however for 10G-PON and 100G-PON the recovery might not be fast enough to amplify without patterning.

The gain and phase recovery times of the bulk SOA were shown to be very similar with increasing bias; unlike the measurements for the Qdot device in which

the gain recovery time was consistently around twice as fast as the phase recovery for increasing bias density.

The performance of the SOAs the PON context should be considered in all locations of the span:

Booster

When operating as a booster the high power incident upon the SOA was identified as a limitation in the operation of the bulk SOA. The gain of the Qdot SOA recovers to equilibrium 1.5 times faster than the bulk SOA indicating that it could provide pattern-effect-free amplification at high bias current densities. However the slower phase recovery of the Qdot could be a problem at high bit rate operation.

As it is difficult to design a Qdot SOA to have low PDG it could be possible to install polarisation maintaining fibre in the short distance between the transmitter and the booster amplifier, however this could be particularly expensive at the ONUs in the upstream direction.

In-Line

An in-line amplifier is used to compensate for power losses caused by fibre attenuation thus high gain is a key requirement. A bulk SOA with gain of 28dB was designed and measured in Chapter 4. Qdot SOAs tend to have lower gain because their gain spectrum is inhomogeneously broadened, the highest reported Qdot SOA gain is 25dB [39] which may not be sufficient for the requirements of PON amplification.

Preamplifier

Preamplifiers receive an input signal with low power and so good sensitivity, high gain, low noise and low polarisation dependence are key requirements. The lowest reported noise figure of a Qdot SOA at the wavelengths of interest for PON is 7dB [39] which is similar to that of the bulk SOA measured in Chapter 4. The aforementioned difficulty of designing a Qdot SOA with low PDG is a limitation of operation in this region.

A proposal for the operation of 10GPON is the implementation of backward integration in which two signals will be transmitted through the amplifier simultaneously. In a bulk SOA it is well documented how the signals will interact however this is unexplored in Qdot SOAs. At these future higher bit rates the speed of the phase recovery is crucial due to the lower tolerance to dispersion.

In the context of GPON a low alpha factor is desired for minimizing chirp and phase nonlinearities during amplification of short pulses. The Qdot SOA was measured to have the lowest alpha factor which could be beneficial for reducing chirp in 10G-PON. Further studies at different wavelengths are required.

The active region of the Qdot SOA permits a faster carrier recovery time which could be beneficial to extend the reach of Passive Optical Networks with reduced patterning when operating as a booster. However, there are several limitations of a Qdot SOA in operation in a PON.

The wide bandwidth of the Qdot SOA (Figure 5.6) could be considered to be detrimental to the amplification of a PON due to the increased ASE in the network. Additionally the aforementioned difficulty of designing a Qdot SOA with low PDG is a limitation of operation causing inconsistent amplification across the TE and TM modes.

The lower confinement factor of a Qdot SOA leads to an increased device length causing a higher drive current and higher power consumption. The highest reported Qdot SOA gain of 25dB [39] had a drive current of 2A which is a factor of ten higher than the drive current of a traditional (bulk) SOA [108]. This significantly increased power consumption will require an analogous increase in cooling; a parameter difficult to achieve in the desired flexibility posed in the street cabinet solution to extended reach GPON.

The nature of GPON operation in the access network alludes to a higher sensitivity to capital and operating expenditure than in a long haul network. Fabrication of a high yield of consistent performing Qdot SOAs with high gain and low power consumption will be critical to these being embraced by the telecommunication operators. However as these are more difficult to fabricate in mass production it is unknown if they are a viable solution on a commercial scale.

Bibliography

[1] "Cisco Visual Networking Index: Forecast and Methodology, 2010-2015," Cisco White Paper, 1 June 2011.

[2] C. T. Hultgren and E. P. Ippen, "Ultrafast Refractive-Index Dynamics in AlGaAs Diode-Laser Amplifiers," *Applied Physics Letters*, vol. 59, no. 6, pp. 635–637, 1991.

[3] K. L. Hall, E. T. Thoen, and E. P. Ippen, "Nonlinearities in Active Media (Chapter 2)," in *Semiconductors and Semimetals*, A. Kost and E. Garmire, Eds. San Diego: Academic Press, 1999, vol. 59: Nonlinear Optics in Semiconductors II.

[4] P. Borri, W. Langbein, J. M. Hvam, F. Heinrichsdorff, M. H. Mao, and D. Bimberg, "Spectral hole-burning and carrier-heating dynamics in InGaAs quantum-dot amplifiers," *IEEE Journal of Selected Topics in Quantum Electronics*, vol. 6, no. 3, pp. 544–551, 2000.

[5] L. Spiekman, D. Piehler, P. Iannone, K. Reichmann, and H. Lee, "Semiconductor Optical Amplifiers for FTTx," in *Proc. Int. Conf. Transparent Optical Networks,Rome, Italy*, July 2007, pp. 48–50.

[6] C. Michie, A. E. Kelly, J. McGeough, S. Karagiannopoulos, and I. Andonovic, "Optically amplified passive optical networks: a power budget analysis," *Journal of Optical Networking*, vol. 8, no. 4, pp. 370–382, 2009.

[7] R. P. Davey and D. B. Payne, "The future of optical transmission in access and metro networks an operators view," in *Proceedings European Conference on Optical Communications*, September 2005, pp. 53–56.

[8] *ITU-T G.651.1 Characteristics of a 50/125 μm multimode graded index optical fibre cable for the optical access network (07/2007).*

[9] *ITU-T G.652 Characteristics of a single-mode optical fibre and cable (06/2005).*

[10] G. P. Agrawal, *Fibre Optic Communication Systems.* New York, USA: John Wiley and Sons, 1997.

[11] H. Bulow, "System outage probability due to first and second order PMD," *IEEE Photonics Technology Letters*, vol. 10, no. 5, pp. 696–698, 1998.

[12] E. Desurvire, *Erbium Doped Fibre Amplifiers.* New York, USA: Wiley, 1994.

[13] R. I. Laming, M. N. Zervas, and D. N. Payne, "Erbium doped amplifier with 54dB gain and 3.1dB noise figure," *IEEE Photon. Technol. Lett*, vol. 4, no. 12, pp. 1345–1347, 1992.

[14] J. Nilsson, S. Y. Yun, S. T. Hwang, J. M. Kim, and S. J. Kim, "Long-wavelength erbium-doped fibre amplifier gain enhanced by ASE end reflectors," *IEEE Photon. Technol. Lett*, vol. 10, no. 11, pp. 1551–1553, 1998.

[15] T. Whitley, R. Wyatt, D. Szebesta, and S. Davey, "Towards a practical $1.3\mu m$ optical fibre amplifier," *BT Technol. J.*, vol. 11, no. 2, pp. 115–127, 1993.

[16] I. Ogawa, F. Ebisawa, N. Yoshimoto, K. Takiguchi, F. Hanawa, T. Hashimoto, A. Sugita, M. Yanagisawa, Y. Inoue, Y. Yamada, Y. Tohmori, T. Ito, K. Magari, Y. Kawaguchi, A. Himeno, and K. Kato, "Lossless hybrid integrated 8 channel wavelength selector module," in *Proc. Int. Conf. Optical Fibre Communications, San Diego, Calfornia*, February 1998, paper PD4.

[17] F. Ebisawa, I. Ogawa, Y. Akahori, K. Takiguchi, Y. Tamura, T. Hashimoto, A. Sugita, Y. Yamada, N. Suzaki, N. Yoshimoto, Y. Tohmori, S. Mino, T. Ito, K. Magari, Y. Kawaguchi, A. Himeno, and K. Kato, "High speed 32 channel optical wavelength selector using PLC hybrid integration," in *Proc. Int. Conf. Optical Fibre Communications, San Diego, Calfornia*, February 1999, pp. 18–20, paper ThB1.

[18] T. Kato, J. Sasaki, T. Shimoda, H. Hatakeyama, T. Tamanuki, M. Yamaguchi, M. Kitamura, and M. Itoh, "10Gb/s photonic cell switching with hybrid 4x4 optical matrix switch module on planar waveguide platform," in *Proc. Int. Conf. Optical Fibre Communications, San Diego, California*, February 1998, paper PD3.

[19] R. Sato, Y. Suzuki, I. Ogawa, N. Yoshimoto, T. Hashimoto, T. Ito, Y. Yanagisawa, Y. Tohmori, Y. Yamada, K. Kato, and H. Toba, "Wide Temperature Operation of Hybrid Integrated Wavelength Converter Module," in *Proc. Int. Conf. Optical Amplifiers and Their Applications*, July 1998, paper BC5.

[20] S. Nakamura, Y. Ueno, and K. Tajima, "168Gb/s all-optical wavelength conversion with a symmetric-Mach-Zehnder-type-switch," *IEEE Photon. Technol. Lett*, vol. 13, no. 19, pp. 1091–1093, 2001.

[21] P. Thijs, L. Tiemeijer, P. Kuindersma, J. Binsma, and T. Van Dongen, "High Performance 1.5m Wavelength InGaAs-InGaAsP Strained Quantum Well Lasers and Amplifiers," *IEEE J. of Quantum Electron.*, vol. 27, no. 6, pp. 1426–1439, 1991.

[22] Y. Lee, T. Ban, S. Makino, H. Hayashi, K. Nagatsuma, R. Mita, S. Tanaka, Y. Matsuoka, T. Sugawara, S. Tsuji, and M. Aoki, "High-Speed and High-Responsivity Back-Illuminated Photodiode with a High Reflective Reflector for 25-Gbps Receiver of 100-Gbps Ethernet," in *Proc. Int. Conf. Optical Fibre Communications, San Diego, California*, March 2009.

[23] D. Spirit and M. O'Mahony, Eds., *High capacity optical transmission explained*. John Wiley and Sons, 1995.

[24] A. Sano, H. Masuda, Y. Kisaka, S. Aisawa, E. Yoshida, Y. Miyamoto, M. Koga, K. Hagimoto, T. Yamada, T. Furuta, and H. Fukuyama, "14-Tb/s (140 x 111-Gb/s PDM/WDM) CSRZ-DQPSK Transmission over 160 km Using 7-THz Bandwidth Extended L-band EDFAs," in *European Conference on Optical Communication 2006, Cannes, France*, 24-28 September 2006, postdeadline Th4.1.1.

[25] U. Feiste, R. Ludwig, C. Schubert, J. Berger, C. Schmidt, H. G. Weber, B. Schmauss, A. Munk, B. Buchold, D. Briggmann, F. Kueppers, and

F. Rumpf, "16OGbit/s transmission over 116 km field installed fibre using 16OGbit/s OTDM and 40Gbit/s ETDM," *Electronics Letters*, vol. 37, no. 7, pp. 443–445, 2001.

[26] M. Nakazawa, T. Yamamoto, and K. R. Tamura, "1.28Tb/s-70 km OTDM transmission using third- and fourth-order simultaneous dispersion compensation with a phase modulator," *Electronics Letters*, vol. 36, no. 24, pp. 2027–2029, 2000.

[27] S. Kawanishi, H. Takara, K. Uchiyama, I. Shake, and K. Mori, "3 Tbit/s (160 Gbit/s19 ch) OTDM/WDM transmission experiment," in *Proc. Int. Conf. Optical Fibre Communications, San Diego, California*, February 1999, paper PD1.

[28] F. J. Effenberger, K. McCammon, and V. O'Byrne, "Passive Optical Network Deployment in North America," *Journal of Optical Networking*, vol. 6, no. 7, pp. 808–818, 2007.

[29] "2007-2008: Early stage deployment of Orange very high speed broadband," France Telecom Press Release, 15 December 2006.

[30] T. Rand-Nash, R. Roth, R. Ram, and R. Kirchain, "Characterizing the CapEx and OpEx Tradeoffs in Next Generation Fiber-to-the-Home Networks," in *Proc. Int. Conf. Optical Fibre Communications, San Diego, Califonia*, February 2008, nthD2.

[31] P. P. Iannone, H. H. Lee, K. C. Reichmann, X. Zhou, M. Du, B. Palsdottir, K. Feder, P. Westbrook, K. Brar, J. Mann, and L. Spiekman, "Hybrid CWDM amplifier shared by multiple TDM PONs," in *Proc. Int. Conf. Optical Fibre Communications, Anaheim, California*, March 2007, pDP-13.

[32] K. Suzuki, F. Fukada, D. Nesset, and R. Davey, "Amplified Gigabit PON systems," *Journal of Optical Networking*, vol. 6, no. 5, pp. 422–433, 2007.

[33] N. Genay, P. Chanclou, P. Saliou, Q. Liu, T. Sorret, and L. Guillo, "Solutions for Budget Increase for the Next Generation Optical Access Network," in *Proc. Int. Conf. Transparent Optical Networks,Rome, Italy*, July 2007, pp. 317–320.

[34] D. A. Neaman, *Semiconductor Physics and Devices: Basic Principles*. McGraw and Hill, 2003.

[35] G. P. Agrawal and N. K. Dutta, *Long Wavelength Semconductor Lasers*. New York, USA: Van Nostrand Reinhold, 1986.

[36] N. K. Dutta and Q. Wang, *Semconductor Optical Amplifiers*. World Scientific, 2006.

[37] T. Akiyama, H. Kuwatsuka, T. Simoyama, Y. Nakata, K. Mukai, and M. Sugawara, "Nonlinear gain dynamics in quantum dot optical amplifiers and its application to optical communication devices," *Journal of Quantum Electronics*, vol. 37, no. 8, pp. 1059–1065, 2001.

[38] T. W. Berg and J. Mork, "Saturation and noise properties of quantum-dot optical amplifiers," *IEEE J. Quantum Electronics*, vol. 40, no. 11, pp. 1527–1539, 2004.

[39] T. Akiyama, M. Ekawa, M. Sugawara, K. Kawaguchi, H. Sudo, A. Kuramata, H. Ebe, and Y. Arakawa, "An Ultrawide-Band Semiconductor Optical Amplifier Having an Extremely High Penalty-Free Output Power of 23dBm Achieved with Quantum Dots," *Photonics Technology Letters*, vol. 17, no. 8, pp. 1614–1616, 2005.

[40] G. Eisenstein, G. Raybon, and L. Stulz, "Deposition and Measurements of Electron-Beam-Evaporated SiO_x Antireflection Coatings on InGaAsP Injection Laser Facets," *Journal of Lightwave Technology*, vol. 6, no. 1, pp. 12–16, 1988.

[41] J. Shim, J. Kim, D. Yang, Y. Eo, and S. Arai, "Facet Reflectivity of a Spot-Size Converter Integrated Semiconductor Optical Amplifier," *Journal of Quantum Electronics*, vol. 38, no. 6, pp. 665–673, 2002.

[42] I. Moerman, P. P. Van Daele, and P. M. Demeester, "A Review on Fabrication Technologies for the Monolithic Integration of Tapers with III-V Semiconductor Devices," *Journal of Selected Topics in Quantum Electronics*, vol. 3, no. 6, pp. 1308–1320, 1997.

[43] T. Saitoh and T. Mukai, "Travelling Wave Semiconductor Laser Amplifiers," in *Coherence, Amplification and Quantum Effects in Semiconductor Lasers*, Y. Yamamoto, Ed. New York: John Wiley and Sons, 1991.

[44] P. Brosson, "Analytical model of a semiconductor optical amplifier," *J. Lightwave Tech.*, vol. 12, no. 1, pp. 49–54, 1994.

[45] T. Saitoh and T. Mukai, "Gain saturation characteristics of travelling wave semiconductor laser amplifiers in short optical pulse amplification," *IEEE Journal of Quantum Electronics*, vol. 26, no. 12, pp. 2086–2094, 1990.

[46] Y. S. Cho and W. T. Choi, "Analysis and Optimization of Polarisation-Insensitive Semiconductor Optical Amplifiers with Delta-Strained Quantum Wells," *Journal of Quantum Electronics*, vol. 37, no. 4, pp. 574–579, 2001.

[47] A. Ougazzaden, D. Sigogne, A. Mircea, E. V. K. Rao, A. Ramdane, and L. Silvestre, "Atmospheric pressure MOVPE growth of high performance polarization insensitive strain compensated MQW InGaAsP/InGaAs optical amplifier," *Electronics Letters*, vol. 31, no. 15, pp. 1242–1244, 1995.

[48] L. F. Tiemeijer, P. J. A. Thijs, T. van Dongen, J. J. M. Binsma, and E. J. Jansen, "Polarization resolved, complete characterization of 1310nm fiber pigtailed multiple-quantum-well optical amplifier," *Photonics Technology Letters*, vol. 14, no. 6, pp. 1524–1533, 1996.

[49] N. Yasuoka, K. Kawaguchi, H. Ebe, T. Akiyama, M. Ekawa, K. Morito, M. Sugawara, and Y. Arakawa, "Quantum-Dot Semiconductor Optical Amplifiers With Polarization-Independent Gains in 1.5μm Wavelength Bands," *IEEE Photon. Technol. Lett*, vol. 20, no. 23, pp. 1908–1910, 2008.

[50] G. Eisenstein, R. S. Tucker, J. M. Wiesenfeld, P. B. Hansen, G. Raybon, B. C. Johnson, T. J. Bridges, F. G. Storz, and C. A. Burrus, "Gain Recovery Time of Traveling-Wave Semiconductor Optical Amplifiers," *Applied Physics Letters*, vol. 54, no. 5, pp. 454–456, 1989.

[51] K. L. Hall, G. Lenz, A. M. Darwish, and E. P. Ippen, "Subpicosecond Gain and Index Nonlinearities in InGaAsP Diode-Lasers," *Optics Communications*, vol. 111, no. 5-6, pp. 589–612, 1994.

[52] J. Pankove, *Optical Processes in Semiconductors*. New York: Dover Publications Inc, 1971.

[53] M. Goeppert-Mayer, "Elementary processes with two-quantum transitions," *Ann. Phys. (Leipz.)*, vol. 9, pp. 273–294, 1931.

[54] W. Kaiser and C. G. B. Garrett, "Two-Photon Excitation in CaF_2:Eu^{2+}," *Phys. Rev. Lett.*, vol. 7, no. 6, pp. 229–232, 1961.

[55] J. H. Bechtel and W. L. Smith, "Two-photon absorption in semiconductors with picosecond laser pulses," *Phys. Rev. B.*, vol. 18, no. 8, pp. 3515–3522, 1976.

[56] W. H. Knox, C. Hirlimann, D. A. B. Miller, J. Shah, D. S. Chemla, and C. V. Shank, "Femtosecond Excitation of Nonthermal Carrier Populations in GaAs Quantum Wells," *Phys. Rev. Lett.*, vol. 56, no. 11, pp. 1191–1193, 1986.

[57] J. Shah, "Hot electrons and phonons under high intensity photoexcitation of semiconductors," *Solid-State Electronics*, vol. 21, no. 1, pp. 43–50, 1978.

[58] J. Mork, J. Mark, and C. P. Seltzer, "Carrier heating in InGaAsP laser amplifiers due to two-photon absorption," *Appl. Phys. Lett.*, vol. 64, no. 17, pp. 2206–2208, 1994.

[59] N. Storkfelt, B. Mikkelsen, D. Olesen, M. Yamaguchi, and K. Stubkjaer, "Measurement of carrier lifetime and linewidth enhancement factor in 1.5m ridge waveguide laser amplifier," *Photonics Technology Letters*, vol. 3, no. 7, pp. 632–634, 1991.

[60] J. Wang, A. Maitra, C. G. Poulton, W. Freude, and J. Leuthold, "Temporal dynamics of the alpha factor in semiconductor optical amplifiers," *Journal of Lightwave Technology*, vol. 25, no. 3, pp. 891–900, 2007.

[61] S. Melnik, G. Huyet, and A. Uskov, "The linewidth enhancement factor α of quantum dot semiconductor lasers," *Optics Express*, vol. 14, no. 7, pp. 2950–2955, 2006.

[62] A. Zilkie, J. Meier, M. Mojahedi, P. Poole, P. Barrios, D. Poitras, T. Rotter, A. Yang, C. Stintz, K. Malloy, P. Smith, and J. Aitchison, "Carrier Dynamics

of Quantum-Dot, Quantum-Dash, and Quantum-Well Semiconductor Optical Amplifiers Operating at 1.55μm," *IEEE J. Quantum Electronics*, vol. 43, no. 11, pp. 982–991, 2007.

[63] M. P. Kesler and E. P. Ippen, "Subpicosecond Gain Dynamics in GaAlAs Laser-Diodes," *Applied Physics Letters*, vol. 51, no. 22, pp. 1765–1767, 1987.

[64] M. Sheik-Bahae and E. W. Van Stryland, "Ultrafast nonlinearities in semiconductor laser amplifiers," *Physical Review B*, vol. 50, no. 19, pp. 14 171–14 178, 1994.

[65] K. L. Hall, J. Mark, E. P. Ippen, and G. Eisenstein, "Femtosecond Gain Dynamics in InGaAsP Optical Amplifiers," *Applied Physics Letters*, vol. 56, no. 18, pp. 1740–1742, 1990.

[66] G. Eisenstein, J. M. Wiesenfeld, M. Wegener, G. Sucha, D. S. Chemla, S. Weiss, G. Raybon, and U. Koren, "Ultrafast Gain Dynamics in 1.5 μm Multiple Quantum Well Optical Amplifiers," *Applied Physics Letters*, vol. 58, no. 2, pp. 158–160, 1991.

[67] R. Giller, R. J. Manning, and D. Cotter, "Gain and Phase Recovery of Optically Excited Semiconductor Optical Amplifiers," *Photonics Technology Letters*, vol. 18, no. 9, pp. 1061–1063, 2006.

[68] M. Sugawara, N. Hatori, T. Akiyama, Y. Nakata, and H. Ishikawa, "Quantum-dot semiconductor optical amplifiers for high bit-rate signal processing over 40 Gbit/s," *Japanese Journal of Applied Physics Part 2 -Letters*, vol. 40, no. 5B, pp. L488–L491, 2001.

[69] T. W. Berg, J. Mork, and A. Uskov, "Ultrafast signal processing in quantum dot amplifiers through effective spectral holeburning," in *Technical Digest, CLEO, Long Beach, California*, May 2002, p. 662, paper CFH7.

[70] P. Borri, W. Langbein, J. M. Hvam, E. Heinrichsdorff, M. H. Mao, and D. Bimberg, "Ultrafast gain dynamics in InAs-InGaAs quantum-dot amplifiers," *IEEE Photonics Technology Letters*, vol. 12, no. 6, pp. 594–596, 2000.

[71] T. W. Berg, S. Bischoff, I. Magnusdottir, and J. Mork, "Ultrafast gain recovery and modulation limitations in self-assembled quantum-dot devices," *IEEE Photonics Technology Letters*, vol. 13, no. 6, pp. 541–543, 2001.

[72] J. Mork and A. Mecozzi, "Response Function for Gain and Refractive-Index Dynamics in Active Semiconductor Wave-Guides," *Applied Physics Letters*, vol. 65, no. 14, pp. 1736–1738, 1994.

[73] K. L. Hall, G. Lenz, E. P. Ippen, and G. Raybon, "Heterodyne Pump-Probe Technique for Time-Domain Studies of Optical Nonlinearities in Waveguides," *Optics Letters*, vol. 12, no. 17, pp. 874–876, 1994.

[74] J. Mork, A. Mecozzi, and C. T. Hultgren, "Spectral Effects in Short Pulse Pump-Probe Measurements," *Appl. Phys. Lett.*, vol. 68, no. 4, pp. 449–451, 1996.

[75] K. L. Hall, Y. Lai, E. P. Ippen, G. Eisenstein, and U. Koren, "Femtosecond Gain Dynamics and Saturation Behaviour in InGaAsP Multiple Quantum-Well Optical Amplifiers," *Applied Physics Letters*, vol. 57, no. 27, pp. 2888–2890, 1990.

[76] J. Mark, N. Tessler, G. Eisenstein, and J. Mork, "Broadband Femtosecond Pump-Probe Setup Operating at 1300 and 1550nm," *Appl. Phys. Lett.*, vol. 64, no. 15, pp. 1899–1901, 1994.

[77] J. Tatum, D. MacFarlane, R. Bowen, G. Klimeck, and W. Frensley, "Ultrafast Characteristics of InGaP-InGaAlP Laser Amplifiers," *IEEE J. of Quantum Electron.*, vol. 32, no. 4, pp. 664–669, 1996.

[78] C. Sun, H. Choi, C. Wang, and J. Fujimoto, "Studies of Carrier Heating in InGaAs/AlGaAs Starined-Layer Quantum Well Diode Lasers Using a Multiple Wavelength Pump Probe Technique," *Appl. Phys. Lett.*, vol. 62, no. 7, pp. 747–749, 1993.

[79] ——, "Femtosecond Gain Dynamics in InGaAs/AlGaAs Strained-Layer Single-Quantum-Well Diode Lasers," *Appl. Phys. Lett.*, vol. 63, no. 1, pp. 96–98, 1993.

[80] K. L. Hall, E. P. Ippen, U. Koren, and G. Raybon, "Carrier Heating and Spectral Hole Burning in Strained-Layer Quantum-Well Laser Amplifiers at 1.5um," *Applied Physics Letters*, vol. 61, no. 21, pp. 2512–2514, 1992.

[81] R. Alizon, D. Hadass, V. Mikhelashvili, G. Eisenstein, R. Schwertberger, A. Somers, J. P. Reithmaier, A. Forchel, M. Calligaro, S. Bansropun, and M. Krakowski, "Cross-saturation dynamics in InAs/Inp quantum dash optical amplifiers operating at 1550nm," *Electronics Letters*, vol. 41, no. 5, pp. 266–268, 2005.

[82] V. Wong and I. Walmsley, "Ultrashort-pulse characterization from dynamic spectrograms by iterative phase retrieval," *Journal of the Optical Society of America B*, vol. 14, no. 4, pp. 944–949, 1997.

[83] D. Reid, "Algorithm for complete and rapid retrieval of ultrashort pulse amplitude and phase from a sonogram," *IEEE J. Quantum Electron.*, vol. 35, no. 11, pp. 1584–1589, 1999.

[84] R. Trebino, Ed., *Frequency-Resolved Optical Gating: the Measurement of Ultrashort Optical Pulses*. Boston, Mass, USA: Kluwer Academic, 2002.

[85] J. M. Dudley, "Complete characterization of ultrashort pulse sources at 1550nm," *IEEE J. Quantum Electron*, vol. 35, no. 4, pp. 441–450, 1999.

[86] B. C. Thomsen, M. A. F. Roelens, R. T. Watts, and D. J. Richardson, "Comparison Between Nonlinear and Linear Spectrographic Techniques for the Complete Characterisation of High Bit-Rate Pulses Used in Optical Communications," *IEEE Photon. Technol. Lett*, vol. 17, no. 9, pp. 1914–1916, 2005.

[87] C. Dorrer and I. Kang, "Simultaneous temporal characterization of telecommunication optical pulses and modulators by use of spectrograms," *Optics Letters*, vol. 27, no. 15, pp. 1315–1317, 2002.

[88] L. Cohen, "Time-Frequency Distributions: A Review," *Proceedings of the IEEE*, vol. 77, no. 7, pp. 941–981, 1989.

[89] D. J. Kane, "Real-time measurement of ultrashort laser pulses using principal component generalized projections," *IEEE Journal on Selected Topics in Quantum Electronics*, vol. 34, no. 2, pp. 278–284, 1998.

[90] ——, "Recent progress toward real-time measurement of ultrashort laser pulses," *IEEE Journal on Selected Topics in Quantum Electronics*, vol. 35, no. 4, pp. 421–431, 1999.

[91] S. I. Grossman, *Elementary Linear Algebra*. Belmont, California: Wadsworth Publishing Company, 1987.

[92] D. J. Kane, G. Rodriguez, and T. S. Taylor, A. J. Clement, "Simultaneous measurement of two ultrashort pulses from a single spectrogram in a single shot," *J. Opt. Soc. Amer. B*, vol. 14, no. 4, pp. 935–943, 1997.

[93] T. Kakitsuka, Y. Shibata, M. Itoh, Y. Kadota, Y. Tohmori, and Y. Yoshikuni, "Influence of Buried Structure on Polarization Sensitivity in Strained Bulk Semiconductor Optical Amplifiers," *IEEE Journal of Quantum Electronics*, vol. 38, no. 1, pp. 85–92, 2002.

[94] M. J. Connelly, "Wideband semiconductor optical amplifier steady-state numerical model," *J. Quantum Electronics*, vol. 37, no. 3, pp. 439–447, 2001.

[95] C. Michie, A. E. Kelly, J. McGeough, I. Armstrong, I. Andonovic, and C. Tombling, "Polarization-Insensitive SOAs Using Strained Bulk Active Regions," *J. Lightw. Technol.*, vol. 24, no. 11, pp. 3920–3927, 2006.

[96] A. Yin, L. Li, and X. Zhanga, "Analysis of 2.5 Gbit/s GPON downlink optical-receiver performance," *Optics Communications*, vol. 282, no. 2, pp. 198–203, 2009.

[97] *ITU-T G.984.2 Gigabit-capable Passive Optical Networks (G-PON): Physical Media Dependent (PMD) layer specification. Amendment 1: New Appendix III Industry best practice for 2.488 Gbit/s downstream, 1.244 Gbit/s upstream G-PON (02/2006).*

[98] A. V. Uskov, T. W. Berg, and J. Mork, "Theory of Pulse-Train Amplification Without Patterning Effects on Quantum-Dot Semiconductor Optical Amplifiers," *IEEE J. Quantum Electron.*, vol. 40, no. 3, pp. 306–320, 2004.

[99] T. Akiyama, N. Hatori, Y. Nakata, H. Ebe, and M. Sugawara, "Pattern-effect-free Semiconductor Optical Amplifier using Quantum Dots," *Electronics Letters*, vol. 38, no. 19, pp. 1139–1140, 2002.

[100] C. Michie, A. E. Kelly, I. Armstrong, I. Andonovic, and C. Tombling, "An Adjustable Gain-Clamped Semiconductor Optical Amplifier (AGC-SOA)," *J. Lightw. Technol.*, vol. 25, no. 6, pp. 1466–1473, 2007.

[101] K. Inoue, "Waveform Distortion in a Gain-Saturated Semiconductor Optical Amplifier for NRZ and Manchester Formats," *IEE Proceedings Optoelectronics*, vol. 144, no. 6, pp. 433–437, 1997.

[102] A. V. Uskov, J. Mork, B. Tromborg, T. W. Berg, I. Magnusdottir, and E. P. OReilly, "On high-speed cross-gain modulation without pattern effects in quantum dot semiconductor optical amplifiers," *Optics Communications*, vol. 227, no. 4–6, pp. 363–369, 2003.

[103] A. V. Uskov, E. P. OReilly, R. J. Manning, R. P. Webb, D. Cotter, M. Laemmlin, N. N. Ledentsov, and D. Bimberg, "On Ultrafast Optical Switching Based on Quantum-Dot Semiconductor Optical Amplifiers in Nonlinear Interferometers," *IEEE Photonics Technology Letters*, vol. 16, no. 5, pp. 1265–1267, 2004.

[104] I. ODriscoll, T. Piwonski, J. Houlihan, G. Huyet, R. J. Manning, and B. Corbett, "Phase dynamics of InAs/GaAs quantum dot semiconductor optical amplifiers," *Appl. Phys. Lett.*, vol. 91, no. 26, pp. 3506–3508, 2007.

[105] I. Kang and C. Dorrer, "Measurements of gain and phase dynamics of a semiconductor optical amplifier using spectrograms," in *Proc. Int. Conf. Optical Fibre Communications, San Diego, California*, February 2004, paper MF43.

[106] T. Vallaitis, C. Koos, R. Bonk, W. Freude, M. Laemmlin, C. Meuer, D. Bimberg, and J. Leuthold, "Slow and fast dynamics of gain and phase in a quantum dot semiconductor optical amplifier," *Optics Express*, vol. 16, no. 1, pp. 170–178, 2008.

[107] L. Occhi, R. Scollo, L. Schares, and G. Guekos, "Effective Alpha Factor in Bulk Semiconductor Optical Amplifiers of Different Lengths," in *Lasers and Electro-Optics Society, San Diego, Calfornia*, November 2001, 105 - 106 vol. 1.

[108] D. Nesset, A. E. Kelly, S. Appathurai, and R. Davey, "Extended Reach GPON Using High Gain Semiconductor Optical Amplifiers," in *Proc. Int. Conf. Optical Fibre Communications, San Diego, California*, February 2008, jWA107.